UNIVERSITY OF CALIFORNIA, SAN DIEGO

Modeling and Optimization Techniques for Sizing and Scheduling Applications in Power and Energy

A dissertation submitted in partial satisfaction of the
requirements for the degree Doctor of Philosophy

in

Engineering Sciences (Mechanical Engineering)

by

Abdulelah Habib

Committee in charge:

Professor Raymond A. de Callafon, Co-Chair
Professor Jan Kleissl, Co-Chair
Professor Mauricio de Oliveira
Professor Philip E. Gill
Professor Tajana Simunic Rosing

2018

The Dissertation of Abdulelah Habib is approved and is acceptable in quality and form for publication on microfilm and electronically:

Co-Chair

Co-Chair

University of California, San Diego

2018

DEDICATION

To my parents, daughter, wife, and siblings.

TABLE OF CONTENTS

LIST OF FIGURES

LIST OF TABLES

ACKNOWLEDGEMENTS

The text and data in Chapter 2, in full, is a reprint of the material as it appears in "Optimal switchable load sizing and scheduling for standalone renewable energy systems", Habib, Abdulelah; Disfani, Vahid R.; Kleissl, Jan; de Callafon, Raymond, *Solar Energy*, 144 (2017), 707 - 720. The dissertation author is the primary investigator and author of this article.

The text and data in Chapter 3, is a reprint of the material as it appears in "Quasi-dynamic load and battery sizing and scheduling for stand-alone solar system using mixed-integer linear programming,". Habib, Abdulelah; Disfani, Vahid R.; Kleissl, Jan; de Callafon, Raymond, *in 2016 IEEE Conference on Control Applications (CCA), 2016*, pp. 1476-1481, 2016. The dissertation author is the primary investigator and author of this article. Some content of this chapter has been corrected in this thesis.

The text and data in Chapter 4, in full, is a reprint of the material as it appears in"Optimal Energy Storage Sizing and Residential Load Scheduling to Improve Reliability in Islanded Operation of Distribution Grids". Habib, Abdulelah; Disfani, Vahid R.; Kleissl, Jan; de Callafon, Raymond, *2017 American Control Conference (ACC)*, Seattle, WA, 2017, pp. 3974-3979. The dissertation author is the primary investigator and author of this article.

The text and data in Chapter 5, in full, is a reprint of the material as it appears in "Market-Driven Energy Storage Planning for Microgrids with Renewable Energy Systems Using Stochastic Programming,". Habib, Abdulelah; Disfani, Vahid R.; Kleissl, Jan; de Callafon, Raymond, *IFAC-PapersOnLine*, vol. 50, iss. 1, pp. 183-188, 2017. The dissertation author is the primary investigator and author of this article

I would like to acknowledge all the support that I have received throughout my graduate studies from my family and my friends. Without their constant support it would be impossible to do all the hard work which has led to this dissertation.

I gratefully acknowledge the mentorship of my both advisors Professor Jan Kleissl and Professor Raymond de callafon. Through their guidance I have found the balance between theory and application at University of California, San Diego. They were very generous in their continuous support, time and funds. I am also thankful to my committee members, Professor Mauricio de Oliveira, Professor Philip E. Gill and professor Tajana imuni Rosing, for their valuable comments and suggestions during the preparation of this dissertation. If there is one person to thank the most is Dr. Vahid Rasouli Disfani who was at the time of my studies a very close friend and mentor during his post doctorate at UC San Diego. Last but not the least,

I acknowledge the support of all my colleagues and collaborators at the University of California, San Diego. I am thankful to my colleague and specially my officemates Zack Pecenak and Ben Kurtz and rest of Solar Resource Assessment and Forecasting Laboratory as well as The Synchrophasor Grid Monitoring and Automation (SyGMA) laboratory. I enjoyed the company of all colleagues, who were part of a unique environment for sharing knowledge and curiosity.

Finally, I would like to show the greatest appreciation to the government of Saudi Arabia represented by King Abdulaziz City for Science and Technology (KACST) for the full scholarship, support and for this unique opportunity. I will always be grateful and loaner to give back to my country and people. Thank Allah the most gracious the most merciful for all this blessing may I be grateful to all that.

VITA

2010	B.S. in Control and Instrumentation System Engineering, King Fahd University of Petroleum and minerals
2011	M.S. in Electrical Engineering, King Abdullah University of Science and Technology
2017	Ph.D. in Engineering Sciences (Mechanical Engineering), University of California, San Diego

PUBLICATIONS

Amir Valibeygi, **Abdulelah H. Habib**, Raymond A de Callafon, "Robust Microgrid Scheduling with Uncertain Renewable Resources," submitted to ACC 2018.

Yunfeng Jiang, **Abdulelah H. Habib**, Xin Zhao, Louis J Shrinkle, Raymond A de Callafon, "Centralized Recursive Optimal Scheduling of Parallel Buck Regulated Battery Modules," In The 56th IEEE Conference on Decision and Control (CDC), Melbourne, Australia Dec 2017.

Abdulelah H. Habib, Vahid R Disfani, Raymond A. de Callafon and Jan Kleissl, "Optimal switchable load sizing and scheduling for standalone renewable energy systems," In Solar Energy, Volume 144, 2017, Pages 707-720, ISSN 0038-092X.

Abdulelah H. Habib, Vahid R Disfani, Raymond A. de Callafon and Jan Kleissl, "Market-Driven Energy Storage Optimization for Microgrids with Renewable Energy Systems Using Stochastic Programming," IFAC 2017 World Congress, Toulouse, France July 2017.

Abdulelah H. Habib, Vahid R Disfani, Raymond A. de Callafon and Jan Kleissl, "Optimal Energy Storage Sizing and Residential Load Scheduling to Improve Reliability in Islanded Operation of Distribution Grids," In American Control Conference (ACC), 2016, Seattle, USA May 2017.

Abdulelah H. Habib, Elizabeth L Ratnam, Vahid R Disfani, Raymond A. de Callafon and Jan Kleissl, "Optimization-based Residential Load Scheduling to Improve Reliability in the Distribution Grid ," In The 55th IEEE Conference on Decision and Control (CDC), Las Vegas, USA Dec 2016.

Abdulelah H. Habib, Vahid R Disfani, Raymond A. de Callafon and Jan Kleissl, "Quasi-dynamic Load and Battery Sizing and Scheduling for Stand-Alone Solar System Using

Mixed-integer Linear Programming," In The IEEE Conference on Control Applications (CCA), Buenos Aires, Argentina Sep 2016.

Raymond A. de Callafon, **Abdulelah H. Habib** and Jan Kleissl, "Scheduling of Dynamic Electric Loads Using Energy Storage and Short Term Power Forecasting," In The IEEE Conference on Control Applications (CCA), Buenos Aires, Argentina Sep 2016.

Abdulelah H. Habib, Jan Kleissl and Raymond A. de Callafon, "Model Predictive Load Scheduling Using Solar Power Forecastin," In American Control Conference (ACC), 2016, Boston, USA June 2016.

Abdulelah H. Habib, Vahid Disfani, Zack Pecenak, Jan Kleissl, and Raymond A. de Callafon, "Reliability of Dynamic Load Scheduling with Solar Forecast Scenarios," 2016 Annual IEEE Systems Conference (SysCon) (IEEE SysCon 2016), Orlando, USA April 2016.

Abdulelah H. Habib, Vahras Zamani, Jan Kleissl, and Raymond A. de Callafon, "Sizing Of Photovoltaic Reverse Osmosis For Solar Desalination Based On Historical Data In Coastal California," International Desalination Association World Congress 2015, IDA.

Abdulelah Habib, Vahraz Zamani, and Jan Kleissl, "Solar Desalination System Model for Sizing of Photovoltaic Reverse Osmosis (PVRO) ," In ASME 2015 Power Conference, pp. V001T01A009-V001T01A009. American Society of Mechanical Engineers, 2015.

ABSTRACT OF THE DISSERTATION

Modeling and Optimization Techniques for Sizing and Scheduling Applications in Power and Energy

by

Abdulelah Habib

Doctor of Philosophy in Engineering Sciences (Mechanical Engineering)

University of California, San Diego, 2018

Professor Raymond A. de Callafon, Co-Chair
Professor Jan Kleissl, Co-Chair

The work summarized in this thesis focuses on the application of optimization techniques to solve power system design problems concerned with sizing/scheduling of loads and energy storage systems with optimal energy dispatch. Three critical power system problems are discussed in the thesis.

The first portion of this thesis solves the sizing and scheduling problem of stand-alone loads and generators for optimal energy utilization. The main application of this work is water treatment or desalination plants which are powered by stand-alone solar

farms in off-grid setup. The techniques can also be applied to large loads operating in island modes - such as motors or pumps, steel manufacturing, and data centers. Mixed integer linear programming is used for sizing and scheduling the loads, whereas historical solar data is used to optimally schedule the available resources in a selected location. The approach is illustrated for both static and dynamic loads.

The second portion of this thesis focuses on methods to mitigating macrogrid power outages by utilizing available Distributed Energy Resources (DER) to supply load locally, but across several customers. The algorithm schedules load and demand to meet certain objective functions such as minimizing power losses or maximizing solar energy utilization and is implemented in the framework of mixed integer linear programming. Reliability metrics increased significantly through power sharing and the approach is illustrated on power data from actual households when subjected to a power outage.

Finally, optimization methods are applied to size a Battery Energy Storage Systems (BESS) from an economic perspective. As BESS can mitigate effects of intermittent energy production from renewable energy sources they play a critical role in peak shaving and demand charge management. The trade-off between BESS investment costs, lifetime, and revenue from utility bill savings along with microgrid ancillary services are taken into account to determine the optimal size of a BESS. The optimal size of a BESS is solved via a stochastic optimization problem considering wholesale market pricing. A stochastic model is used to schedule arbitrage services for energy storage based on the forecasted energy market pricing while accounting for BESS cost trends, the variability of renewable energy resources, and demand prediction. The approach is illustrated with an application to various realistic case studies based on pricing and demand data from the California Independent System Operator (CAISO). The case study results give insight in optimal BESS sizing from a cost perspective, based on both long-term installation schedules and daily BESS operation.

Chapter 1

Introduction

1.1 Highlights

1. Billions of people are lacking power access. Electrification problem and the need of water is a key element for surviving.
2. The grid outage problem and how we proposed a solution.
3. The rapped wholesale ISO price model changing needs a solution that microgrid might be. Determining when and what size of storage to be installed and how to operate the storage is also a contribution in this thesis.

The need for island system (stand-alone) has been driven by poor electrification of rural areas and supply power to the weak infrastructure countries. More than 1.5 Billion of people are lacking power access or unstable connectivity which is a real challenge for surviving UN (2014). The majority of those people are in rural areas of developing countries, largely in Africa and South-East Asia Doll and Pachauri (2010). In India, for instance, it was identified that electricity through renewable energy-based decentralized generation options can be financially more attractive in comparison to extending the grid Nouni et al. (2008). This a motivation to study how can sizing this renewable energy in rural areas specially in solving the problem of water and food nexus which guided the first

part of this thesis. A application was to investigate the water treatment and desalination powered by island (stand-alone) power application which is solar. This was a motivation to look into the sizing and load scheduling in a planning of some of the power system infrastructure. In this work, we tried to integrate this application with renewables (solar power to be specific) and investigate how such process' efficiency can be improved. This problem would be easier if the site/ location was grid connected. Sizing and scheduling in island power system (stand-alone system) are two different problems. In Chapter 2 and 3, the mathematical formulation is described for both problem separately as well as the scheduling problem by itself.

Another related topic is the effect of poor/ weak electricity infrastructure on customers and society. Power system outages are huge issue both modern and developing countries. Each year eight million customers suffer from power outages in the USA only. The second part of the thesis focuses on how can power sharing improves the effect of grid outages. This contribution is valid for both modern and developing countries, but it also set the floor for state of the art new outage management system as part of the future shared economy. This thesis shed some light on this model and its application with real data from residential network in Chapter 4.

The rapid changing pattern of the grid which introduced the duck curve or more even the negative price phenomena sooner that most model expected/forecasted. The idea of a microgrid is one approach to solve this problem where this thesis is looking into size and scheduling in a given microgrid.

The power system applications studied in this thesis are convex application (or ways to convexify the non-convex ones were applied), such load sizing and load scheduling both on grid-connected and island application. The focus is not to investigate any new optimization techniques rather than applying some of the existing ones.

Chapter 2

Load sizing and scheduling for island system (stand-alone) application

The variability of solar energy in off-grid systems dictates the sizing of energy storage systems along with the sizing and scheduling of loads present in the off-grid system. Unfortunately, energy storage may be costly, while frequent switching of loads in the absence of an energy storage system causes wear and tear and should be avoided. Yet, the amount of solar energy utilized should be maximized and the problem of finding the optimal static load size of a finite number of discrete electric loads on the basis of a load response optimization is considered in this paper. The objective of the optimization is to maximize solar energy utilization without the need for costly energy storage systems in an off-grid system. Conceptual and real data for solar photovoltaic power production is provided the input to the off-grid system. Given the number of units, the following analytical solutions and computational algorithms are proposed to compute the optimal load size of each unit: mixed-integer linear programming and constrained least squares. Based on the available solar power profile, the algorithms select the optimal on/off switch times and maximize solar energy utilization by computing the optimal static load sizes. The effectiveness of the algorithms is compared using one year of solar power data from San Diego, California and Thuwal, Saudi Arabia. It is shown that the annual system solar

energy utilization is optimized to 73% when using two loads and can be boosted up to 98% using a six load configuration.

2.1 Introduction

Increasing global energy demand and human population growth have triggered a need for standalone renewable applications. Recent estimates show that 1.4 billion people do not have access to energy services and one billion are suffering from unreliable electricity services IEA, International Energy Agency (2013). Standalone application of clean energy, (E.g., fresh water pumping), has become more critical for humanity IEA, International Energy Agency (2013); UN (2014). Often such systems are powered by solar photovoltaic (PV) due to ubiquitous high solar resource availability and scalability. However, solar production exhibits high variability over a broad range of time scales Wan (2012). Power variability is the main obstacle facing solar energy in standalone or islanded mode applications. High penetrations of solar power sources create large power swings which influence electric power quality Nguyen et al. (2015), and can cause loss of load or generation curtailment Energy (2010). Variability of solar PV generation is a result of seasonal and diurnal changes in the sunpath as well as short-lived cloud cover. Solar variability limits the operation of off-grid loads at maximum capacity Saber and Venayagamoorthy (2012); Egido and Lorenzo (1992); Sreeraj et al. (2010).

Optimal load switching can be applied to microgrids with any hybrid forms of renewable energy resources such as solar and wind Mohammadi et al. (2012); Kobayakawa and Kandpal (2015); Lee et al. (2014); Atia and Yamada (2015) to capture as much renewable energy as possible. Although partial or modulated load operation is conducive to the problem, there are numerous types of load units which can only be switched on or off, such as non-dimmable lighting, standard electric motors, and Magnetic Resonance Imaging (MRI) machines at hospitals and load aggregation such as demand side manage-

ment Shafie-khah et al. (2016); Negnevitsky and Wong (2015). Dispatching such binary load units, which are referred as switchable loads hereafter, to follow available renewable energy resources have been discussed in the literature for different microgrid applications such as water desalination Smaoui et al. (2015), pumping systems Bakelli et al. (2011), irrigation systems Olcan (2015), and cooking appliancesMandelli et al. (2016); Fux et al. (2013); Bouabdallah et al. (2015).

Different optimization techniques are used for planning and design of such systems. For instance, mixed-integer linear programming (MILP) has been used in many fields, such as unit commitment of power production Viana and Pedroso (2013) and power transmission network expansion Bahiense et al. (2001); Zhang et al. (2012), as well as scheduling problem of the generation units in off-grid in order to maximize supply performance of the system Morais et al. (2010). Nonlinear approaches have also been applied to load scheduling Hung and Robertazzi (2008). For example, neural networks and genetic algorithms have been applied to size stand-alone PV Mellit et al. (2010a); Mellit and Kalogirou (2008); Mellit et al. (2010b). The on/off control optimization problem is similar to the unit commitment problem in power systems and bio-fuelChen et al. (2015); Amir et al. (2008). However, limited studies have been conducted on the optimal load sizing in a standalone (islanded) grid application with switchable loads. Most of other research has been in the demand/supply side while very few looked into the unit/load sizing for many reasons, such as, the load is assumed to be fixed and has to meet by any supply way Ashok (2007) or the accessibility of designing load for certain application is harder and not easy process. This work focuses on optimal load sizing for standalone applications in rural areas or off-grid sites. While the present paper assumes an off-grid system, similar challenges exist for a power system with a weak grid connection, i.e. with a line carrying capacity that could only balance variability that is a small fraction of local solar generation or load capacity.

Energy storage systems (ESS) have been applied to solve the variability challenges Pickard and Abbott (2012a); Kousksou et al. (2014).An alternative or complementary approach is optimal sizing and scheduling of load units which follow power generation variability to maximize solar energy utilization and load uptime. Clearly, the solar energy utilization could be improved with an ESS, but an ESS that eliminates solar variability would need to be large enough to store several days' worth of solar power which is uneconomical at present. Smaller ESS would experience significant cycling and deep discharge events if not properly maintained, increasing maintenance costs and requiring replacement much before the end-of-life of a PV system. Our objective is to improve solar utilization without an ESS and use load demand response only and show that high efficiencies can still be obtained. In practice, a combination of a small ESS with high cycle life such as an ultracapacitor ESS and the proposed load sizing and scheduling system would probably be the best solution. The ESS would absorb solar variability at time scales of seconds to minutes while the loads would balance variability at longer time scales. This approach would allow limiting ESS energy capacity making it more economical. While practical challenges of implementing such a system are significant, e.g. in maintaining system stability during switching, this paper focuses on the critical algorithmic work that permits such a system to operate efficiently and economically.

In a properly planned system the solar system would be optimally sized to power the load required for the intended application. This paper does not consider this scenario. Often in practice the conditions are not as plannable. Load growth will occur and a solar power system may be initially oversized to accommodate such growth. Sizing the solar system may also be limited by land ownership and topographic constraints. The solutions proposed in this paper apply in such a context where solar capacity is fixed and loads are sized to optimize solar energy utilization.

This paper proposes an optimization model to capture the maximum amount of

variable solar generation, which sizes and schedules a finite number of loads to track available solar PV power. The objective is to maximize solar utilization, given the projected power generation of the renewable energy resources. Here, solar utilization is defined as percentage of energy captured by the units over total solar energy produced. This is akin to terms such as solar utilization factor Vermeulen and Nieuwoudt (2015) and loss of power supply (LPS) Gupta (2011) which are commonly used in the literature. The loads are assumed to switch between a binary ”on” or ”off” statuses, where both the switching times and the size of the static power demand (static load size) determines the ability to track available solar power.

The main contribution of this paper is to develop both analytical solutions and computational approaches based on Equality Constrained Least Squares (ECLS), Inequality Constrained Least Squares (ICLS), and Mixed-Integer Linear Programming (MILP) in order to solve the optimization problem. The rest of the paper is organized as follows. The mathematical formulation is given in Section 2.2 along with an analytical example and the motivation for a computational procedure for optimal load size selection. One year of solar resource data for San Diego is analyzed and discussed in Section2.3. Section 2.4 presents different computational procedures for optimal load size selection based on a bi-linear optimization problem involving a mix of binary and real numbers. The simulation results are presented and discussed in Section 2.5. Finally, Section 2.7 concludes the paper.

2.2 Problem Formulation

The sizing and scheduling problem computes the distribution of the optimal load size of a finite number load units, given an available (solar) power profile. For the optimal load size selection, the loads are assumed to operate in a binary manner, off or on, and therefore only the static load size is optimized.

2.2.1 Static Load Response Optimization Problem

To formalize the notation for the optimization approach presented in this paper, we assume knowledge of the (solar) power delivery $S(t)$ sampled at regular time intervals $t = t_k = k\Delta_T$, where $1/\Delta_T$ is a fixed sampling frequency and k is the sample index. In this way, we have a data set of T points on the solar power production $S(t_k),\ k = 1, ..., T$. Typically, $S(t_k)$ is close to a daily periodic function and $S(t_k) \geq 0$ over a daily time interval $t_k \in [t_b, t_e]$, where b is the beginning and e is the ending of the day, with a maximum value

$$S_{max} = \max_k S(t_k),$$

that is typically equal to the AC rating of the solar power system. The data $S(t_k)$ and S_{max} may be available from historical solar power measurements or from solar radiation measurements in conjunction with a model of the solar power conversion efficiency.

In the static load response optimization we consider n loads, where each load $i = 1, ..., n$ is characterized only by a static power value x^i that can be either turned on or off. Given the number n of loads, the objective of the static load response optimization is to find the optimal distribution of static load values $x^i,\ i = 1, 2, \ldots, n$ so that the time sampled solar power delivery $S(t_k)$ can be approximated as closely as possible to maximize the energy captured.

As indicated in Figure 2.1, the power mismatch $E(t_k)$ at any time t_k can be characterized by

$$E(t_k) = S(t_k) - \sum_{i=1}^{n} u_k^i x^i$$

where $u_k^i \in [0, 1]$ are n binary numbers reflecting the on/off switch state of the individual

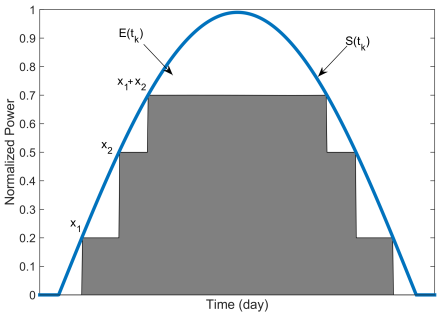

Figure 2.1. Problem illustration for one clear and symmetric day. Loads x^i are scheduled hourly to follow the increase or decrease in solar power generation $S(t_k)$.

loads $i = 1,\ldots,n$ with their (to be determined) static load size x^i. Defining the vectors

$$\begin{aligned} u_k &= \begin{bmatrix} u_k^1 & u_k^2 & \ldots & u_k^n \end{bmatrix}, \quad u_k^i \in [0,1] \\ x &= \begin{bmatrix} x^1 & x^2 & \ldots & x^n \end{bmatrix}^T, \quad x^i > 0 \end{aligned} \tag{2.1}$$

the static power mismatch $E(t_k)$ at a particular time t_k can be written with an inner product

$$E(t_k) = S(t_k) - u_k x,$$

of the time dependent binary switch state vector u_k and the static load size distribution vector x. Static load response optimization can now be written as

$$\arg\min_{u_k,x} \sum_{k=1}^{N} E(t_k)^2, \;\; E(t_k) = S(t_k) - u_k x \tag{2.2}$$

where the variables u_k and x are given in (2.1). The optimization in (2.2) is a least squares optimization in which both the time dependent binary switch state vector u_k and the static load size distribution vector x must be determined on the basis of the T data points on the solar production $S(t_k),\ k = 1,\ldots,T$.

Clearly, the least squares optimization in (2.2) is non-standard for several reasons. First of all, the error $E(t_k)$ is bi-linear due to the product of the optimization variable u_k

and x. Furthermore, the optimization variable u_k is a binary vector, whereas the elements x^i of the static load size distribution. Vector x must likely satisfy (linear) constraints

$$x^i \geq x^{i-1} \geq 0 \tag{2.3}$$

to ensure a unique load distribution solution with real valued positive loads. An additional linear constraint

$$\sum_{i=1}^{n} x^i = |x|_1 = CS_{max} \tag{2.4}$$

where C can be chosen in the range of $0.5 < C < 1$ ensures that the sum of the load distribution is bounded to avoid oversizing of the loads in trying to match the anticipated maximum power production S_{max}. Finally, the number of loads (n) also needs to be determined. It is clear that a larger value n of will enable smaller power mismatch errors $E(t_k)$ but would likely increase the investment cost as the per kWh cost of a load unit typically decreases with the size of the unit.

The process can be described in a flow chart as Figure 2.2 illustrates, starting with annual solar irradiance data for at least one year to capture the seasonal changes. Then followed by a power model to compute solar power and then sort solar power annual data followed by inputting number of desired units then the optimal unit sizing will be computed then followed by a daily unit scheduling.

2.3 Solar Resource Data and its Distribution

To capture the interannual variability of solar irradiance, solar resource data should be collected for several years, such as in the production of a typical meteorological year (TMY). In this paper, only one year of solar power generation is used to demonstrate the model application, but most large solar system developers rely on multidecadal modeled power production based on site adoption of long-term satellite records with short-

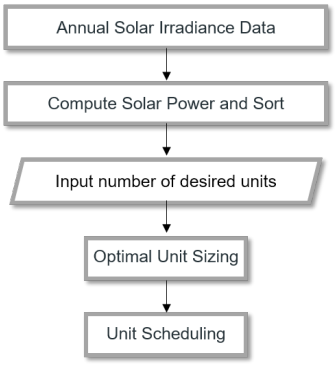

Figure 2.2. Flow chart of the proposed optimization process in this paper.

term local measurements for their financial calculations Thevenard and Pelland (2013). Such long-term data would be preferable in practice although interannual variability of solar energy generation is small. For example, Pitz-Paal et al. (2011) specifies that the interannual variability of GHI for 7-10 years of measurement at Potsdam, Germany and Eugene, USA is about 5%.

Here, only one year of data was available which allows characterizing most of the important seasonal and diurnal variability.

2.3.1 Case Study 1: San Diego, USA

Multidecadal PV power projections are typically based on the measured and modeled GHI which is transposed to the direct, diffuse, and reflected radiation at the plane-of-arrayBouabdallah et al. (2013a); Wissem et al. (2012); Bouabdallah et al. (2013b) and input into a PV performance model. We bypass the complexity in the PV power modeling by using a solar power generation dataset available at two sites. AC power production and GHI data were collected from a (91.6 kW_{DC} and 100 kW_{AC}) fixed tilt (non-tracking) polycrystalline PV system (Figure 2.3). The system was installed at 10 $^{\circ}$ tilt and facing south, at the UC San Diego campus at 32°53′01.4”N 117°14′22.6”W. Data for one year, *i.e.,* May 2011 through April 2012, were used and averaged over 15 minutes.

The raw data is available at 1 s resolution and the algorithm can be applied to data at any temporal resolution. Nevertheless, switching loads over such short timescales is generally impractical and we assume instead that a small energy storage system modulates high frequency solar variability to create a supply that is stable over 15 min intervals. The solar power data for these specific sites are not symmetric over a day, and overcast conditions occur more frequently in the mornings.

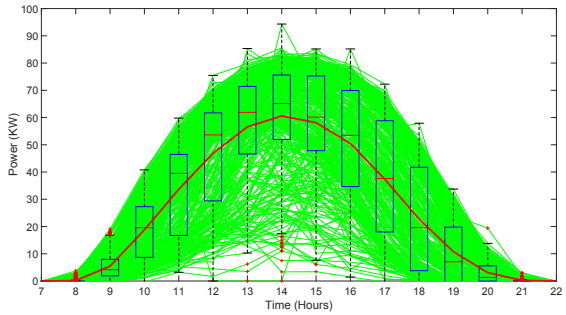

Figure 2.3. 365 days of solar PV output data from the UC San Diego campus (green) superimposed with the annual average (red). Hourly boxplots (black) show the median, 25^{th} and 75^{th} percentiles, and range.

The impacts of solar PV generation variability on the utilization of different combinations of discrete loads is illustrated through 2-dimensional (2D) histograms in Figure 2.4. In each subplot, similar to Figure 2.3, one year of solar power data is superimposed over one day and different numbers of units n are used to track the solar power generation. The quantization idea of the solar power data $S(t_k)$ for different numbers of units is illustrated. $N = 2^n - 1$ is the number of discrete combinations of units for each case described in (2.1), which implies that with more units more discrete load levels can be served resulting in a better match with the solar generation. Qualitatively, the best combination of load sizes is expected to be the one that is able to best track the solar generation levels (or minimize power mismatch as in (2.2)) that are (i) large and (ii) occur frequently.

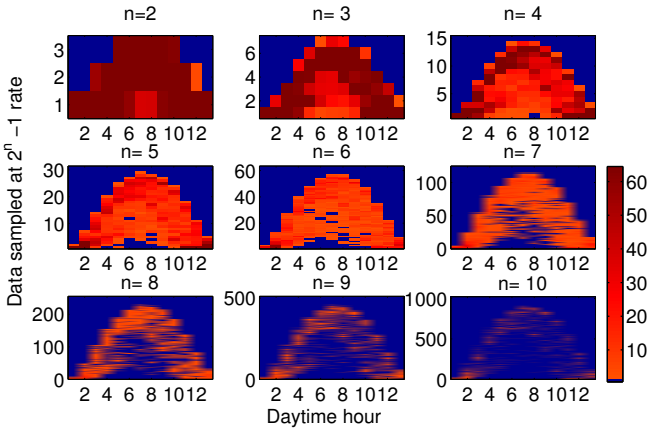

Figure 2.4. 2D histogram of number of occurrences of a combination of discrete loads for $n = 2$ to 10 as a function of time of day for one year of solar power generation data shown in Figure 2.3. Only hours with non-zero power data, i.e., only daytime hours, are shown. For example, for $n = 2$, either two units (at different capacity) can be turned on individually or together resulting in 3 discrete loads. For $n = 10$, almost 1,000 discrete load levels exist, The colors show how often each combination of loads is run to utilize the energy from solar PV generation.

2.3.2 Case Study 2: Thuwal, Saudi Arabia

Another case was selected to prove the robustness of the algorithms to different input data. Thuwal, north of Jeddah, is a city located in the west coast of Saudi Arabia as shown in Figure 2 of Habib et al. (2015). Thuwal solar meteorology is predominantly clear and at a lower latitude and is therefore quite different from San Diego with days such as clear day (D1) in Figure 2.10 being more common. Data from a monocrystalline Silicon solar PV power plant at (22°18′28.5”N 39°06′17.1”E) with tilt 20° and azimuth of 133° and 145° (split in two different arrays) was collected by King Abdullah University of Science and Technology (KAUST).

2.4 Optimization Techniques

This section is initiated by an analytical solution for a small number $n \leq 2$ of loads is presented when the available power follows a symmetric daily profile. The analytical

approach is followed by the motivation for a computational procedure to compute optimal load size distribution for a larger number $n \geq 2$ of loads when the available daily power profile is non-symmetric. After that three different optimization techniques are presented, discussed and compared.

2.4.1 Analytical and Motivating Example

Consider a (symmetric) time dependent power function $y = S(t)$ which must be followed by the rectangular power demands created by a simple on/off switching of a static load over a specified time period. System efficiency is optimized by finding the largest rectangular window (representing energy demand by the switchable load units) to be drawn under the power function $S(t)$. For a single load subjected to a symmetric $S(t)$, this problem reduces to selecting an optimal on/off switch time $\bar{t}$ to define the width of the rectangle $2\bar{t}$ and height $\bar{y} = S(\bar{t})$, as indicated in Figure 2.5.

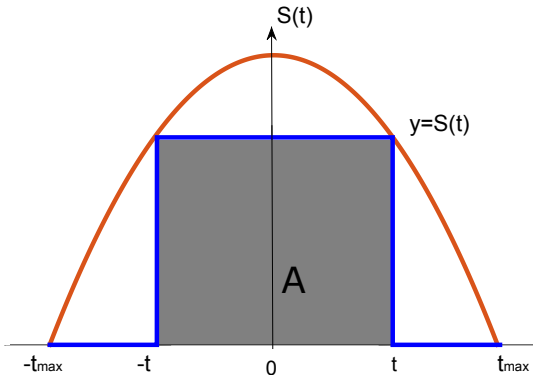

Figure 2.5. Single static unit sizing and scheduling optimization over a symmetric power function $S(t)$, resembling solar power output on a clear day.

The function $A(t)$ that parametrizes the area of the rectangle in Figure 2.5 is equal to $A(t) = 2tS(t)$ and can be written in terms of y as $A(y) = 2S^{-1}(y)y$. The derivative or Jacobian of this function is given as

$$A'(t) = 2S(t) + 2tS'(t), \text{ or } A'(y) = 2S^{-1}(y) + 2y(S^{-1}(y))'$$

By setting $A'(y) = 0$, the optimal value for the load size $\bar{y} = f(\bar{t})$ and the resulting switch time $\bar{t}$ can be found. In this case, it is clear that $A'(y) = 0$ leads to the analytical expression

$$S^{-1}(y) = -\bar{y}(S^{-1}(y))' \tag{2.5}$$

where solving it for y gives the optimal load size $\bar{y}$.

To make this approach applicable to a symmetric solar PV power curve, a clear sky power solar function $S(y)$ can be modeled as a trigonometric function or a parabola. Global horizontal irradiance (GHI) models have been extensively studied in the literature in Reno et al. (2012); Bouabdallah et al. (2013a); Wissem et al. (2012); Bouabdallah et al. (2013b) take for example equation 20 Reno et al. (2012) as bellow

$$GHI = 951.39cos(t)^{1.15}$$

In this paper, a simplified fitting curve is presented using trigonometric and parabola functions as below (see Appendix for accuracy discussion),

$$S(t) = y = a\ cos(bt) + a_1 sin(bt) = a\ sin(bt + c) \tag{2.6}$$

where $a = 0.9903,\ a_1 = -0.001192,\ b = 0.006952$, and $c = 1.572$ based on data obtained from a clear solar day, where axes interception are $(0, \pm y_{max}) = (0, 0.9903)$ and $(\pm t_{max}, 0) = (\pm 226, 0)$. The inverse function S^{-1} is thus as follows,

$$t = S^{-1}(y) = \alpha\ \arcsin(\beta y) + \gamma \tag{2.7}$$

where $\alpha = 143.8,\ \beta = 1.01,$ and $\gamma = -226.1$. More details on the computation of the numerical values of a, b can be found in Appendix A. The first derivative of (2.7) can be

expressed as

$$t' = (S^{-1}(y))' = \frac{\alpha\beta}{\sqrt{1+\beta^2 y^2}} \tag{2.8}$$

Solving the analytic expression (2.5) numerically for an optimal integer value $\bar{t}$, with $S^{-1}(y)$ given in (2.7) and $(S^{-1}(t))'$ given in (2.8) with a trigonometric function to compute the optimal values of $\bar{y}$ analytically, with the following numerical value of $A'(y) = 0$

$$S^{-1}(y) + y(S^{-1}(y))' = 0 \rightarrow \frac{y}{\alpha\beta\sqrt{1-y^2/\alpha^2}} - \frac{\gamma - arcsin(y/\alpha)}{\beta} = 0$$

then leads to

$$\begin{aligned} S(\bar{t}) = \bar{y} &= 0.6489 \\ \bar{t} &= \pm 123 \end{aligned} \tag{2.9}$$

for the optimal switch time $\bar{t}$ and normalized load size $\bar{y}$.

The resulting optimal switch time and load size lead to a maximum (rectangular) area of $2\bar{t}\bar{y} = 2 \cdot 0.6489 \cdot 123 = 159.6294$. With the known (symmetric) solar power curve $S(t)$, we can also compute $\sum_{-x_{max}}^{x_{max}} S(t)$ over the integer values $t \in [-226, 226]$ to be 284.8962 and obtain

$$\text{Solar utilization (SU)} = \frac{\text{Total Energy Captured by Units}}{\text{Total Solar Energy}} = \frac{2\bar{t}\bar{y}}{\sum_{-t_{max}}^{t_{max}} S(t)dt} = 56.03\%.$$

This means that for a single load, the optimal rectangular area achieved under the given symmetric power curve $S(t)$ captures 56% of the total (solar) energy. Similar results can be obtained by a straightforward line search algorithm for the scalar value of t as provided in Appendix B.

The approach of finding optimal on/off switching time and load size for a symmetric power curve can also be extended to the case of multiple loads. However, the solution is only analytically tractable for $n = 2$ loads where the Jacobian becomes a two dimensional vector or a three dimensional vector with an additional equality constraint as indicated below.

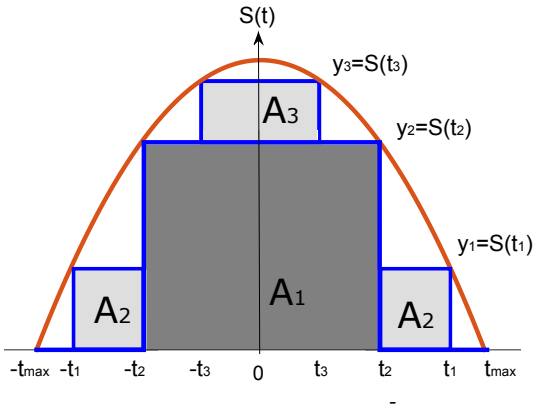

Figure 2.6. Analytical optimization results for a functional clear sky model and two units. A_1, A_2, and A_3 are the energy captured by loads 1, 2, and both loads together.

Figure 2.6 illustrates the optimal load size distribution and switching to maximize solar utilization for $n = 2$ loads. Under this scenario there exists 3 optimal switch times t_1, t_2 and t_3 for two (optimal) load sizes y_1, y_2, where $y_3 = y_1 + y_2$ is used to indicate when both loads are on. The dark gray shaded area is due to switch time t_2, where the area is $A_1 = 2t_2y_2$. The area of the light gray shaded areas are functions of t_1, t_2 and t_3, where the area of the light gray rectangular areas is the sum of $A_2 = 2(t_1 - t_2)y_1$ and $A_3 = 2t_3(y_3 - y_2)$. The objective is to maximize the sum of the shaded areas

$$A(y_1, y_2, y_3) = \sum_{i=1}^{2^n-1=3} A_i = 2S^{-1}(y_2)\, y_2 + 2(S^{-1}(y_1) - S^{-1}(y_2))\, y_1 + 2S^{-1}(y_3)(y_3 - y_2)$$

to solve for the optimal switch times and load sizes as shown in Figure 2.6. The area $A(y_1, y_2, y_3)$ can be reduced to a function of only two variables $\bar{A}(y_1, y_2)$ by substituting

$y_3 = y_1 + y_2$ to obtain

$$\bar{A}(y_1, y_2) = 2y_1(S^{-1}(y_1) - S^{-1}(y_2) + S^{-1}(y_1 + y_2)) + 2y_2 S^{-1}(y_2). \tag{2.10}$$

The maximum solar utilization can now be expressed as an optimization problem:

$$\begin{aligned} &\max_{y_1, y_2, y_3} A(y_1, y_2, y_3) \\ &\text{subject to} \quad 0 \leq y_1 \leq y_2 \leq y_3 < y_{max} \\ &\qquad\qquad y_3 = y_1 + y_2, \end{aligned} \tag{2.11a}$$

which alternatively can be written as

$$\begin{aligned} &\max_{y_1, y_2} \bar{A}(y_1, y_2) \\ &\text{subject to} \quad 0 \leq y_1 \leq y_2 < y_{max} \end{aligned} \tag{2.11b}$$

where $S(y)$ is given in (2.7), and y_{max} is the y intersection of $S(y)$. We consider only the positive values $y > 0$ of the symmetric trigonometric approximation $S^{-1}(y)$ as indicated in Figure 2.6.

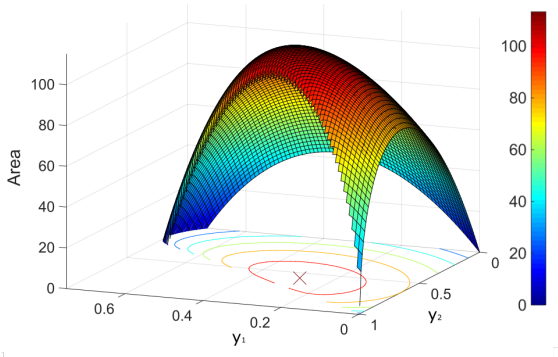

Figure 2.7. Area surface plot of equation (2.10) as function of y_1 and y_2. The z-axis and the colorbar show the area.

Since the optimization problem has affine equality constraints, its solution set is convex. Moreover, the objective function is a concave function. Thus, it has a single maximum or minimum $1/A(y_1, y_2, y_3)$ as indicated in Figure 2.7. As a result, solving the optimization in (2.11b) by an iterative gradient method will lead to the global maximum solution. The following Jacobian matrix, which is derived in Appendix C,

$$\nabla J = \begin{bmatrix} \frac{\partial A}{\partial y_1} \\ \\ \frac{\partial A}{\partial y_2} \end{bmatrix} = \begin{bmatrix} S^{-1}(y_1) - S^{-1}(y_2) + S^{-1}(y_1 + y_2) + y_1 (S^{-1}(y_1))' \\ \\ (S^{-1}(y_2))'(y_1 + y_2) + S^{-1}(y_2) \end{bmatrix}$$

can be used in an iterative gradient based method, leading to the optimal load size solutions $[\bar{y}_1, \bar{y}_2, \bar{y}_3] = [\bar{y}_1, \bar{y}_2, \bar{y}_1 + \bar{y}_2] = [0.2727,\ 0.5758,\ 0.8485]$. The resulting solar utilization for 2 loads is then characterized by

$$\text{SU} = \frac{A(\bar{y}_1, \bar{y}_2, \bar{y}_3)}{\sum_{-t_{max}}^{t_{max}} S(t) dt} = 79.49\%$$

indicating a significant improvement over the single load solar utilization of 56.0307% over the same symmetric solar power curve.

The analytic approach indicates that maximizing solar utilization is equivalent to finding the largest sum of rectangle windows that can be drawn under the power function $S(t)$. Extending this concept to n number of loads where $n > 2$ would entail

$$A(y_1, \cdots, y_{2^{n-1}}) = \sum_{i=1}^{2^n} 2 \left[S^{-1}(y_i) - S^{-1}(y_{i+1}) \right] y_i, \tag{2.12a}$$

where $y_{2^n} = 0$ and

$$y_i = bin(i)^T \times \begin{bmatrix} y_1 \\ y_2 \\ \vdots \\ y_n \end{bmatrix} \quad , i = \{1, 2, \cdots, 2^n - 1\}, \tag{2.12b}$$

where $bin(i)$ is a reversed vertical vector format representing the binary value of i. The number of variables of the new area function $\bar{A}(y_1, \cdots, y_n)$ in (2.12a) reduces to n variables instead of $2^n - 1$ by substituting (2.12b).

In summary the optimization problem appears to be convex over our solution set. However, relying on $S^{-1}(y)$ for $y > 0$ is not possible, as $S^{-1}(y)$ is not guaranteed to exist. Furthermore, a power curve $S(t)$ may not be symmetric, especially for PV systems operating on non-clear day conditions. To overcome these obstacles, this paper proposes optimization approaches that exploit the convexity of the optimization problem that selects the optimal load size distribution. Although the analytic approach is only viable for a small number of loads under symmetric power curves, we will use the optimally computed solar utilization as a benchmark for the solar utilization obtained from the optimization approaches presented in the following.

2.4.2 Equality Constrained Least Squares Optimization

Although the optimization in 2.2 to minimize the Least Squares of the static power mismatch $E(t_k)$ is bi-linear, it is clear that the entries of the time dependent binary switch state vector u_k is given by a limited number of binary combinations. The number of binary combinations depends on the choice of n and the number of data points T. Once the time dependent binary switch state vector u_k is fixed, the optimization in (2.2) reduces to a standard Least Squares (LS) problem to find the optimal value of the static

load size distribution vector x.

To ensure a unique solution for the static load size distribution vector x, the constraint (2.3) can be included in the LS optimization implicitly by simply ordering the T data points of the (solar) power data $S(t_k)$. The ordering uses the fact that both $S(t_k) \geq 0$, $x^i > 0$ and the fact that a larger value of $S(t_k)$ would require the switching of a larger sum of loads $u_k x$. To set up the solution to the optimization to (2.2), the solar data $S(t_k)$ that may be periodic due to daily patterns and irregular due to weather patterns, is sorted such that

$$S(t_{\bar{k}+1}) \geq S(t_{\bar{k}}),\ \bar{k} = 1, ..., T-1 \tag{2.13}$$

The ordering in (2.13) ensures that $S(t_{\bar{k}})$ is monotonically non-decreasing function represented as the unshaded curve in Figure 2.8 In addition, it allows the ordering of the n numerical values $x^i > 0$ in the vector x to become unambiguous by properly ordering the n binary values $u^i_{\bar{k}}$ in the binary vector $u_{\bar{k}}$ for each value of $\bar{k} = 1, ..., T-1$.

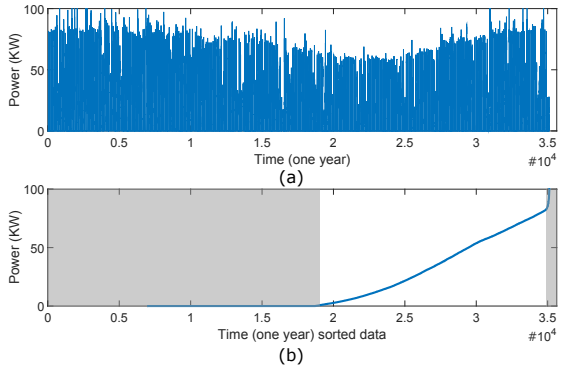

Figure 2.8. (a) Time series plot for 12 months of solar power data starting from May 2011 through April 2012. (b) Sorted solar power data $S(\bar{t}_k)$ sampled at a 15 minute interval satisfying equation (2.13).

The ambiguity in the ordering of the n numerical values $x^i > 0$ in x given in (2.3) is implicitly included due to the fact

$$S(t_{\bar{k}+1}) \geq S(t_{\bar{k}}) \ \Rightarrow\ u_{\bar{k}+1} x \geq u_{\bar{k}} x,\ \ \bar{k} = 1, ..., T-1 \tag{2.14}$$

and the fact that $x^i > 0$. In this way, the values of x_i can be ordered if we order the values of $u_{\bar{k}}^i \in [0,1]$ contained in the time ordered binary switch state vector $u_{\bar{k}}$ by the choice of a positive real linear function

$$f(u_{\bar{k}}) = \sum_{i=1}^{n} f^i u_{\bar{k}}^i,\ f^i > 0 \tag{2.15}$$

that satisfies the property

$$f(u_{\bar{k}+1}) \geq f(u_{\bar{k}}),\ \bar{k} = 1, ..., T-1 \tag{2.16}$$

The rationale behind the choice of the function $f(\cdot)$ in (2.15) is as follows. For a given value of n, there are $2^n - 1$ possible binary combinations of the vector $x_{\bar{k}}$, excluding the value 0. Ordering the values of the time ordered binary switch state vector $u_{\bar{k}}$ according to (2.16), allows us to choose a fixed x (independent of $\bar{k}$) with $x^i > 0$ to satisfy (2.14).

An obvious choice for the desired function $f(\cdot)$ in (2.15) is to use the fact that $u_{\bar{k}}^i \in [0,1]$ and that the vectors $u_{\bar{k}}$ with length n can be seen as a n bit binary number representing a signed integer number $d_{\bar{k}} > 0$. The conversion from an n bit binary number $u_{\bar{k}}$ to a signed integer number $d_{\bar{k}}$ is given by

$$f(u_{\bar{k}}) = d_{\bar{k}} = \sum_{i=1}^{n} u_{\bar{k}}^i \cdot 2^{n-i}, \tag{2.17}$$

which clearly satisfies the conditions of the function $f(\cdot)$ given in (2.15) and (2.16). With the choice of $f(u_{\bar{k}}) = d_{\bar{k}}$ and ordering the integer numbers $d_{\bar{k}}$ according to (2.15), the static load optimization problem in (2.2) can be rewritten as

$$\begin{gathered} \hat{x} = \arg\min_{x} \sum_{\bar{k}=1}^{T} E(t_{\bar{k}})^2,\ \ E(t_{\bar{k}}) = S(t_{\bar{k}}) - u_{\bar{k}} x \\ f(u_{\bar{k}+1}) \geq f(u_{\bar{k}}),\ \bar{k} = 1, ..., T-1 \end{gathered} \tag{2.18}$$

with $f(u_{\bar{k}})$ given in (2.17). It should be noted that for a given value of n, the binary numbers and the ordering of $u_{\bar{k}}$ in (2.18) are completely known. As a result, only an optimization over x is required reducing the optimization in (2.2) to an equivalent standard least squares (LS) optimization given in (2.18). With the known time ordered binary switch state vector $u_{\bar{k}}$, the time ordered error $E(t_{\bar{k}})$ for $\bar{k} = 1, ..., T$ in (2.2) can be written in a matrix notation $E = S - Ux$ where the matrices are given by

$$\begin{aligned} S &= \begin{bmatrix} S(t_1) & S(t_2) & \cdots & S(t_T) \end{bmatrix}^T \in R^{T\times 1}, \\ E &= \begin{bmatrix} E(t_1) & E(t_2) & \cdots & E(t_T) \end{bmatrix}^T \in R^{T\times 1}, \\ U &= \begin{bmatrix} u_1^1 & u_1^2 & \cdots & u_1^n \\ u_2^1 & u_2^2 & \cdots & u_2^n \\ \vdots & & \ddots & \vdots \\ u_{2^n-1}^1 & u_{2^n-1}^2 & \cdots & u_{2^n-1}^n \end{bmatrix} \otimes \mathbf{1}_{1\times L} \in R^{T\times n} \\ x &= \begin{bmatrix} x^1 & x^2 & \cdots & x^n \end{bmatrix}^T \in R^{n\times 1} \end{aligned} \tag{2.19}$$

and where the block rows of the matrix U will be repeated entries given of the time ordered binary load switch vector $\begin{bmatrix} u_{\bar{k}}^1 & u_{\bar{k}}^2 & \cdots & u_{\bar{k}}^n \end{bmatrix}$ due to Kronecker product with the $1 \times L$ unity vector $\mathbf{1}_{1\times L}$ where $L = T/(2^n - 1)$. The repeated entries are needed to ensure that $U \in R^{T\times n}$, as there are only $2^n - 1$ binary load switch combinations (excluding all loads off), while the available number of (solar) power data points $T >> 2^n - 1$. The typical value of L for the repeating entries in the block rows of U is $L = 20$, using $20 \cdot (2^n - 1)$ points of ordered (solar) power data for computation of the optimal load size distribution. The standard LS minimization of (2.18) can be rewritten as

$$\hat{x} = \arg\min_x \|S - Ux\|_2$$

where the solution can be computed by $\hat{x} = [U^T U]^{-1}[U^T S]$.

The standard LS solution in (2.18) will solve the Least Squares error of the static power mismatch, but does not ensure yet that the sum of the load distribution is bounded as in (2.4) to avoid oversizing of the loads in trying to match the anticipated maximum power production S_{max} Miller and de Callafon (2012). The additional linear equality constraint on the sum of the load distribution can easily be incorporated via an Equality Constrained Least Square (ECLS) problem

$$\hat{x}, \hat{\lambda} = \arg\min_{x,\lambda} \sum_{\bar{k}=1}^{T} E(t_{\bar{k}})^2 + \lambda (Dx - C)), \quad E(t_{\bar{k}}) = S(t_{\bar{k}}) - u_{\bar{k}} x \tag{2.20}$$

that also includes a Lagrange multiplier λ and the unit equality constraint vector $D = [1\ 1\ \cdots\ 1] = \mathbf{1}_{1\times n}$ and a chosen value of C in the range $0.5 \leq C \leq 1$ to satisfy (2.4). The ECLS solution is now given by

$$\begin{bmatrix} \hat{x} \\ \hat{\lambda} \end{bmatrix} = \begin{bmatrix} U^T U & \mathbf{1} \\ \mathbf{1} & 0 \end{bmatrix}^{-1} \begin{bmatrix} U^T S \\ C \end{bmatrix}.$$

with U and S as given in (2.19). Since the optimal value C in the range $0.5 \leq C \leq 1$ to avoid oversizing of the loads by bounding the sum of the load distribution as in (2.4) is unknown, an additional line search along C can be used to determine the optimal load oversizing constraint.

2.4.3 Inequality Constrained Least Squares Optimization

Although the ECLS approach presented above computes the optimal load size distribution $x = [x^1\ x^2\ \cdots\ x^n]^T$, the optimal solution $\hat{x}$ to (2.20) still depends on the choice of the time ordered binary load switch vector $u_{\bar{k}}$ due to the bi-linear nature of the optimization problem in (2.2). Even when the (solar) power data $S(t_k)$ has been ordered,

it is still not clear when exactly the loads will be turned on/off. Referring to Figure 2.9 to illustrate this concept, it is not clear what the optimal load switch time m_1 for the first load 1 will be and how many samples m_2 the first load should remain on before the second load is switched on at $m_1 + m_2$ samples. Clearly, the optimal static values $\hat{x}^1$ and $\hat{x}^2$ of the loads depend on these switching times.

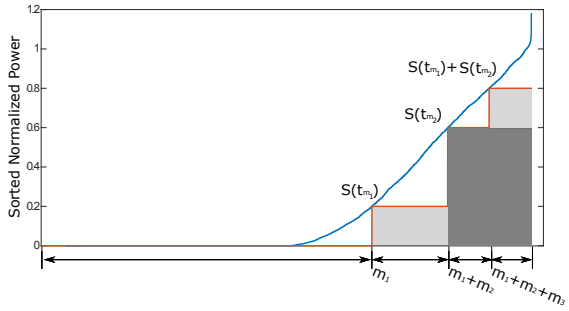

Figure 2.9. Illustration of variable switching time in optimal load switching and load size optimization.

To explicitly incorporate the ordering constraint (2.3) and allow for variability in the switch time, both the optimization variable x and the matrix U in (2.19) can be modified., while still allowing for a convex optimization. First we define

$$x = T\bar{x}, \quad T = \begin{bmatrix} 1 & 1 & \cdots & 1 \\ 0 & 1 & \cdots & 1 \\ \vdots & & \ddots & \vdots \\ 0 & 0 & \cdots & 1 \end{bmatrix} \in R^{n \times n}$$

where the upper diagonal matrix T ensures that $\bar{x}$ now reflect the incremental change in the load size distribution. In this way the ordering constraint (2.3) can be enforced

explicitly by $\bar{x} > 0$. Secondly, we define

$$U(m) = \begin{bmatrix} U_1^1 & U_1^2 & \cdots & U_1^n \\ U_2^1 & U_2^2 & \cdots & U_2^n \\ \vdots & & \ddots & \vdots \\ U_{2^n-1}^1 & U_{2^n-1}^2 & \cdots & U_{2^n-1}^n \end{bmatrix} \in R^{T \times n}$$

where now the block rows of U are defined by

$$\begin{bmatrix} U_k^1 & U_k^2 & \cdots & U_k^n \end{bmatrix} = \begin{cases} \begin{bmatrix} u_k^1 & u_k^2 & \cdots & u_k^n \end{bmatrix} \otimes \mathbf{1}_{1 \times m_k}, & k = 1, 2, \ldots, 2^n - 2 \\ \begin{bmatrix} u_k^1 & u_k^2 & \cdots & u_k^n \end{bmatrix} \otimes \mathbf{1}_{1 \times T - \sum m}, & k = 2^n - 1 \end{cases}$$

in which the integer vector

$$m = \begin{bmatrix} m_1 & m_2 & \cdots & m_{2^n-1} \end{bmatrix} \text{ with } m > 0, \ \sum m < T$$

is the set of $2^n - 1$ possibilities of incremental switching time values in the case of n loads.

The incremental switching time values m allow variable timing when loads are switched, similar as in Figure 2.9 for the case of $n = 2$ loads. Moreover, given the vector of incremental switching time values m, the optimal incremental load size distribution can be computed with a Inequality Constrained Least Squares (ICLS) problem

$$\hat{x} = \arg\min_{\bar{x}} \|S - U(m)T\bar{x}\|_2, \text{ subject to } A\bar{x} \leq b \tag{2.21}$$

where the matrix A and b can be used to enforce inequality constraints. In particular, the

choice

$$A = \begin{bmatrix} -I_{n\times n} \\ U(m)T \end{bmatrix}, \; b = \begin{bmatrix} \mathbf{0}_{n\times 1} \\ S \end{bmatrix}$$

enforces the ordering constraint (2.13) via $\bar{x} \geq 0$ and ensures load power demand is always under the (solar) power curve via $U(m)T\bar{x} = U(m)x \leq S$ to avoid oversizing of the loads directly.

The solution to the ICLS problem can be solved with standard convex optimization tools and will lead directly to optimal results for the static load distribution, given the integer vector

$$m = \begin{bmatrix} m_1 & m_2 & \cdots & m_{2^n-1} \end{bmatrix} \text{ with } m > 0, \; \sum m < T$$

of $2^n - 1$ possibilities of incremental switching time values. An additional line search or non-linear optimization can be used on top of the ICLS problem to compute an optimal set of incremental switching time values to further improve the solar utilization of the static load distribution. Theoretically, such an additional search along the switching time values via an additional iterative or gradient based optimization should lead to the globally optimal solution to the bi-linear optimization problem of (2.2), as one can use the full number of T data points on the (solar) power data, while using the smallest number of optimization variables. A drawback is that the iterative search for switching time values may get stuck in a local minimum. This was performed based on gradient search over m using the Nonlinear programming solver (fmincon) in the MATLAB optimization toolbox

2.4.4 Mixed-integer Linear Programming (MILP) Method

Since the optimization problem (2.2) is a bi-linear optimization problem involving a mix of binary and real numbers, a limited range of optimization solvers can be applied and none of which may guarantee global optimality. To guarantee the optimality, we employ the Big-M relaxation method Griva et al. (2009) to convert the optimization problem into a mixed-integer linear programming (MIPL) problem. The convexity of MILP therefore fulfills the zero duality gap. In addition, MILP has the capability of determining the exact switching schedule of load units, which the other approaches discussed in this paper lack. In fact, solving the optimization problem through MILP is equivalent to simultaneous solution to planning and scheduling problems.

There exist many mature MILP solvers which are capable of solving large-scale MILP problems with millions of variables within a reasonable time frame Bonami et al. (2012). Proper selection of optimization variables and use of the disjunctive methods discussed in Bahiense et al. (2001) make it possible to reformulate the original problem as an MILP problem.

Denoting the binary variable $u_i(t_k)$ as the on/off status of the unit i at time step t_k, the optimization problem (2.2) is presented as below,

$$\begin{aligned} &\min_{u_i,x_i} \sum_{t_k=1}^{T} [S(t_k) - \sum_{i=1}^{n} y_i(t_k)] \\ &\text{subject to} \quad u_i(t_k) \in \{0,1\}, \forall t_k \\ &\qquad\qquad S(t_k) \geq \sum_i y_i(t_k), \forall t_k \\ &\qquad\qquad y_i(t_k) = u_i(t_k) x_i, \end{aligned} \tag{2.22}$$

where i and t_k are the index for units and time steps respectively. $S(t_k)$ denotes the solar power timeseries of length T. $x \in R^n$ is the vector of load sizes. $y_i(t_k)$ also denotes the

committed demand by load i at time t_k.

The last constraint in (2.22) is a bi-linear equality constraint and makes (2.22) nonconvex. To resolve the nonconvexity issue, the big-M technique is used to replace the constraint with the two following sets of constraints,

$$\begin{cases} y_i(t_k) \leq u_i(t_k)M, \\ y_i(t_k) \geq 0, \end{cases} \tag{2.23a}$$

$$\begin{cases} y_i(t_k) \leq x_i, \\ y_i(t_k) \geq x_i + (u_i(t_k) - 1)M, \end{cases} \tag{2.23b}$$

where M is a big-enough positive number, e.g. 10^6 as utilized in the numerical examples here. The constraint sets (2.23a) and (2.23b) are binding and relaxed respectively when $u_i(t_k) = 1$, guaranteeing $y_i(t_k) = x_i$. Likewise, $y_i(t_k)$ exactly equal to zero $u_i(t_k) = 0$.

One great advantage of this method is that the input data can be one certain day (clear or cloudy), that is the data does not need to be sorted as compared to the other approaches. In addition, as no change is required in the order of PV power profile while solving the optimization problem via MILP, additional constraints and technologies such as minimum uptime and downtime of load units and employing energy storage systems could be considered in the optimization process. Since this paper is focused on optimal load sizing, these options will be discussed in detail in the future research works.

MILP was implemented using the CVX toolbox and Gurobi 6.50 to solve the integer problem in our optimization. To reduce computational expense, down-sampling the original data was needed. As the sequence of PV data does not affect the optimization results, down-sampling with the ratio of $1 : n$ can be performed by arbitrarily selecting one data point from every n data points from either the original or sorted data set further

discussed in Section 2.5.3.

2.5 Results

In this paper, two levels of optimization are performed. The first level is toward unit sizing for a given number of units. After the size of the units is determined, they are scheduled through an optimization process to capture the maximum solar power. For example Figure 2.10, which will be discussed more in section 2.6, illustrates the scheduling results on three sample days for different number of units.

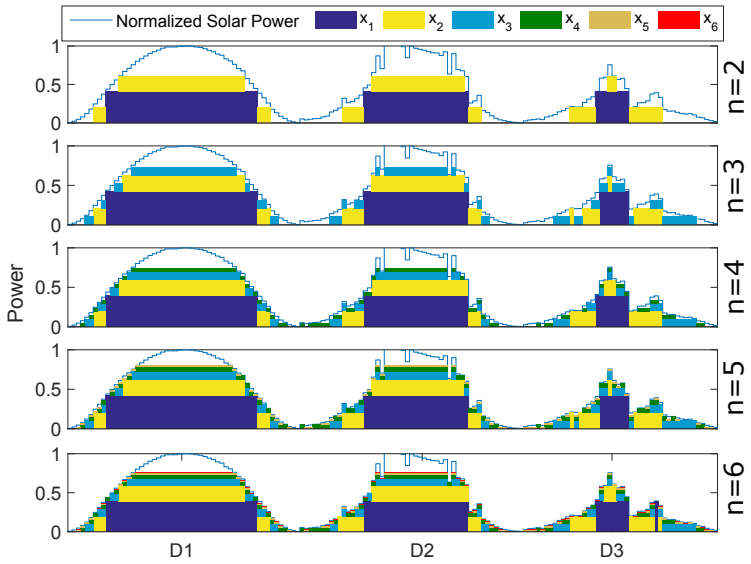

Figure 2.10. Scheduling results for four different days (D1 clear, D2 mostly clear with scattered clouds, and D3: overcast. The unit sizes of the Inequality Constrained Least Squares (ICLS) method are presented.

San Diego solar power data, described earlier in Section 2.3 is investigated in the following subsection using the different optimization techniques. This is followed by an additional case study and concluded with a discussion.

2.5.1 Equality Constrained Least Squares Optimization (ECLS) Results

The optimal unit sizes x are obtained from equation (2.20). Subsequently, the operation is simulated for one year of solar power data. These results do not constrain the units with any minimum up or down time meaning the units are instantly turned on or off. After that the solar utilization (SU) was calculated by dividing energy consumed by the loads over the solar power data for one year.

Table 2.1. ECLS results for unit sizes and solar utilization for n between 2 and 6.

n	x_1	x_2	x_3	x_4	x_5	x_6	$\sum(x)$	SU
2	0.4670	0.1450					0.6120	0.7071
3	0.5068	0.2025	0.0857				0.7950	0.8277
4	0.5111	0.2269	0.1175	0.0585			0.9140	0.9117
5	0.4769	0.2138	0.1117	0.0565	0.0290		0.8880	0.9571
6	0.4476	0.2015	0.1060	0.0544	0.0287	0.0158	0.8540	0.9790

A Sensitivity analysis for ECLS method was performed for $n = 3$ showing the 75th percentile of the maximum solar utilization in 42 points and showing the range of the unit sizes. The maximum solar utilization for $n = 3$ as shown in Table 2.1 is 0.8277 but for other x combinations the solar utilization can be as low as 0.7542 (Figure 2.11). Unit size appears to be closely related to solar utilization. For example the size of x_1 varies between 0.5752 and minimum is 0.4385 with quartiles of 0.5418, 0.5068, 0.5418. This results in a 9% change in solar utilization with this unit size range. The smallest unit sizes are associated with the smallest solar utilization. Then there appears a bifurcation where the largest and mid-size units achieve medium solar utilization. The largest solar utilization are associated with medium-to-large unit sizes.

2.5.2 Inequality Constrained Least Squares (ICLS) Results

The Inequality Constrained Least Squares (ICLS) optimization results are shown in Table 2.2 and will be discussed in section 2.6.

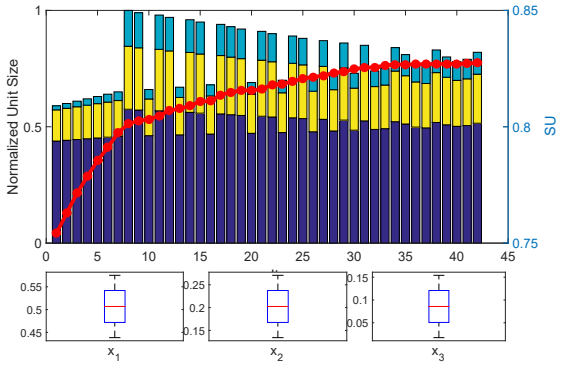

Figure 2.11. Sensitivity analysis for the CLS method. Blue line is solar utilization while stacked bars represent total load size split into the contributions of unit 1 (blue), 2 (yellow), and 3 (turquoise). A Box-Whisker plot for the unit size distribution for each unit is shown on the bottom.

Table 2.2. Same as Table 2.1, but for ICLS method.

n	x_1	x_2	x_3	x_4	x_5	x_6	$\sum(x)$	SU
2	0.4078	0.1994					0.6053	0.7274
3	0.4210	0.2076	0.1028				0.7314	0.8601
4	0.3957	0.1954	0.0989	0.0467			0.7367	0.9273
5	0.4180	0.2063	0.1034	0.0508	0.0228		0.8013	0.9614
6	0.3913	0.1935	0.0973	0.0473	0.0233	0.0115	0.7642	0.9796

2.5.3 MILP Optimization Results

To mitigate the adverse effect of down-sampling on the simulation results in this paper, down-sampled data points are selected uniformly from sorted data set, which represents the original data set more accurately. Figure 2.12 examines the impact of downsampling on computational speed and solar utilization for the case of 3 units $(n = 3)$. The final solar utilization is the nearly the same for different down-sampling rates (with in 1% variation) while the computational cost varies remarkably. Table 2.3 shows the best solar utilization obtained in Figure 2.12.

For comparison Thuwal, Saudi Arabia case was performed using the ICLS approach and the results are shown in Figure 2.13. The resulting unit sizes are expected to be larger than San Diego due to the lack of cloudy days driving the need for smaller,

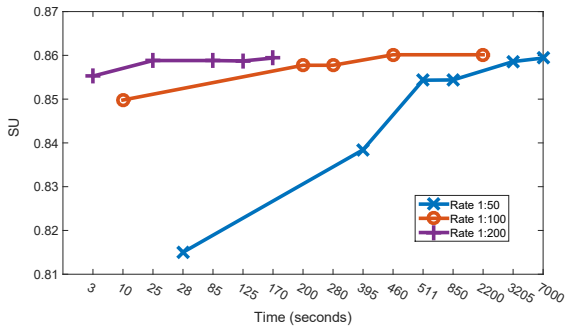

Figure 2.12. Convergence rate for system efficiency for difference down-sampling rates. The x-axis is nonuniform and shows computational cost on a MATLAB based modeling system named CVX using gurobi solver.

Table 2.3. Same as Table 2.1, but for Mixed-Integer Linear Programming.

n	x_1	x_2	x_3	x_4	x_5	x_6	$\sum(x)$	SU
2	0.3933	0.1899					0.5832	0.7274
3	0.4126	0.1899	0.1008				0.7033	0.8586
4	0.4074	0.2100	0.0914	0.0438			0.7526	0.9243
5	0.3811	0.2150	0.1082	0.0515	0.0240		0.7798	0.9597
6	0.4505	0.2049	0.0837	0.0598	0.0327	0.0162	0.8478	0.9765

more adaptive units.

2.6 Discussion

Looking at the solar utilization comparison between the three optimization approaches shows close results for each n number of units as shown in Figure 2.14. Figure 2.14 shows summary of optimal unit size achieved by each method as well as solar utilization. ECLS was chosen as the reference case and assigned a solar utilization of 1 as shown in Figure 2.15. Theoretically the ICLS optimization approach should lead to the largest solar utilization, as it uses the full data set and the smallest number of optimization variables. ICLS indeed yielded the best results, but improvements compared to ECLS only ranged from 3.9% to 0.1% decreases as n increases. However, MILP results were slightly less than ICLS. From Figure 2.14, it is also clear that as n increases the different among the approaches decreases.

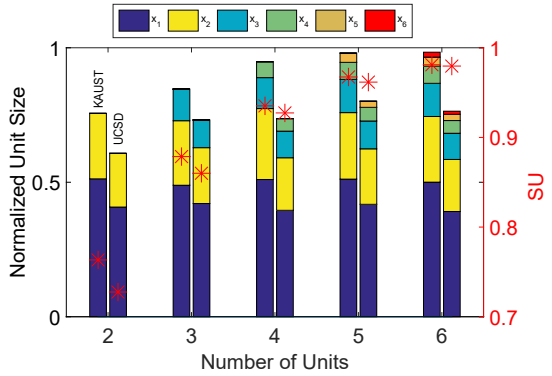

Figure 2.13. Comparison of results for the ICLS optimization between San Diego and Thuwal.

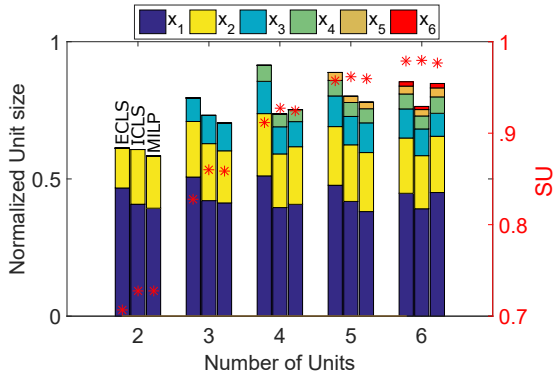

Figure 2.14. Unit sizes for difference optimization approaches and different number of units n. ICLS is Inequality Constrained Least Squared, ECLS is Equality Constrained Least Squared, and MILP is Mixed-integer Linear Programming.

Figure 2.13 summarizes the differences between the unit sizes for both case studies (San Diego, USA and Thuwal, Saudi Arabia) as well as the optimal solar utilization obtained. Keep in mind that these results are normalized for both solar power and unit size. The main difference between the two sites is larger units are preferred in the Thuwal case with an average size increase of 25%. For $n = 2$ the solar utilization for Thuwal was larger compared to San Diego, mainly due to a higher clear day count over the year. As n increases both site solar utilization tend to get closer until they nearly match for $N = 6$.

Each method proposed in this paper carries advantages and drawbacks when solving the unit sizing problem, as summarized in Table 2.4. From a global optimality

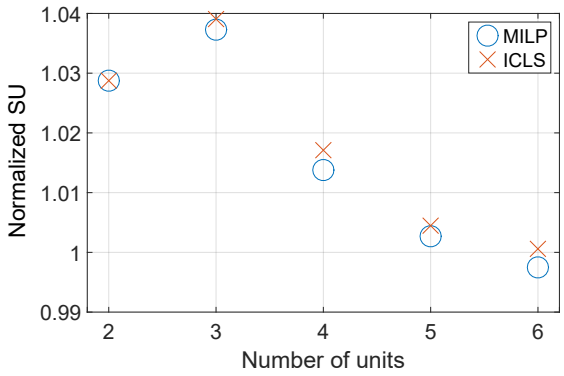

Figure 2.15. Normalized solar utilization for the ICLS and MILP versus ECLS as reference case.

point of view, the analytic approach is proven to achieve the global optimum, but it can not be generalized for all solar day patterns. The other approaches on the other hand were proven to be robust and suitable for real sizing problems. MILP approach guarantees global optimality, but its computation expense increases exponentially with the number of decision variables and constraints. ECLS required downsampling as well, and that explains the decreases in solar utilization difference between different methods as n increases, where downsampling get more accurate. Finally, ICLS is not guaranteed to converge to the global optimal, rather could get stuck in a local minimum. Thus, the final solution highly depends on initial conditions. This could be avoided by slightly perturbing the initial or final solution and restarting the optimization and thereby exploring the solution space

The analytic approach can not be generalized for all solar day patterns; it requires a functional form for the solar data and function inverse has to be known which limits this approach to be applied to run yearly data. For that reason, the analytic method can not be used for real sizing problems. The MILP technique is the most flexible approach especially given the ability of adding more constraints to the problem, such as battery or minimum up and downtime. It can also solve a daily pattern which is suitable for

schedule peruses with global optimality claims in case of convergence, still the number of variables play a big role in convergence and determining optimality. The main obstacles with the MILP are the high computational cost due to a large number of variables as well as the approximation or the relaxation applied to the problem. ECLS and ICLS are both scalable to solve multiple number of years with fast computation time. The main disadvantages of these approaches are that they do not consider the daily solar profile in addition to that they have limited capability to add constraints or improve the case as in adding batteries or minimum up and downtime.

Sample results were selected in Figure 2.10 for $n = 2$ up to $n = 6$ using the ICLS approach as shown in Table 2.2 and Figure 2.14. The algorithm solves for the optimal unit sizing over one year which contains various daily patterns based on the prevailing weather conditions. For the clear day (D1), clearly a large area of the peak of the day is wasted but lost energy is reduced as the number of units n increases. On the other hand, on the most cloudy day D3, the loss was reduced. This is a reflection of the input data where clear midday periods that yield normalized power output close to 1 are less common than cloudy days and morning and evening periods. Consequently, the unit sizes are selected to track lower power outputs more closely and clear midday periods are curtailed. If the algorithm was intended to solve the optimization over just one of the days pattern or for a different site, the results would be different.

Moreover, the computational time for the different methods was performed in a 3.4 GHz Intel Core i7 processor with 32 GB of RAM. As discussed earlier the analytic approach can not solve the planning problem, but it is very fast routine since it only computes derivative of existing function and substitute variables. MILP is the slowest, for the full set of variables, whereas Figure 2.12 shows it takes 7000 seconds to solve for input with 1:50 samples ratio and only 170 second for 1:200 downsample ratio. As discussed before the ICLS optimization is expected to return the optimal sizing of units,

it does not require removing the zero solar radiation data. The main advantage of ICLS is that it searches for the optimal unit size and switching time by avoiding the equidistant constraints giving by the ECLS method. The main disadvantage for ICLS, it is sensitive to the initial condition, especially for larger n ($n > 4$) which means that global optimality is not guaranteed. The computation time for ICLS varies from 11 seconds for $n = 2$ to around 150 seconds for $n = 6$. ECLS is the fastest approach even though it has to search for the optimal C given in (2.20). ECLS forces the results of the switch time to be equidistant outdistance spaced from each other which is not the optimal decision. Also it requires removal of zeros in the input data; otherwise the results and the solar utilization will be negatively affected. Each run of ECLS costs 0.01 seconds so solution time is dependent on the resolution of the line-search (C). For our purposes, ECLS is the fastest approach. Assuming the resolution of the line-search is 100 steps, ECLS is 10 times faster than ICLS for $n = 2$ and 140 faster for $n = 6$.

Table 2.4. Comparison of the advantages and disadvantages of the optimization algorithms.

	ICLS	ECLS	MILP	Analytic
Advantage	-Fast -Considering all sorted data -Not equidistant	-Fast -Unique minimum for fixed constraint	-Convex (Global optimality)* -Any data profile for limited variables - More constraints could be added	-Fast -Exact (no approx.) -Guarantees global optimum
Disadvantage	-No guaranteed global optimality -Sensitive to initial conditions	-Down-sampling required -Equidistant -Requires line-search for constraint	-Computationally expensive -Requires down-sampling	-Only for symmetric, i.e., clear days -Can not be used for planning algorithms

* Note: convexity for MILP approach is assumed in case of convergence

2.7 Conclusions

Solar PV is a desirable energy source for many standalone applications. Variability of solar irradiance is one of the main challenges of PV utilization. State-of-the-art optimization techniques were developed and applied to optimize the solar utilization by

sizing a given number of load units based on one year of data collected in San Diego and Saudi Arabia. The algorithm switches the units on and off to "load follow" the available solar power during the day to maximize the solar energy utilization. The primary output of the algorithms is the optimum sizing for a given number of units, but unit scheduling is a byproduct of the analysis. Three different optimization methods are proposed to solve for the optimal unit size: Equality Constrained Least Squares (ECLS), Inequality Constrained Least Squares (ICLS), and Mixed-Integer Linear Programming (MILP). The performance of the three methods was compared with two case studies. Results for the San Diego case indicate a solar utilization (i.e., percentage of energy captured by units over available energy) differed by less than 5% between the algorithms. It was shown the utilization increased from 73% for two units up to 98% for six units for San Diego case. As expected, the ICLS optimization yields the largest utilization. The results obtained will differ by location and may even vary year-to-year due to spatio-temporal patterns in the solar resources and cloud coverage as evident from the differing results between San Diego, USA and Thuwal, KSA. The methodology proposed in this paper allows computationally efficient solutions even when several years of solar resource data are available and yield the optimal sizing for the given data. For practical applications, the economics also need to be considered as smaller units typically cost more per kW and an optimization based on cost would therefore yield larger and prefer fewer units. Within our framework, it is possible to assign a cost function to the number of units and to the solar utilization to provide solutions for practical applications.

Appendices

Appendix A: Clear Day Fitting

To obtain a function close to a clear day solar power data for the analytical optimization, San Diego data from a clear day was used as a template to fit a quadratic function

$$S_1(x) = p_1 t^2 + p_2 t + p_3,$$

and a combination of sin and cos functions

$$S_2(x) = a_1 sin(bt) + a_2 cos(bt)$$

as shown in Figure 2.16. The quadratic function parameters were $p_1 = -2.001 \times 10^{-11}, p_2 = 9.035 \times 10^{-6}, p_3 = -0.04926$. Once shifting $S_1(t)$ to be symmetric over the y-axis $p_1 = -2.001 \times 10^{-5}, p_2 = -7.884 \times 10^{-6}, p_3 = 0.9708$
. The sin and cos parameters were $a_1 = a_2 = 0.99, b = 0.007$. For the symmetric $S_2(t)$, $a_1 = 0.99, a_2 = 8.3 \times 10^{-4}, b = 7 \times 10^{-6}$.

Both functions are suitable to be used as fitting for clear sky model, where the $S_2(x)$ resulted in better fitting. This was discussed in detailed in the the motivation section 2.4.1. The San Diego solar data was recorded at 15 min resolution. The function where shifted to be symmetric over the y-axis to simplify calculation.

Appendix B: Numerical Optimization

An alternative way to the Jacobian method in section 2.4.1 is the numerical search or the line-search for all possible numbers which can draw the rectangle. By doing so the line-search started from around zero up to the peak of the parabola which is around 1. The results were very close the Jacobian method and difference is due the

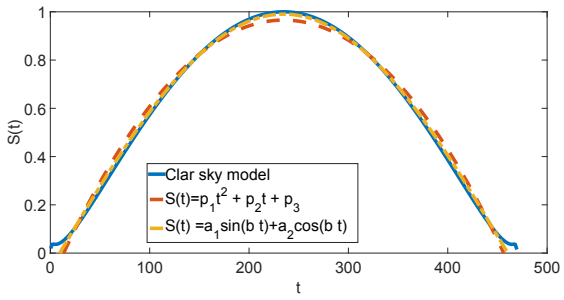

Figure 2.16. Clear day solar power data normalized by the peak fitted with quadratic polynomial and a combination of sin and cos.

sampling errors. The area of the simulation results is 15985 while the analytical result is $2 \times 123 \times 0.6489 = 15963$. The error is 0.14%

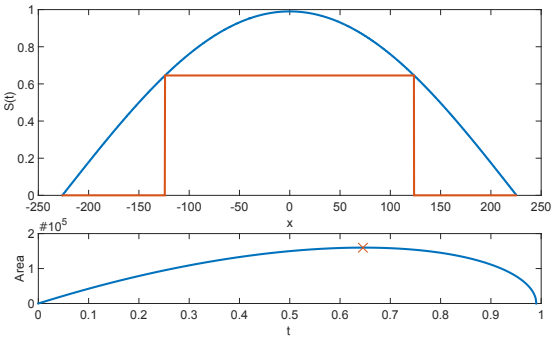

Figure 2.17. Numerical optimization of sizing a single rectangle under a parabola.

Appendix C: Newton's Method

Showing the results of the optimization using the Jacobian method is not straightforward, since the area function is nonlinear for more than 2 variables.

$$A(y_1, y_2, y_3) = y_1(S^{-1}(y_1) - S^{-1}(y_2)) + y_2 S^{-1}(y_2) + (y_3 - y_2)S^{-1}(y_3)$$

substituting $y_3 = y_1 + y_2$

$$\bar{A}(y_1, y_2) = y_1(S^{-1}(y_1) - S^{-1}(y_2) + S^{-1}(y_1 + y_2)) + y_2 S^{-1}(y_2)$$

$$\nabla J = \begin{bmatrix} \frac{\partial A}{\partial y_1} \\ \\ \frac{\partial A}{\partial y_2} \end{bmatrix} = \begin{bmatrix} S^{-1}(y_1) - S^{-1}(y_2) + S^{-1}(y_1 + y_2) + y_1(S^{-1}(y_1))' \\ \\ (S^{-1}(y_2))'(y_1 + y_2) + S^{-1}(y_2) \end{bmatrix}$$

This problem was solved by plotting the derivative of the area over all variables ($\frac{\partial A}{\partial y_1}$ and $\frac{\partial A}{\partial y_2}$) and equate them to zero or find their intersection. Since the area function is 2D and so its derivative Figure 2.18 shows each of the ∇J equation surface graph plotted over each other and sliced over the area function at zero.

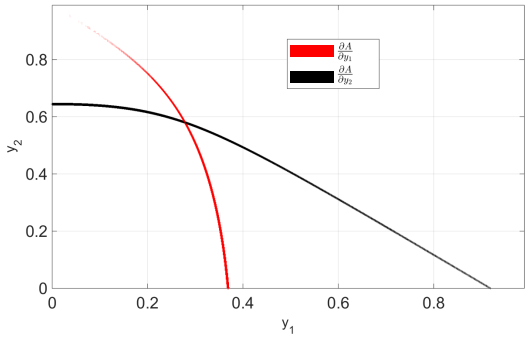

Figure 2.18. A slice of the 3-dimensional graph in Figure 2.7 at area = 0 showing the intersection of the area derivative with respect to the variables (x_1 and x_2).

The text and data in Chapter 2, in full, is a reprint of the material as it appears in "Optimal switchable load sizing and scheduling for standalone renewable energy systems", Habib, Abdulelah; Disfani, Vahid R.; Kleissl, Jan; de Callafon, Raymond, *Solar Energy*, 144 (2017), 707 - 720. The dissertation author is the primary investigator and author of this article.

Chapter 3

Quasi-Dynamical Load sizing and scheduling

Considering the intermittency of renewable energy systems, a sizing and scheduling model is proposed in this Chapter for a finite number of static electric loads. The model objective is to maximize solar energy utilization with and without storage. For the application of optimal load size selection, the energy production of a solar photovoltaic is assumed to be consumed by a finite number of discrete loads in an off-grid system using mixed-integer linear programming. Additional constraints are battery charge and discharge limitations and minimum uptime and downtime for each unit. For a certain solar power profile the model outputs optimal unit size as well as the optimal scheduling for both units and battery charge and discharge (if applicable). The impact of different solar power profiles and minimum up and down time constraints on the optimal unit and battery sizes are studied. The battery size required to achieve full solar energy utilization decreases with the number of units and with increased flexibility of the units (shorter on and off-time). A novel formulation is introduced to model quasi-dynamic units that gradually start and stop and the quasi-dynamic units increase solar energy utilization. The model can also be applied to search for the optimal number of units for a given cost function.

3.1 Introduction

Standalone solar energy systems are increasingly deployed in rural and off grid areas, especially to provide basic societal needs, for example, water treatment, pumping, and cooking or heating Rickerson et al. (2012). The main obstacles in optimal sizing and scheduling problems of electric power systems are the variability and intermittency of renewable energy generation. The most challenging scenario is the standalone or islanded mode where high penetration of variable renewable power sources such as wind and solar causes power variability that is large enough to affect electric power quality and efficiency Wan (2012) and Nguyen et al. (2015). Solar energy production depends foremost on the solar resource availability, which suffers from high variability over a broad range of time scales.

Sizing of power generators for standalone application was discussed in many papers such as Egido and Lorenzo (1992) and Kellogg et al. (1998), where solar energy was sized to meet the load. In this paper, we consider the opposite case where both the generators, unit load size, and number of units are designed to optimize system efficiency or minimize energy loss. Such a tool is helpful if a complete microgrid (generators and loads) is designed from scratch, such as for a desalination plant without local grid power supply, or if additional loads are connected to an existing off-grid solar system.

Load scheduling plays an important role in optimizing efficiency as well. It has been applied in many ares, for example thermal loads and domestic appliances Ferhatbegovic et al. (2011). Optimal scheduling a wind farm with a storage system constrained by states of charge of the battery was considered in Ma and Chen (2015). Game theory and customers effect on the grid and EVs was studied in Kim et al. (2013). Load scheduling is also used in water network system where the number of pumps are scheduled to meet the water demand and optimize the cost Sun et al. (2014). Forecasts for

solar generation and uncontrollable loads are required inputs for the scheduling problem yet solar forecast research is still ongoing and errors can be substantial especially on short time scales. In our previous work we defined number and size of units and solved the scheduling problem with the solar forecast. We also proposed ideas to overcome forecast error in standalone cases Habib et al. (2016b).

Energy storage systems can solve the variability and intermittency problem Pickard and Abbott (2012b) and balance forecast errors, but energy storage will add cost and complexity to the standalone system. An alternative way is load sizing, where loads on the standalone system are adjusted to accommodate power variability to consume as much as possible of the available solar energy thereby reducing energy losses. While the need for energy storage can be substantially reduced through scheduling, the addition of a battery can be cost effective for standalone applications be it wind Savkin et al. (2014) or solar PV Vieira and Mota (2010). The sizing and scheduling of such a battery will also be optimized in this work.

This paper is organized as follows, some background and problem explanation are discussed in Section 3.2. In Section 3.3 the problem formulation is given explaining the optimization techniques, objective functions and the constraints. Also the two principal optimization approaches are presented in this section. In Section 3.4 different scenarios are discussed and compared for different solar generation pattern, e.g., clear, cloudy and partially cloudy days as well as different minimum up and downtime constraints both with and without storage.

3.2 Background

Planning algorithms for solar standalone applications are needed to overcome solar radiation variability. The standalone PV sizing problem inputs are solar PV and the load. Energy storage is an optional component. PV power performance models are well

understood and PV output timeseries can be generated globally and for different days of the year given existing solar resource databases and models. For brevity we will deal with sample daily solar power profiles from a PV system at UC San Diego and normalized it to one for generality. In practice, sizing decisions should be based on several years of solar resources data to capture the annual variability and possible even inter-annual variability. While typical meteorological year (TMY) or typical solar year are often used for this purpose, large solar system developers increasingly rely on multidecadal modeled power production based on site adaption of long-term satellite records with short-term local measurements for their financial calculations Thevenard and Pelland (2013). Such long-term data would be preferable in practice although interannual variability of solar energy generation is small. For example, Pitz-Paal et al. (2011) specifies that the interannual variability of GHI for 7-10 years of measurement at Potsdam, Germany and Eugene, USA is about 5%.

The sizing of load is determined to maximize the solar utilization factor that will be referred to in this paper as efficiency (Eff). We proposed a unit sizing design for each a clear and a cloudy day. The approach can be extended to yearly data which allows characterizing most of the important seasonal and diurnal variability. Considering longer timeseries merely adds computational cost to the implementation of our proposed model. If computation power is limited, the sizing could be based on these two or a few more characteristic days with a weighing factor based on the probability of occurrence of a daily pattern is for a selected location.

In our previous work we targeted the sizing of standalone PV reverse osmosis units (PVRO) by searching among different unit numbers and sizes. A financial model allowed the optimization to achieve the lowest water cost Habib et al. (2015). Then we developed a mathematical data driven optimization to optimally size the PVRO units in Habib et al. (2017). In Habib et al. (2016b,a), we developed a model predictive

load scheduling to optimally schedule units. In this paper we describe a method that can consider all of these objectives at the same time; we provide a model to optimally size, choose the number of units, and schedule. The addition of energy storage is also considered. The algorithm can also be applied to problems where units sizes and numbers are known and only the scheduling is of interest.

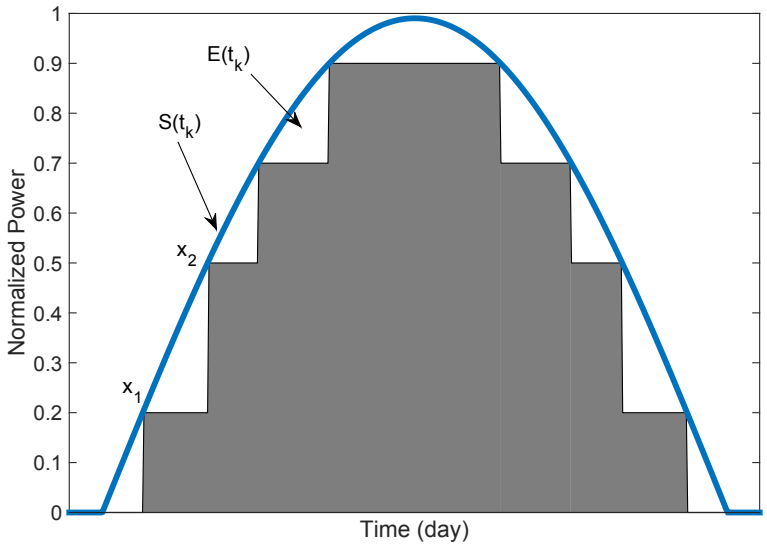

Figure 3.1. Problem illustration for one clear and symmetric day. Loads x^i are scheduled hourly to follow the increase or decrease in solar power generation $S(t_k)$.

3.3 Problem Formulation

The optimization problem tackled in this paper is generally presented as

$$
\begin{aligned}
\min_{\mathbf{U},\mathrm{X},\bar{\mathrm{P}}_{\mathbf{b}},\mathrm{P_s}} \quad & \mathbf{f}(\mathbf{U},\mathrm{X},\bar{\mathrm{P}}_{\mathbf{b}},\mathrm{P_s}) \\
\text{s.t.} \quad & \mathbf{g}(\mathbf{U},\mathrm{X},\bar{\mathrm{P}}_{\mathbf{b}},\mathrm{P_s}) \leq 0 \\
& \mathbf{h}(\mathbf{U},\mathrm{X},\bar{\mathrm{P}}_{\mathbf{b}},\mathrm{P_s}) = 0 \\
& \phi(\mathbf{U},\mathbf{R},\mathbf{Q},\mathbf{W},\mathbf{V}) \leq 0 \\
& \psi(\mathbf{U},\mathbf{R},\mathbf{Q},\mathbf{W},\mathbf{V}) = 0 \\
& \mathbf{R},\mathbf{Q},\mathbf{W},\mathbf{V} \subset \{0,1\}^{|\mathbf{U}|} \\
& \mathbf{U} \subset \{0,1/2,1\}^{|\mathbf{U}|}
\end{aligned}
\tag{3.1}
$$

where the decision variables $\mathrm{X} = [x_1, x_2, \cdots, x_n]^T$ and

$$
\mathbf{U} \quad = \quad \begin{bmatrix} u_1^1 & u_1^2 & \cdots & u_1^k \\ u_2^1 & u_2^2 & \cdots & u_2^k \\ \vdots & & \ddots & \vdots \\ u_n^1 & u_n^2 & \cdots & u_n^k \end{bmatrix}
$$

are load vector and switching matrices, respectively, such that $u_i^{t_k}$ denotes the portion of the load i which is turned on at time t_k, and x_i is the size of unit i. The size of the battery connected is a scalar and called P_b, while P_s is a column vector representing the battery scheduled discharging power at all t. The variable matrices $\mathbf{V}$ and $\mathbf{W}$ respectively denote the start-up and shut-down signals, whereas the variable matrices $\mathbf{R}$ and $\mathbf{Q}$ are defined such that $\mathbf{U} = \frac{\mathbf{R}+\mathbf{Q}}{\mathbf{2}}$. Also, the functions $\mathbf{f}$, $\mathbf{g}$ and $\mathbf{h}$ denote the mathematical formulations of the objective function, inequality constraints, and equality constraints respectively. The functions ϕ and ψ also represent the inequality and equality constraints that involve

U and the binary matrices.

3.3.1 Objective Function

As indicated in Figure 3.1, the power mismatch between available solar power and power used by load units at any time t_k can be characterized by

$$E(t_k) = S(t_k) - \sum_{i=1}^{n} u_k^i x^i$$

for the case without a battery. Considering a battery system that is discharged by $P_s^{t_k}$ at time t_k, the definition of power mismatch changes to

$$E(t_k) = S(t_k) + P_s(t_k) - \sum_{i=1}^{n} u^i(t_k) \cdot x^i$$

Therefore, the objective function is to minimize the mismatched power and maximize the efficiency (defined as matched energy over total solar energy)

$$\mathbf{f}(\mathbf{U}, \mathrm{X}, \bar{\mathrm{P}}_{\mathbf{b}}, \mathrm{P_s}) = \mathbf{1}^T \cdot (S + \mathrm{P_s} - diag(\mathrm{X}) \cdot U \cdot \mathbf{1}) \tag{3.2}$$

where S is a column vector denoting the PV power available at all time steps. The objective function in (3.2) is nonlinear due to the bilinear product function, *i.e.* $diag(\mathrm{X}) \cdot U$. To remove nonlinearity, a new decision variable matrix $\mathbf{Y} = diag(\mathrm{X}) \cdot U$ is defined which denotes the scheduled power. Thus, the objective function becomes linear as

$$\mathbf{f}(\mathbf{U}, \mathrm{X}, \bar{\mathrm{P}}_{\mathbf{b}}, \mathrm{P_s}) = \mathbf{1}^T \cdot (S + \mathrm{P_s} - \mathbf{Y} \cdot \mathbf{1}) \tag{3.3}$$

Adding the definition of **Y** to the set of constraints guarantees identical solutions for Eqs. (3.1) and (3.3). The definition of **Y** moves nonlinearity from objective function to constraints. The big-M method is the common solution to remove such nonlinearities Griva et al. (2009), when **U** is a binary matrix. In this paper, a novel application of big-M

method is proposed to remove these nonlinearities when the elements of **U** belong to the set of $\{0, 1/2, 1\}$.

3.3.2 Constraints

Resource Adequacy

To prevent frequency issues, the maximum total load that the microgrid can supply must be less than the total PV energy available at each time interval:

$$\mathbf{1}^T.\mathbf{Y} \leq \mathrm{S} + \mathrm{P_s}, \tag{3.4}$$

Definition of Scheduled Power

In order to apply the new format of big-M method, two auxiliary binary matrices R and Q are defined such that $\mathbf{U} = \frac{\mathbf{R}+\mathbf{Q}}{\mathbf{2}}$ and $R - Q \geq 0$. These two constraints guarantee that the vector $U = [0, 1/2, 1]$ is uniquely mapped to the vectors $R = [0, 1, 1]$ and $Q = [0, 0, 1]$.

With the definitions of the matrices R and Q, the constraint $\mathbf{Y} = diag(\mathrm{X}) \cdot U$ is equivalent to the following set of constraints,

$$\begin{aligned}
-\mathbf{Y} &\leq \mathbf{0} \\
\mathbf{Y} - \frac{\mathbf{R}+\mathbf{Q}}{2} M &\leq \mathbf{0} \\
\mathbf{Y} - \frac{\mathbf{1}\cdot\mathbf{1^T}\cdot\mathbf{diag}(\mathbf{X})}{2} - \frac{\mathbf{R}+\mathbf{1}\cdot\mathbf{1^T}-\mathbf{Q}}{2} M &\leq \mathbf{0} \\
-\mathbf{Y} + \frac{\mathbf{1}\cdot\mathbf{1^T}\cdot\mathbf{diag}(\mathbf{X})}{2} - \frac{\mathbf{R}+\mathbf{1}\cdot\mathbf{1^T}-\mathbf{Q}}{2} M &\leq \mathbf{0} \\
\mathbf{Y} - \mathbf{1}\cdot\mathbf{1^T}\cdot\mathbf{diag}(\mathbf{X}) &\leq \mathbf{0} \\
-\mathbf{Y} + \mathbf{1}\cdot\mathbf{1^T}\cdot\mathbf{diag}(\mathbf{X}) - \frac{\mathbf{1}\cdot\mathbf{1^T}-\mathbf{R}+\mathbf{Q}}{2} M &\leq \mathbf{0}
\end{aligned} \tag{3.5}$$

where M is a real constant number, e.g, 10^6.

In (3.5) the first two and the last two constraints correspond to the case that $u = 0$

and $u = 1$, respectively. the third and fourth inequalities guarantee any $\mathbf{y} = x/2$ if the corresponding u is 0.5, while they are relaxed otherwise.

Dynamic Model Constraint

One of the novelties in this paper is to consider dynamics of load switching in the start up and shut down processes. The dynamics in this paper is modeled by adding an intermediate step $u = 1/2$ for the load units while switching on or off.

To model these dynamics, several constraints must be considered. First, no immediate transitions between $u = 0$ and $u = 1$ are allowed. Second, if $u(t) = 1/2$, then at the following timestep $u(t+1) = 1 - u(t-1)$, which means that u may not stay in the state $u = 1/2$ for any two consecutive time steps and no switching is allowed during dynamics. These constraints are summarized as:

$$\begin{aligned}
u_i^t - u_i^{t-1} &\leq 1/2 \quad \forall_{i,t} \\
u_i^{t-1} - u_i^t &\leq 1/2 \quad \forall_{i,t} \\
r_i^{t+1} &\leq 1 - r_i^{t-1} + (1 - r_i^t + q_i^t)M \quad \forall_{i,t} \\
r_i^{t+1} &\geq 1 - r_i^{t-1} - (1 - r_i^t + q_i^t)M \quad \forall_{i,t} \\
q_i^{t+1} &\leq 1 - q_i^{t-1} + (1 - r_i^t + q_i^t)M \quad \forall_{i,t} \\
q_i^{t+1} &\geq 1 - q_i^{t-1} - (1 - r_i^t + q_i^t)M \quad \forall_{i,t}
\end{aligned} \tag{3.6}$$

Minimum Up-time and Minimum Down-time

To avoid increased wear and tear to load units and inconvenience to microgrid customers because of frequent start-ups and shut-downs, a set of constraints are defined to guarantee that the unit is switched on (off) for at least m^+ (m^-) time steps before it is switched off (on). These constraints are called minimum up (down) time and are defined

as:

$$\begin{aligned} r_{i,t_k} - \sum_{h=t_k-m_i^+ +2}^{t_k} v_{i,h} \leq 0 \quad \forall_{m_i^+ \leq t_k \leq T} \\ (1-r_{i,t_k}) - \sum_{h=t_k-m_i^-}^{t_k} w_{i,h} \leq 0 \quad \forall_{m_i^- \leq t_k \leq T}, \end{aligned} \tag{3.7}$$

where the matrix $\mathbf{V} \subset \{0,1\}^{|\mathbf{V}|}$ and $\mathbf{W} \subset \{0,1\}^{|\mathbf{W}|}$ are denoted as start-up and shut-down matrices respectively, and their elements are defined as:

$$\begin{aligned} v_{i,t_k} - w_{i,t_k} &= r_{i,t_k} - r_{i,t_k-1} && \forall_{1\leq i\leq N} \forall_{2\leq t_k \leq T} \\ v_{i,t_k} + w_{i,t_k} &\leq 1 && \forall_{1\leq i\leq N} \forall_{2\leq t_k \leq T} \\ v_{t,1} &= w_{i,1} = 0 && \forall_{1\leq i\leq N} \end{aligned} \tag{3.8}$$

Battery Constraints

There are also some constraints associated with the battery such as maximum charge and discharge power, minimum and maximum limits of state of charge (SOC), and initial and final SOC, which are described as:

$$\begin{aligned} \mathrm{P_s} &\leq \bar{\mathrm{P}}_b \cdot \mathbf{1} \\ {\mathrm{P_s}}^T \cdot \mathbf{1} &= 0 \\ \sum_{h=1}^{t} \bar{\mathrm{P}}_b^h + \mathrm{E}_b^0 &\leq \bar{\mathrm{E}}_b \\ \sum_{h=1}^{t} \bar{\mathrm{P}}_b^h + \mathrm{E}_b^0 &\geq 0, \end{aligned} \tag{3.9}$$

where the efficiency of the battery is assumed to be 1, and E_b^0 denotes the initial energy stored in the battery. As ${\mathrm{P_s}}^T \cdot \mathbf{1}$ is equal to the net energy stored in the battery during the entire day, the second constraint in (3.9) keeps the final SOC of the battery on its initial value.

3.3.3 Static and Quasi-Dynamic MILP Strategies

Static MILP

Static MILP considers loads to be either on or off, i.e. transient dynamics are neglected. In this case, **R** and **Q** in equation (3.5) have to be equal which forces **U** to be in the set of $\{0, 1\}$. Static MILP still allows optimizing the size of a given number of units, minimum up and down time constraints, and the battery size and battery schedule for a given solar power profile.

Quasi-Dynamic MILP

The quasi-dynamic MILP strategy is more sophisticated than static MILP. Here the units are assumed to go from off state to half operational state and finally to the final state, and vice versa. So the loads will go from 0% to 50% and then to 100% of unit size x_i. This case is more realistic since most large loads are ramped up over a period of time before they reach to steady state. The quasi-dynamic strategy also yields all the variables in the static strategy; the only difference is that **U** is in the set $\{0, 1/2, 1\}$.

3.4 Numerical Results

In this section results from both static and quasi-dynamic MILP strategies are presented using using the CVX toolbox and Gurobi 6.50. Figure 3.2 illustrates the results corresponding to three different representative solar power profiles of D1 clear day, D2 cloudy day and D3 partly cloudy day. The units are scheduled and stacked as area plots. The numeric values for units and battery are shown in Table 3.2. Without storage (upper row in the figure) the total unit power cannot exceed the solar power. With storage (lower row) the total unit power can temporarily exceed solar power.

The optimal unit sizes clearly decrease on the overcast day with small solar resource as units of the size of x_1 in D1 would rarely be able to run. The addition of

storage also effects the unit sizes. Storage will allow the units to ride through short-lived dips in solar power by utilizing battery energy which results in larger unit sizes and increased solar utilization. This is most apparent in the D3 case at around 1100 Local Standard Time (LST) where the green units ride through the temporary cloud cover on partial battery power and both blue and green units are enlarged for the storage case.

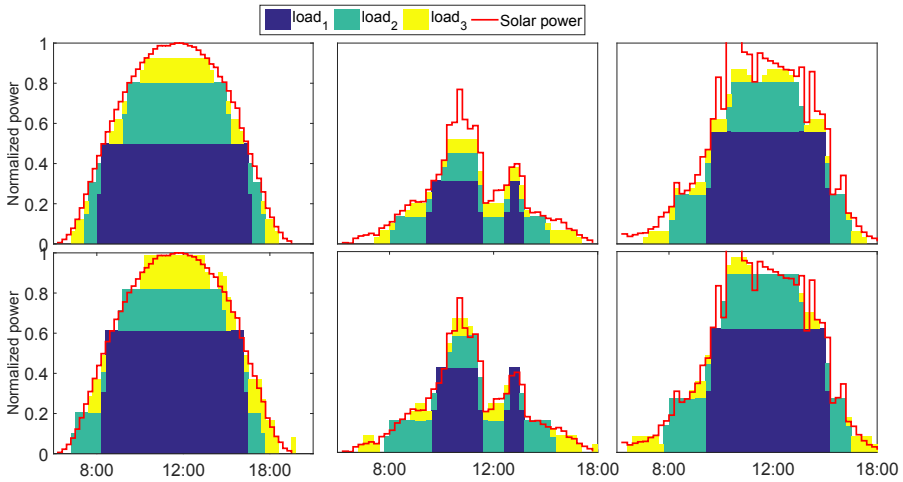

Figure 3.2. Results of load sizing and scheduling without (top) and with (bottom) storage for the Quasi-Dynamic MILP strategy for three different days and three units. The clear day (first from left) is referred to D1, the overcast day in the middle is D2, and the partially cloudy day (right) is D3. The minimum on and off times are 3 time steps (45 minutes) for all units. The initial storage of the battery is $\frac{\bar{P}_b}{2}$ and equal to [0.07, 0.13, 0.14]/2 for D1, D2, and D3 respectively

In both Table 3.1 and Table 3.2 different unit sizes and efficiency for the case $n = 3$ are shown with different minimum up time and down time constraints. The left hand side column shows different minimum uptime and downtime constraints for each unit represented in terms of time steps in square brackets. At the right of the same column day types are shown as D1, D2, and D3. The middle column shows results for unit sizes and solar energy utilization or efficiency (Eff) without battery. Finally the last column displays the results with storage and the optimal battery size $\bar{P}_b$ required to achieve Eff equal to one which corresponds to utilizing all solar power on a given day.

All results including the battery sizes are normalized as per unit (pu) of the maximum solar power production on the clear day. Eff equal one can be achieved as the battery model is assumed ideal without losses from charging or discharging.

Table 3.1. Static MILP strategy results (pu) for three units and different on and off times (left column)

$\begin{bmatrix} m_1^+ \\ m_2^+ \\ m_3^+ \end{bmatrix}$	$\begin{bmatrix} m_1^- \\ m_2^- \\ m_3^- \end{bmatrix}$	Day type	Without Storage				With Storage			
			x_1	x_2	x_3	Eff (%)	x_1	x_2	x_3	$\bar{P}_b$
$\begin{bmatrix} 3 \\ 3 \\ 3 \end{bmatrix}$	$\begin{bmatrix} 3 \\ 3 \\ 3 \end{bmatrix}$	D1	0.50	0.30	0.12	0.90	0.54	0.33	0.12	0.11
		D2	0.32	0.14	0.07	0.82	0.40	0.16	0.08	0.18
		D3	0.56	0.24	0.09	0.87	0.62	0.27	0.11	0.13
$\begin{bmatrix} 3 \\ 2 \\ 1 \end{bmatrix}$	$\begin{bmatrix} 3 \\ 2 \\ 1 \end{bmatrix}$	D1	0.55	0.25	0.12	0.92	0.57	0.30	0.12	0.10
		D2	0.29	0.15	0.11	0.84	0.38	0.18	0.12	0.12
		D3	0.56	0.24	0.09	0.88	0.64	0.23	0.13	0.10
$\begin{bmatrix} 7 \\ 6 \\ 5 \end{bmatrix}$	$\begin{bmatrix} 3 \\ 2 \\ 1 \end{bmatrix}$	D1	0.60	0.30	0.08	0.89	0.57	0.31	0.11	0.11
		D2	0.25	0.20	0.11	0.81	0.33	0.24	0.10	0.18
		D3	0.58	0.22	0.08	0.86	0.67	0.23	0.10	0.16
$\begin{bmatrix} 3 \\ 2 \\ 1 \end{bmatrix}$	$\begin{bmatrix} 7 \\ 6 \\ 5 \end{bmatrix}$	D1	0.50	0.30	0.16	0.91	0.52	0.32	0.14	0.10
		D2	0.25	0.20	0.11	0.81	0.55	0.22	0.11	0.19
		D3	0.56	0.24	0.13	0.84	0.54	0.30	0.19	0.17

For three time steps (45 min) up and down time Table 3.1 shows that clear and partly cloudy days (D1 and D3) were associated with larger units compared to the overcast day D2, as expected. Maybe unexpectedly, D3 had larger x_1 units compared to D1 but $x_{2,3}$ were smaller. D2 had smaller units to align with the smaller range of the solar resource and significant cloud variability. Efficiency was largest for the clear day as expected.

Four different minimum uptime and downtime combinations were performed for 3 different daily patterns to illustrate the model sensitivity to different constraints. Larger minimum uptime and down time reduce the flexibility of scheduling and are expected to reduce efficiency and trigger larger unit sizes. When flexibility increases (from [3 3 3] to [3 2 1]) efficiency increases by about two percentage points and the required battery size for Eff= 1 decreases by 10% to 60%. The results for different minimum on and off times for the same case are inconclusive and dependent on the time scales of solar resource fluctuations on different days.

Adding storage always increase Eff as our model solves for the co-optimization problem for both battery size and units size. All unit sizes increase when batteries are added especially on the more variables days D2 and D3. For all minimum uptime and downtime cases D2 requires the largest battery size to smooth out the variability even though the total solar production on D2 is far smaller than on D1 or D3.

Applying different minimum up and down times for different units are shown in the second row of results; the largest unit still has a 3 time step requirement, but the smallest unit does not have any constraint. The unit sizes for D3 remain largely unaffected, while for D1 x_1 is in fact larger and x_2 correspondingly smaller and vica versa for D2. The main noticeable difference here is the battery size of D2 which resulted in smaller size and due to the smaller minimum up/downtime constraints for the smaller units x_2 and x_3.

The last 2 cases are distinguishing both uptime downtime and units as shown in row 3 of the results, where the largest units x_3 has to be on for 7 times step (105 min) but downtime is only 45 min, and so on. These cases are based on the load application assuming the units need to be on for double or more the time that they need to be off. Effects are mostly restricted to a redistribution of the unit sizes (e.g. for D2 x_2 increases while x_1 decreases) while the total unit sizes $x_1 + x_2 + x_3$ changes only slightly. Eff

Table 3.2. Quasi-dynamic model results (pu)

$\begin{bmatrix} m_1^+ \\ m_2^+ \\ m_3^+ \end{bmatrix}$	$\begin{bmatrix} m_1^- \\ m_2^- \\ m_3^- \end{bmatrix}$	Day type	Without Storage				With Storage			
			x_1	x_2	x_3	Eff (%)	x_1	x_2	x_3	$\bar{P}_b$
$\begin{bmatrix} 3 \\ 3 \\ 3 \end{bmatrix}$	$\begin{bmatrix} 3 \\ 3 \\ 3 \end{bmatrix}$	D1	0.50	0.30	0.12	0.93	0.54	0.32	0.12	0.07
		D2	0.32	0.14	0.07	0.85	0.42	0.18	0.08	0.13
		D3	0.56	0.24	0.07	0.87	0.71	0.22	0.11	0.14
$\begin{bmatrix} 3 \\ 2 \\ 1 \end{bmatrix}$	$\begin{bmatrix} 3 \\ 2 \\ 1 \end{bmatrix}$	D1	0.54	0.30	0.13	0.94	0.61	0.27	0.11	0.05
		D2	0.34	0.15	0.11	0.86	0.39	0.20	0.10	0.10
		D3	0.56	0.24	0.09	0.88	0.57	0.29	0.14	0.10
$\begin{bmatrix} 7 \\ 6 \\ 5 \end{bmatrix}$	$\begin{bmatrix} 3 \\ 2 \\ 1 \end{bmatrix}$	D1	0.67	0.18	0.13	0.92	0.51	0.36	0.13	0.10
		D2	0.40	0.15	0.11	0.83	0.34	0.25	0.12	0.18
		D3	0.56	0.24	0.06	0.86	0.68	0.22	0.08	0.14
$\begin{bmatrix} 3 \\ 2 \\ 1 \end{bmatrix}$	$\begin{bmatrix} 7 \\ 6 \\ 5 \end{bmatrix}$	D1	0.55	0.37	0.25	0.91	0.63	0.35	0.18	0.10
		D2	0.41	0.16	0.09	0.82	0.35	0.24	0.13	0.17
		D3	0.59	0.36	0.24	0.84	0.54	0.37	0.20	0.17

generally decreases with the reduced flexibility. In terms of storage, increasing the on time requirement did not effect much the D1 results, while the storage size increase substantially for D2 and D3. Lastly, flipping the previous cases assuming the load required longer off time, the effect is mainly in the unit sizes of D1 and D3. The Eff and $\bar{P}_b$ remains similar as expected because the same solar profile results in similar battery scheduling.

Table 3.2 shows results for the Quasi-Dynamic MILP strategy. The main change from the Static MILP results is increasing Eff in almost all cases since the half-on units effectively add additional discretizations beyond the 2^3 unit size combinations for the three units. Therefore the loads can better track the solar curve. For the same reason $\bar{P}_b$

became smaller. In general, unit sizes stayed the same or increased and in some cases like the last case in D1 ([3, 2, 1] and [7, 6, 5]) no small units resulted. For the clear day D1 usually x_3 is small as the middle of the day favors large base-load and the two smaller units primarily capture the shoulders of the day. However, long downtime constraints appear to favor larger units probably because the units are unable to capture the evening shoulder after the downtime requirement.

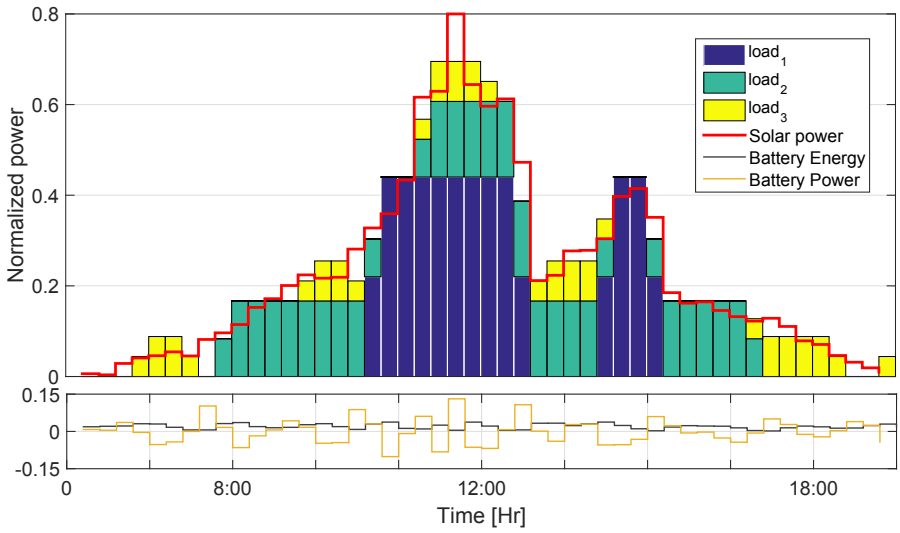

Figure 3.3. Overcast day example of load sizing and scheduling with storage for quasi-dynamic MILP (top). Same as the bottom center graph in Fig. 3.2, but the power and the energy of the battery are shown as well (bottom).

An overcast day example of load sizing and scheduling with storage is given in Figure 3.3. The initial energy stored in the battery E_b^0 is half of the battery size which is 0.13 pu and an additional constraint was added to the end charge state of the battery $\mathrm{E}_b^t = \mathrm{E}_b^0$ or ($\mathrm{P_s} \leq \bar{\mathrm{P}}_b \cdot \mathbf{1}$). For the first few time steps after sunrise the battery charged allowing the smallest unit x_3 to be on for one hour. Then x_3 was shut down allowing the battery to charge up allowing x_2 to be turned on 30 min before the solar power was sufficient. Following the charging and discharging battery curves shows that the battery was never charging or discharging for more than four consecutive time steps. The battery shifts

Table 3.3. Different number of units (n) comparison for static MILP.

				D1				
n	2	3	4	5	2	3	4	5
$\bar{P}_b$	0	0	0	0	0.28	0.11	0.07	0.05
x_1	0.67	0.50	0.48	0.49	0.67	0.54	0.49	0.50
x_2	0.25	0.30	0.32	0.18	0.28	0.33	0.33	0.32
x_3		0.12	0.12	0.14		0.12	0.13	0.20
x_4			0.06	0.12			0.05	0.08
x_5				0.05				0.07
Eff	0.82	0.90	0.93	0.94	1	1	1	1
				D2				
n	2	3	4	5	2	3	4	5
$\bar{P}_b$	0	0	0	0	0.40	0.18	0.09	0.05
x_1	0.31	0.41	0.31	0.31	0.45	0.40	0.36	0.23
x_2	0.14	0.14	0.15	0.26	0.15	0.16	0.22	0.21
x_3		0.07	0.08	0.15		0.08	0.15	0.16
x_4			0.05	0.08			0.06	0.12
x_5				0.05				0.05
Eff	0.67	0.82	0.89	0.93	1	1	1	1
				D3				
n	2	3	4	5	2	3	4	5
$\bar{P}_b$	0	0	0	0	0.36	0.13	0.08	0.07
x_1	0.56	0.56	0.56	0.40	0.69	0.62	0.58	0.51
x_2	0.24	0.24	0.24	0.36	0.24	0.27	0.28	0.36
x_3		0.09	0.24	0.18		0.11	0.12	0.18
x_4			0.09	0.08			0.06	0.08
x_5			0.04	0.06				0.06
Eff	0.80	0.87	0.91	0.93	1	1	1	1

small amounts of energy to allow units to come on earlier during increasing solar power production and turn off later during decreasing solar power production.

Table 3.3 summarizes the results for different n from two units up to five units to illustrate the ability of the model to simulate a varying number of units as well the size of each unit. The left side shows the sizing without storage based on optimal Eff. Eff increased from 82% for two units up to 94% for five units in the clear case and from 67% to 93% in the overcast case. On the right side storage is considered. For the clear day the

system reaches optimal efficiency by using 28% pu battery size for two units and reduces up to 5% pu in the case of 5 units. For the overcast storage sizes decrease from 40% to 5%.

The optimization code was performed in a 3.4 GHz Intel Core i7 processor with 32 GB of RAM. The computational time varies based on the day and the number of units, for the case of $n = 2$ and an overcast day the computational time for the static method takes 2.5 seconds while quasi-dynamic method takes 10 seconds the computational time.

3.5 Conclusions

Considering the intermittency of renewable energy systems, a sizing and scheduling model is proposed for a finite number of static or quasi-dynamic electric loads. The model objective is to maximize system efficiency, which is also defined as solar utilization, with and without storage. For the application of optimal load size selection, the power production of a solar PV is assumed to be consumed by a finite number of discrete loads in an off-grid system using mixed-integer linear programming with constraints, such as, battery charge and discharge limits, and minimum uptime and downtime for each unit. The method was applied to three characteristic daily solar profiles. Different minimum up and down time constraints are also investigated.

By means of a case study, three different days results indicate a system efficiency increased from 82% for two units up to 94% for five units for the clear day and from 67% to 93% for the overcast day. Including battery storage for the clear day, the system requires a 28% pu battery size to reach 100% efficiency for two units, but the battery size reduces to 5% pu for five units.

The results obtained are specific to the location and days presented differ by location and may even vary year-to-year due to spatio-temporal patterns in the solar resources and clouds coverage. The methodology proposed in this paper allows computationally

efficient solutions even when several years of solar resource data are available and yield the optimal sizing for the given data.

For practical applications, the economics also need to be considered as smaller units typically cost more per kW and an optimization based on cost would therefore yield larger and fewer units. Within our framework, it is possible to assign a cost function to the number of units and to the efficiency to allow satisfying needs of practitioners. Similarly, the competition between reduced battery size and larger unit capital cost for more units could be considered in such an economic optimization.

The text and data in Chapter 3, in full, is a reprint of the material as it appears in "Quasi-dynamic load and battery sizing and scheduling for stand-alone solar system using mixed-integer linear programming,". Habib, Abdulelah; Disfani, Vahid R.; Kleissl, Jan; de Callafon, Raymond, *in 2016 IEEE Conference on Control Applications (CCA), 2016,* pp. 1476-1481, 2016. The dissertation author is the primary investigator and author of this article. The following section is a correction on some of this chapter content.

3.6 Correction

$$\mathbf{X} = \begin{bmatrix} x_1 \\ x_2 \\ \vdots \\ x_n \end{bmatrix}$$

$$\mathrm{S} = \begin{bmatrix} S(t_1) \\ S(t_2) \\ \vdots \\ S(t_N) \end{bmatrix}$$

$$\mathrm{P_s} = \begin{bmatrix} P(t_1) \\ P(t_2) \\ \vdots \\ P(t_N) \end{bmatrix}$$

$$\mathrm{P_s} \leq \bar{P}_b \cdot \mathbf{1}$$

$$f(\mathbf{U}, \mathbf{X}, \bar{P}_b, \mathrm{P_s}) = \mathbf{1}^T \cdot (\mathrm{S} + \mathrm{P}_s - diag(\mathbf{X}) \cdot \mathbf{U} \cdot \mathbf{1})$$

$$\mathbf{Y} = diag(X) \cdot \mathbf{U}$$

$$f(\mathbf{U}, \mathbf{X}, \bar{P}_b, \mathrm{P_s}) = \mathbf{1}^T \cdot (\mathrm{S} + \mathrm{P}_s - \mathbf{Y} \cdot \mathbf{1})$$

$$\begin{aligned} \min_{\mathbf{U},\mathbf{X},P_b,\mathrm{P_s}} \quad & f(\mathbf{U}, \mathbf{X}, \bar{P}_b, \mathrm{P_s}) \\ \text{s.t.} \quad & g(\mathbf{U}, \mathbf{X}, \bar{P}_b, \mathrm{P_s}) \leq 0 \\ & h(\mathbf{U}, \mathbf{X}, \bar{P}_b, \mathrm{P_s}) = 0 \\ & \phi(\mathbf{U}, \mathbf{R}, \mathbf{Q}, \mathbf{W}, \mathbf{V}) \leq 0 \\ & \psi(\mathbf{U}, \mathbf{R}, \mathbf{Q}, \mathbf{W}, \mathbf{V}) = 0 \\ & \mathbf{R}, \mathbf{Q}, \mathbf{W}, \mathbf{V} \subset \{0,1\}^{|\mathbf{U}|} \\ & \mathbf{U} \subset \{0,1\}^{|\mathbf{U}|} \end{aligned} \tag{3.10}$$

$$
\begin{aligned}
-\mathbf{Y} &\leq \mathbf{0} \\
\mathbf{Y} - \mathbf{U}M &\leq \mathbf{0} \\
\mathbf{Y} - \mathbf{1}\cdot\mathbf{1}^{\mathbf{T}}\cdot\mathbf{diag}(\mathbf{X}) &\leq \mathbf{0} \\
-\mathbf{Y} + \mathbf{1}\cdot\mathbf{1}^{\mathbf{T}}\cdot\mathbf{diag}(\mathbf{X}) + (\mathbf{U} - \mathbf{1}\cdot\mathbf{1}^{\mathbf{T}})M &\leq \mathbf{0}
\end{aligned}
\tag{3.11}
$$

where M is a real constant number, e.g, 10^6.

With

$$\mathbf{U} = [0,1],$$

$$
\begin{aligned}
-\mathbf{Y} &\leq \mathbf{0} \\
\mathbf{Y} - \tfrac{\mathbf{R}+\mathbf{Q}}{2}M &\leq \mathbf{0} \\
\mathbf{Y} - \tfrac{\mathbf{1}\cdot\mathbf{1}^{\mathbf{T}}\cdot\mathbf{diag}(\mathbf{X})}{2} - \tfrac{\mathbf{R}+\mathbf{1}\cdot\mathbf{1}^{\mathbf{T}}-\mathbf{Q}}{2}M &\leq \mathbf{0} \\
-\mathbf{Y} + \tfrac{\mathbf{1}\cdot\mathbf{1}^{\mathbf{T}}\cdot\mathbf{diag}(\mathbf{X})}{2} - \tfrac{\mathbf{R}+\mathbf{1}\cdot\mathbf{1}^{\mathbf{T}}-\mathbf{Q}}{2}M &\leq \mathbf{0} \\
\mathbf{Y} - \mathbf{1}\cdot\mathbf{1}^{\mathbf{T}}\cdot\mathbf{diag}(\mathbf{X}) &\leq \mathbf{0} \\
-\mathbf{Y} + \mathbf{1}\cdot\mathbf{1}^{\mathbf{T}}\cdot\mathbf{diag}(\mathbf{X}) - \left(\tfrac{\mathbf{R}+\mathbf{Q}}{2} - \mathbf{1}\cdot\mathbf{1}^{T}\right)M &\leq \mathbf{0}
\end{aligned}
\tag{3.12}
$$

where M is a real constant number, e.g, 10^6 and

$$\mathbf{U} = \frac{1}{2}(\mathbf{R}+\mathbf{Q}) \qquad\qquad \mathbf{R}-\mathbf{Q} \geq 0$$

$$\mathbf{U} = [0,1/2,1],\ \ \mathbf{R} = [0,1,1],\ \ \mathbf{Q} = [0,0,1]$$

Chapter 4

Optimal Energy Storage Sizing and Residential Load Scheduling to Improve Reliability in Islanded Operation of Distribution Grids

Despite the increase of modern residential rooftop solar PhotoVoltaic (PV) installation with smart inverters, islanded operation during grid blackouts is limited for most PV owners. This paper presents an optimization method to construe an resource sharing algorithm for islanded operation during blackouts by using shared PV energy. The optimization methods determine if rooftop PV power is either used directly or distributed to neighbors within a residential subsystem. Residential customers, each with a fixed size rooftop PV system are assumed to be connected by a single point of common coupling to a distribution network. The algorithm derives the optimal power distribution to improve the reliability of electricity supply to each residential customer and the results are benchmarked against the isolated self-consumption only mode. In addition, an energy storage system (ESS) is added to quantify the improvement in reliability, whereas a comparison is made between a distributed and centralized ESS deployment strategy.

4.1 Introduction

System level power outages or blackouts typically result in millions of dollars in losses for industry, commercial, and residential customers Horowitz et al. (2010); Liscouski and Elliot (2004); FERC (2012). The main cause of these outages may be equipment failures due to a natural disaster, e.g. the 2011 blackout induced by Hurricane Sandy, where 8 million customers lost power for several days resulting in losses of around US$ 50B Blake et al. (2013); Mansfield and Linzey (2013).

To improve reliability in the presence of a blackout we consider the notion of a (grid)subsystem. A subsystem is defined here as a distributed set of loads and generation assets, identified residential customers, connected to a medium voltage network at a point of common coupling (PCC) and has the ability to be operated independently in case of grid outages (emergency operation mode). Voltage collapse, electric faults, or other drops in power quality at the PCC may trigger the subsystem to operate in island mode Lasseter (2011). An Energy Storage System (ESS) may be used in a subsystem to mitigate the effects of a blackout or intermittency of solar photovoltaic (PV) or wind penetration Jaworsky and Turitsyn (2013); Belloni et al. (2016) and provide ancillary services such as peak shaving and voltage regulation. An ESS also can be applied to the problem of harmonic distortion which may occur in the islanding mode of the subsystem Balasubramaniam et al. (2016) and voltage regulation with many successful examples Yang et al. (2014); Hanley et al. (2008).

In loss-of-load conditions, subsystem power generation capacity is often insufficient to meet all loads. Therefore, an optimization method is required to schedule the critical assets within the subsystem and maximize the utilization of available energy (or minimize unused or lost energy). This problem is commonly referred to as load scheduling or shedding and Mixed-integer Linear Programming (MILP) is a promising

method to exploit convex optimization routines to solve the load scheduling problem. MILP has been used in a variety of areas of power systems such as power distribution network expansion Bahiense et al. (2001); Zhang et al. (2012), unit commitment of power production Viana and Pedroso (2013), and the decentralized energy management problem of a microgrid Ioli et al. (2015).

In this paper, MILP is applied to an optimization-based problem for scheduling loads of a group of conjoined premises or residential customers ("houses"), each with a possible rooftop solar PV system. In the MILP formulation, the optimization aims to minimize the daily solar generation loss. For illustration of the effectiveness of the proposed optimization, actual residential customers load and PV data are used from a case study from the Australian grid Ratnam et al. (2015). Two main operational strategies were considered: isolated self-consumption for each house and an interconnected sharing strategy Habib et al. (2016c). In addition, the possibility of adding an ESS is included in the MILP to improve the reliability of supply and energy losses. Satisfying intuitive expectations, the optimization results show that a majority of the customers score higher reliability of electricity supply when connecting to the subsystem via inter-connected sharing with an ESS.

4.2 Problem Description

4.2.1 Strategies for solar energy sharing in a subsystem

Consider a subsystem with generation units connected to a distribution system via a main circuit breaker (CB) at the point of common coupling (PCC). The main CB is used to isolate the subsystem from the main network in case of power quality disruption or power outages. A residential group of customers ('houses') denoted by the index i, each with its own load, PV system, and additional CB is assumed to constitute the

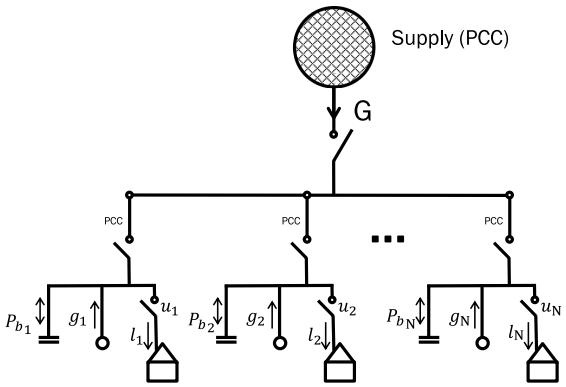

Figure 4.1. Different ESS configuration for power generation and distribution of a residential subsystem of ten houses. u_i controls the ESS operations based on the house load and the solar generation. Where it represents decentralized storage at each house where each house is independently operated (isolated self-consumption) by keeping the PCC switch on.

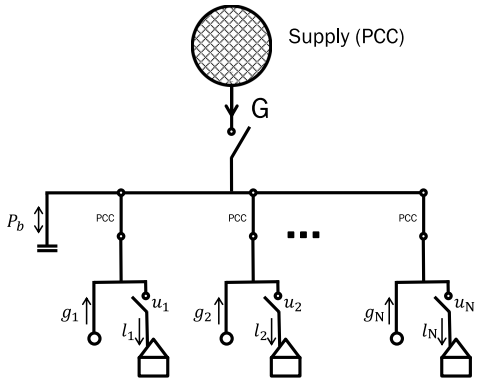

Figure 4.2. Representation of centralized storage for the whole subsystem.

subsystem (Fig. 4.1). The status of the switch connected to the PCC of house i is the decision variable u_i in the optimization problem. If there is insufficient solar power to supply the load at any time step t, then no power is supplied and the solar power is assumed to unutilized (e.g. lost).

Two main operational modes are considered, each with and without ESS. (1) Isolated self-consumption as in Fig. 4.1, where each house is isolated from the subsystem and only able to use whatever available power from PV and/or ESS. (2) Energy sharing, where all houses can supply their electric loads from any PV system and/or a central-

ized ESS. In Fig. 4.2, the decision which houses to (dis)connect is coordinated by an optimization problem that operates with a 30 minutes time step. Minimum up-time and down-time constraint for a supplied load were considered for all strategies as certain appliances require a certain minimum operation time to be effective (e.g. dishwasher).

4.2.2 Model Assumptions

Without loss of generality, the following assumption are made on both the ESS model and power distribution model to formulate a solution to the proposed optimal power scheduling problem. In the ESS model, no power losses or degradation occur in the charge/discharge process, although limits to over charge/discharge are included. Nonlinear effects in energy storage and splly are ignored in the ESS model as well. In usual power distribution analysis lines losses are computed for large geographical distance but in our case, the houses are assumed to be close to each other.

To simplify the analysis, solar power is assumed to be known or represented by a perfect forecast. Load on the side is assumed to be same under grid connected or islanded conditions and no partial load is permitted in this case study. Knowledge of both solar and load is assumed to be known over the simulation period but a moving average is also applicable. Simulation results in this case study are conducted over one year of data.

4.2.3 Illustration of Data

A subset of a dataset with 300 de-identified residential customers with separate meters for load and rooftop PV from a distribution network in Australia was selected. One year was considered for the optimization problem to cover many loads and PV scenarios that may occur. For model validation, the first ten residential customers ($N = 10$) were selected with customers ID [2 13 14 20 33 35 38 39 56 69] as defined in Ratnam et al. (2015) for July 1, 2010, through June 30, 2011.

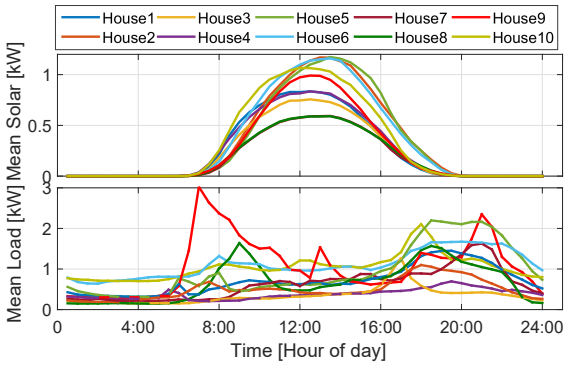

Figure 4.3. Average diurnal cycle of PV generation g_i and load l_i for the $N = 10$ chosen residential customers (houses) over one year.

While the PV rooftop systems vary in size, the total PV rated capacity is rated at 17.3 kW_{AC}. Daily peak solar power averages around 11 kW. The corresponding daytime load peak is around 8 kW with a higher peak in the evening that reaches 13 kW. To understand the diversity of PV generation, the plots in Fig. 4.3 illustrate average PV generation and load for each of the 10 chosen residential customers.

Two sample days (Fig. 4.4) illustrate the varying potential for PV energy to power the subsystem. During the summer season (January in the Southern hemisphere), solar generation is high in comparison to load. On this specific day it happens to exceed load at the solar peak, which is the case on average as well. On the other hand, during the winter season loads are smaller, but solar is much smaller and insufficient to supply all loads at any time of the day.

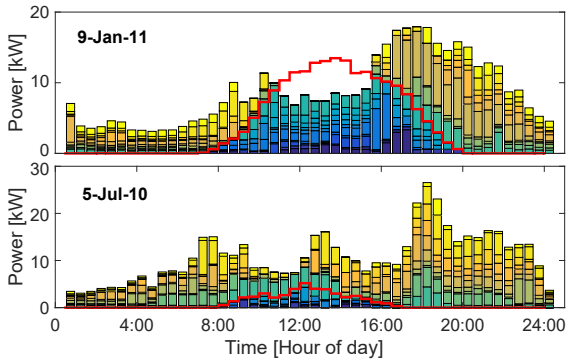

Figure 4.4. Stacked bar chart of load and solar generation (red line) on two sample days in summer (top) and winter (bottom). Each sub bar shows a different house, where the blue colors show load that could be supplied from solar energy in case of an islanded subsystem. Note that January is summer in the southern hemisphere. All results later consider 1 year.

4.3 Problem Formulation

The general form of our optimization problem for residential energy scheduling is of the form

$$\begin{aligned} \max_{\mathbf{U},\mathbf{E_b},\mathbf{E_s},\mathbf{E_0}} \quad & \mathbf{f}(\mathbf{U},\mathbf{E_b},\mathbf{E_s},\mathbf{E_0}) \\ \text{s.t.} \quad & \mathbf{g}(\mathbf{U},\mathbf{E_b},\mathbf{E_s},\mathbf{E_0}) \leq 0 \\ & \mathbf{h}(\mathbf{U},\mathbf{E_b},\mathbf{E_s},\mathbf{E_0}) = 0 \\ & \mathbf{U} \subset \{0,1\}^{|\mathbf{U}|} \end{aligned} \tag{4.1}$$

where the binary decision variable $\mathbf{U} = [u_1, u_2, \cdots, u_N]^\intercal$ is the matrix of switching statuses for all houses at all time steps during a time span such that u_i is the vector of switching statuses for house i. $\mathrm{E_b}$ and $\mathrm{E_0}$ are vectors of size N denoting the ESS energy nameplate capacity and initial stored energy in the ESS, and $\mathrm{E_s}$ is a matrix defining ESS SoC energy at all times. The notation $\mathrm{P_b}$ and $\mathrm{P_s}$ will be used to denote the differential of energy (power). The objective function, inequality constraints, and equality constraints are denoted respectively by **f g** and **h** and discussed in more detail below.

4.3.1 Objective Functions

The main objective function minimizes PV curtailment or maximizes load supply, which can be described as $\mathbf{f}(\mathbf{U})$

$$\mathbf{f}(\mathbf{U}) = \mathbf{1}^{\mathsf{T}}(\mathbf{Y}) \cdot \mathbf{1} - \beta \cdot \mathbf{1}^{\mathsf{T}} \cdot \mathrm{P}_b \tag{4.2}$$

where $\mathbf{1}$ is a vector of ones with length equal to the number of houses N. $\mathbf{L} = [l_1, l_2, \cdots, l_N]^{\mathsf{T}}$ is the load matrix where l_i is the column load vector of house i at all times. The matrix $\mathbf{Y} = \mathbf{U} \circ \mathbf{L}$ denotes the supplied load of any house at any time step where the notation $\circ$ is used to show the Hadamard (element-wise) product of the two matrices. β is a dummy veritable to avoid ESS oversizing.

The switch settings that determines what houses are supplied with power at any time are considered in the objective function (4.2) and the output of the optimization problem.

4.3.2 Constraints

Supply load of any house at any time

The definition of $\mathbf{Y}$ in (4.2) must be reflected in the constraints, thus

$$\mathbf{Y} - \mathbf{U} \circ \mathbf{L} = 0. \tag{4.3}$$

Available Power

In islanding mode, the subsystem cannot provide more than the available solar power. Thus, the total load and ESS charging power that the subsystem can supply must

be less than the total PV energy available at each time step:

$$\mathbf{1}^{\intercal}\cdot\mathbf{Y}+\mathbf{P_s}\leq\mathbf{1}^{\intercal}\cdot\mathbf{G}, \tag{4.4}$$

where $\mathbf{G}=[g_1,g_2,\cdots,g_N]^{\intercal}$ is the PV generation matrix.

Minimum Up-time and Minimum Down-time

A set of constraints are defined to keep a unit which is switched on (off) in the same state for at least m^+ (m^-) time steps before it is switched off (on). This minimum up (down) time constraints decrease the risk of damage to load units and/or inconvenience for residents due to frequent start-ups and shut-downs. They are defined as:

$$\begin{aligned} u(i,t)-\Sigma_{h=t-m_i^+ +1}^{t}v(i,h)\leq 0 \quad & \forall_{m_i^+\leq t\leq T} \\ (1-u(i,t))-\Sigma_{h=t-m_i^- +1}^{t}w(i,h)\leq 0 \quad & \forall_{m_i^-\leq t\leq T}, \end{aligned} \tag{4.5}$$

where the matrices $\mathbf{V}\subset\{0,1\}^{N\times T}$ and $\mathbf{W}\subset\{0,1\}^{N\times T}$ are start-up and shut-down matrices with the elements defined as:

$$\begin{aligned} & v(i,t)-w(i,t)=u(i,t)-u(i,t-1) && \forall_{1\leq i\leq N}\forall_{2\leq t\leq T} \\ & v(i,t)+w(i,t)\leq 1 && \forall_{1\leq i\leq N}\forall_{2\leq t\leq T} \\ & v(i,1)=w(i,1)=0 && \forall_{1\leq i\leq N}, \end{aligned} \tag{4.6}$$

where N is the number of houses and T is the simulation time.

ESS Constraints

Assuming that the efficiency of the ESS is 100%, the ESS constraints are given by

$$-\mathrm{P}_b(i)\leq\mathrm{P_s}(i,t)\leq\mathrm{P}_b(i) \tag{4.7a}$$

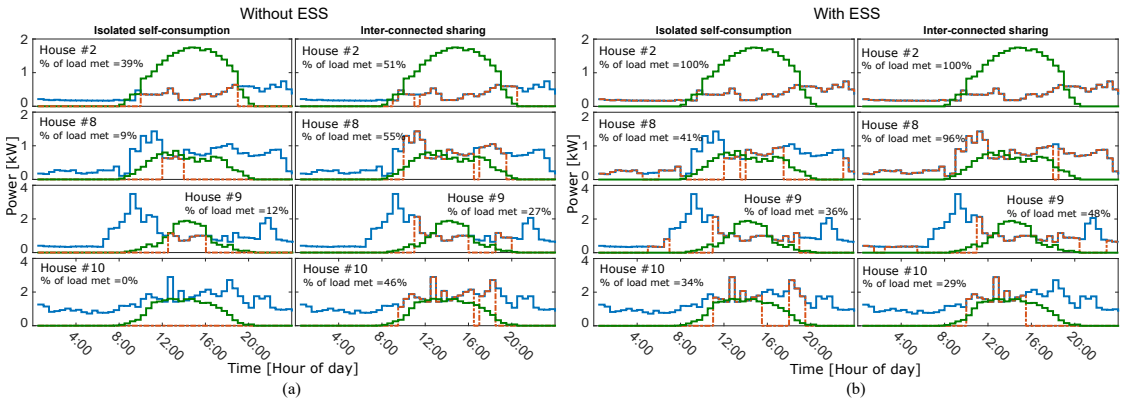

Figure 4.5. Hourly results for four different houses for a summer day (Jan 9), where the blue line shows load, the red line represents supplied load, and the green line shows solar power. Isolated and connected scenarios are compared side-by-side for the case (a) Without ESS, and (b) With ESS. The subsystem solar utilization on Jan 9 is (24, 80.4, 92.2, 100)% and the percentage of load met is (10.8, 35.6, 40.8, 44.6)% for all scenarios from left to right respectively.

$$\mathrm{E}_s(i,t) = \Sigma_{h=1}^{t} \mathrm{P}_s(i,h)\Delta t + \mathrm{E}_0(i) \tag{4.7b}$$

$$\rho_{min}\mathrm{E}_b(i) \leq \mathrm{E}_s(i,t) \leq \rho_{max}\mathrm{E}_b(i) \tag{4.7c}$$

$$\mathrm{E}_s(i,1) = \mathrm{E}_0(i) \tag{4.7d}$$

$$\forall_{i\in N}\, \forall_{t\in T}\, \forall_{t_1\in\{24k \text{ hours}|k\in\mathbb{N}\}}$$

where $\mathrm{P_s}$ denotes the charging/discharging power schedule matrix for the ESS for each time step t and house i. The maximum charging/discharging power of the ESS is limited to the ESS rating Eq. (4.7a). Second Eq. (4.7b) calculates the energy stored in the ESS at each time step t for house i. Further, deep discharge should be avoided for ESS health where ρ_{max} and ρ_{min} are applied in Eq. (4.7c) to be usually around 0.9 and 0.1, respectively. Eq. (4.7d) guarantees that no energy shift happens betweens days by keeping

the level of energy at the end of each day equal to its initial value E_0. The power:energy ratio is assumed to be 4:1, i.e. $4 \times E_b = P_b$. To allow a cleaner analysis without energy shifting from one day to the next, the initial (E_0) and final state of charge (SoC) during a day are set to be equal which is fulfilled by the second constraint in Eq. (4.7d).

As the objective function and constraints contain both binary (integer) and real valued optimization variables and all constraints in (4.1)-(3.9) are linear, the optimization problem is Mixed-Integer Linear Programming (MILP). Therefore commercial MILP solvers such as Gurobi through CVX can solve the problem and used in this paper for the numerical optimization.

4.3.3 Optimization Success Metrics

To compare the simulation results of different strategies with and without ESS, two metrics are considered in this paper. The first metric is the percentage of supplied load (the ratio of supplied load to the total load) determined as

$$\% \text{ of Load Met} = (\mathbf{Y} \cdot \mathbf{1}) \oslash (\mathbf{L} \cdot \mathbf{1}),$$

where $\oslash$ denotes element-wise division.

The other metric is the PV utilization percentage (the ratio of utilized PV generation to total PV generation) defined as

$$\% \text{ PV Generation Utilization} = (\mathbf{1}^\intercal \cdot \mathbf{G}) \oslash (\mathbf{1}^\intercal \cdot \mathbf{L}).$$

4.4 Numerical Results

In this section, the results are presented in three parts. The first two parts are designed to discuss the results of two main scenarios, i.e. subsystem with and without

ESS, each of which considers both isolated self-consumption and inter-connected power sharing cases. The third part summarizes and compares the long-term effects of these four scenarios on the subsystem operation over the course of one year.

4.4.1 Subsystem without ESS

An hourly example for a summer day (Jan 9 in Australia) and four sample houses #(2, 8, 9, 10) is presented in Fig. 4.5(a) for both isolated self-consumption and inter-connected power sharing scenarios. Under ideal conditions of a clear mid-summer day with high solar production, the load of most houses is met during the middle of the day. However, excess solar power is lost and no load is served during hours that do not coincide with peak insolation. For house #2, total solar power generation exceeds total power demand the most. The excess PV energy could not be captured in the isolated self-consumption case while is was shared with the other houses in the inter-connected case.

As a result of the minimum up-time constraints, no load was met for house #2 between 0900 and 1100h. Alternatively, in the power sharing case, more load was met between 0900 to 1100h, because only a small amount of energy from other houses is needed to satisfy the minimum up time constraint. However, some power was not met around 1100h, which might have been used to supply other houses since every house is treated equally to achieve the overall smallest solar power losses. For house #10, the load is higher than solar power at all times except a one-hour period around 1300 h. As a result, its demand is never met in the isolated self-consumption case (the brief period of excess solar power is too short to meet the 1.5(0.5) h minimum up(down)-time). House #10 benefit greatly from power sharing increasing % load met on this day from zero to 46%.

Fig. 4.6 shows average daily results for the subsystem without ESS over the

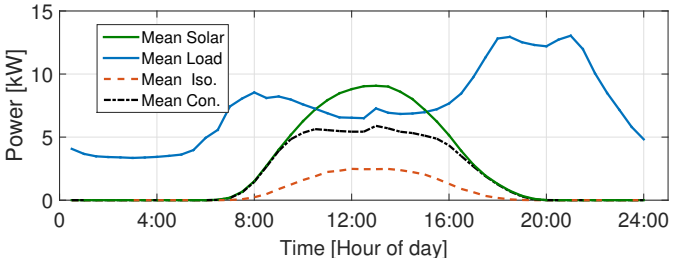

Figure 4.6. Yearly average daily cycle of solar and load (equal to the average of Fig. 4.3) for load met for isolated self-consumption and inter-connected sharing modes for without ESS.

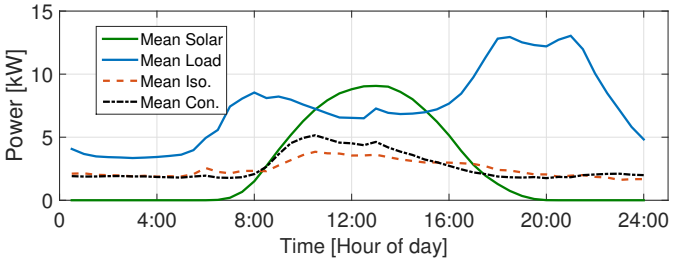

Figure 4.7. ESS allow shifting the load to the shoulders of the day.

course of a year for the isolated self-consumption and the inter-connected sharing. For the isolated self-consumption case, house load is only met during the day when solar generation exceeds load consumption for the minimum up-time. As a result, only 9% of the total load is met as shown in Table 4.1 while the percentage of load met was almost three times scoring 26.3% for the sharing case. Lost power occurs due to several scenarios: (i) At the solar peak (noon time) total solar is higher than total load. (ii) The optimal combination of houses has a discrete load that is usually less than the available solar power. (iii) Minimum up and down times limit the choice of which houses to power causing less discrete load levels. No load can be met during periods of no solar generation at night.

4.4.2 Subsystem with ESS

The optimization solves for the optimal ESS size P_b [E_b] for every house for the isolated self-consumption case as shown in Table 4.2 and for the inter-connected sharing ESS as shown in Table 4.1. The grid connected case resulted in an ESS size of 259.2 kW [64.1 kWh] which is 43% less than the aggregated ESS size for the isolated case. The ESS initial SoC for every day is optimized for the isolated case to average around 5 kWh and 21.6 kWh for the connected case.

Table 4.1. Percent load met and optimal ESS size for different operating strategies over the year.

	% of load met	$P_b[E_b]$ kW [kWh]	% of PV gen. utilized
Iso. without ESS	9.2	0	25.8
Iso. with ESS	33.7	460.1 [115.1]	94.9
Con. without ESS	26.3	0	74.0
Con. with ESS	35.5	259.2 [64.1]	100

Table 4.2. Optimal ESS size E_b and initial SoC E_0 for each house in the isolated self-consumption mode.

Houses	E_b (kWh)	E_0(kWh)	% PV of gen. utilized
1	10.6	5.2	99.3
2	12.7	4.5	82.8
3	8.0	3.1	93.3
4	13.5	6.7	79.6
5	17.2	7.2	99.3
6	11.6	5.5	98.9
7	9.1	3.8	99.0
8	8.5	3.6	99.6
9	11.2	6.0	99.4
10	12.7	5.0	99.1
$\sum E_b$	115.1		

Fig. 4.5(b) illustrates the summer day example with ESS. For the isolated self-consumption case ESS are installed locally and only serve a particular house. The ESS

size is optimized to maximize the local solar utilization. If daily solar energy exceeds daily load as for house #2, excess solar energy during daytime can be stored in the ESS and all load is met. If daily solar energy is smaller than daily load, then times with loss of load remain. For example, houses #(8, 9, 10) were able to meet the smaller load during the night or early morning but missed some of the peaks due to the limitation of solar energy.

In the connected case, the subsystem installs a community ESS operated for the benefit of all. With ESS, the differences between isolated and connected cases are small. Houses #(8, 9) improved the load met with connection but at the expense of house #10. Comparing to the case without an ESS, the ESS demonstrates value by storing unusable solar power that can be shifted to later times to meet load and minimum up-time constraints.

Fig. 4.7 shows the annual average daily cycle for both isolated and connected operation modes with ESS. The isolated self-consumption case supplies 33.7% of the total load while the interconnected sharing case supplies 35.5% of the total load. Adding an ESS flattens the curves of load met by shifting daytime solar energy to night time. The connected case performs better, from 0900 till 1500 h. Although ESS installation is expected to increase the load met for the whole system, the model cannot guarantee the same for individual houses. For example, House #10 captured less load with the ESS case because meeting other houses' load decreases the system loss.

Table 4.2 presents optimal ESS size for each house in the isolated self-consumption mode as well as the corresponding solar utilization factor. The solar utilization factor is over 93% for most houses except houses #(2, 4). For houses #2 and #4, the low PV utilization factor is due to oversized solar systems together with the fact that excess solar energy cannot be exchanged within the subsystem and cannot be shifted between days. The problem is exemplified during two weeks, when solar far exceeds the load demand,

presumably due to the absence of the residents (Fig. 4.8). Most of the solar energy during these two weeks is lost.

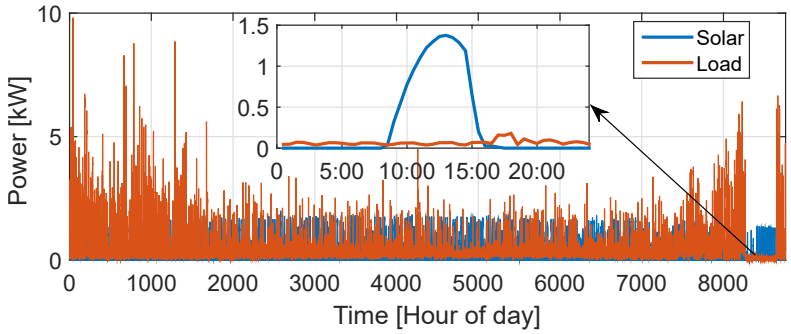

Figure 4.8. Illustration of one year of solar and load data for house#2. The inset shows a day of low demand during a period of absence of the residents.

4.4.3 Effects of Various Scenarios on subsystem Operation

Fig. 4.9 presents the different operation scenarios for all months to capture the seasonal effect on the subsystem. Winter (May till August in Australia) reduces the load met because of the seasonal drop in solar generation. The peak of load met therefore occurs during the highest summer month November. As expected, the isolated self-consumption without ESS captures the least load. The inter-connected sharing mode scores the best for the subsystem over the year. A comparison of different operation modes by house is shown in Fig. 4.10. Adding ESS to the isolated case at least triples the load met for each house. The inter-connected sharing case with ESS supplies the most load for 5 out of 10 houses, while houses #(2, 5, 6) prefer to be isolated with ESS, and houses #(4, 10) achieve the same load met for these two scenarios.

Not only does the power sharing case with ESS show slightly better results than the isolated case with ESS, but it also leads to a 44% reduction in the total size of ESS installation on the subsystem.

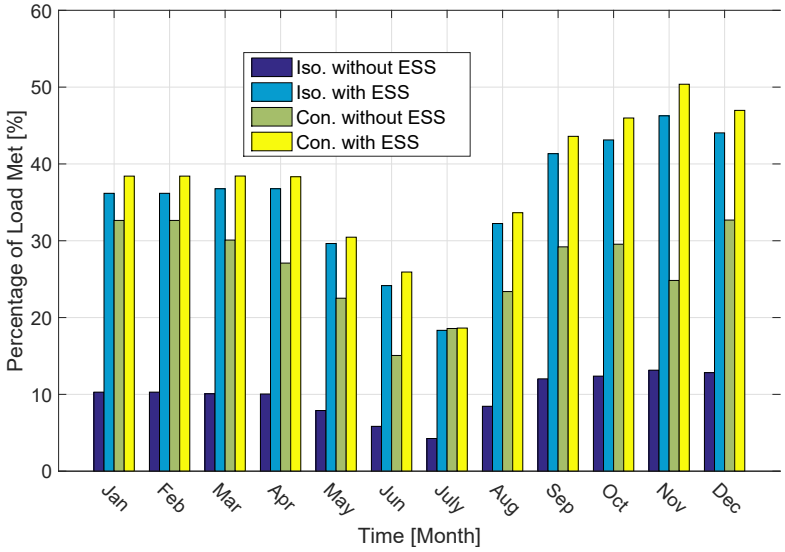

Figure 4.9. Monthly results for the percentage of load met for different strategies averaged over all houses.

4.5 Conclusions

An optimization based residential customer scheduling based on mixed-integer linear programming is proposed to increase the reliability of power delivery for subsystem customers during (macro)grid blackouts or emergency islanded operation. An actual yearly dataset for PV and load of ten residential customers was used as a benchmark study to illustrate the results. The benchmark results illustrate the benefit of the optimal scheduling: an interconnected scenario in which rooftop PV power is shared across the members of the subsystem greatly improves solar energy utilization compared to the isolated scenario in which each residential customer only supplies their own electrical load.

The isolated and interconnected scenarios are also studied in the presence of a local and centralized Energy Storage System (ESS). For that purpose, the proposed optimization is able to compute the optimal ESS size, the daily initial State of Charge (SoC) and the charge/discharge schedule of the ESS for the isolated and the connected

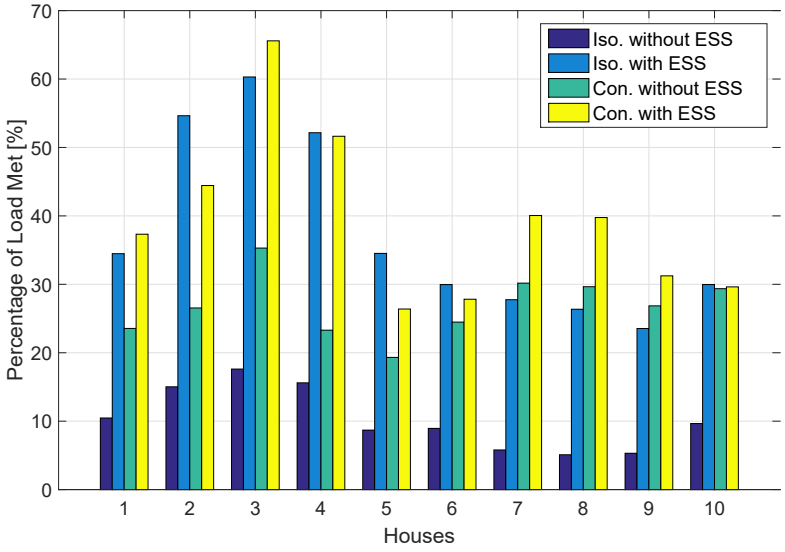

Figure 4.10. Yearly optimization results for all houses using different operation scenarios.

scenarios. This paper shows that, despite variability and intermittency of PV power generation, an ESS can substantially improve electric power reliability by almost four times compared to the situation without a centralized ESS. In addition, the centralized ESS strategy results in a smaller ESS size with a higher percentage of load met and solar utilization.

The decision to install an ESS and whether or not to operate in an isolated and interconnected scenario can be studied by the proposed optimization based residential customer scheduling. With an ESS, residential customers with oversized PV systems fair better when remaining disconnected, but the investments in ESS capacity for the entire subsystem almost double. Therefore, it may be concluded that the interconnected centralized ESS strategy is preferred as it supplies 100% of the load for a smaller capital investment in ESS. As the best strategy may depend on PV size, the results motivate further research on socio-economic considerations and fairness arguments to incentive residential customers with large PV systems to participate.

The text and data in Chapter 4, in full, is a reprint of the material as it appears

in“Optimal Energy Storage Sizing and Residential Load Scheduling to Improve Reliability in Islanded Operation of Distribution Grids”. Habib, Abdulelah; Disfani, Vahid R.; Kleissl, Jan; de Callafon, Raymond, *2017 American Control Conference (ACC)*, Seattle, WA, 2017, pp. 3974-3979. The dissertation author is the primary investigator and author of this article

Chapter 5

Market-Driven Energy Storage Planning for Microgrids with Renewable Energy Systems Using Stochastic Programming

Battery Energy Storage Systems (BESS) can mitigate effects of intermittent energy production from renewable energy sources and play a critical role in peak shaving and demand charge management. To optimally size the BESS from an economic perspective, the trade-off between BESS investment costs, lifetime, and revenue from utility bill savings along with microgrid ancillary services must be taken into account. The optimal size of a BESS is solved via a stochastic optimization problem considering wholesale market pricing. A stochastic model is used to schedule arbitrage services for energy storage based on the forecasted energy market pricing while accounting for BESS cost trends, the variability of renewable energy resources, and demand prediction. The uniqueness of the approach proposed in this paper lies in the convex optimization programming framework that computes a globally optimal solution to the financial trade-off solution. The approach is illustrated by application to various realistic case studies based on pricing and demand data from the California Independent System Operator (CAISO). The case study results give insight in optimal BESS sizing from a cost perspective, based

on both yearly scheduling and daily BESS operation.

5.1 Introduction

The need for a Battery Energy Storage System (BESS) to serve as a buffer for electric energy is palpable for microgrid systems that have a large penetration of intermittent renewable energy sources. A BESS may be economical for both islanded microgrids and a for grid-connected system, as a BESS increases reliability during outages and provides revenue or grid services such as peak shaving, voltage regulation, and arbitrage power trading during normal operation Lasseter (2002); Donadee (2013); Kousksou et al. (2014) .

Applications of a BESS can be found in various settings to assist with renewable power integration. It has been applied to the problem of harmonic distortion, generally known as voltage regulation, which may occur in standalone operation (islanding) of a microgrid Yang et al. (2014); Hanley et al. (2008). Specifically, a BESS can be used to reduces the effects of Photo Voltaic (PV) and wind energy production variability Teleke et al. (2010); Zheng et al. (2015) by different control strategies such as a rule-based control and a model predictive control (MPC). A BESS in conjunction with PV and demand forecasting can help shift renewable generation to times of higher power demand or lower electricity price via an MPC technique Sevilla et al. (2015). A mathematical model for a large BESS system was performed in Zhang et al. (2015) as a reduced four state space equations to model the relation between the bulk power grid and a BESS.

The benefits of BESS in coping with variable renewable energy production are evident, but the costs associated with financing and installing BESS are often prohibitive. In particular for residential settings Holbert and Chen (2015), a BESS may not produce sufficient revenue from energy arbitrage to achieve investment payback without government incentives to fund the BESS. At the same time, BESS costs are anticipated to drop

in the near future and investment banks are expecting the payback time for unsubsidized investment in electric vehicles (EV) combined with rooftop solar and BESS Houchois et al. (2014) to reduce to around six to eight years. Also, the economies of scale due to the adoption of EV and rapid improvement of battery technologies will likely reduce BESS prices. As a result, the projected reduction in pricing of BESS is expected to lead to a return on investment within a time frame of three years by 2030 Nykvist and Nilsson (2015); Sachs (2014).

Optimal BESS sizing from an economical perspective must find the optimal trade-off between critical design parameters that include BESS sizing, BESS life expectancy due to battery degradation and total revenue from utility bill savings due to energy arbitrage. Holistic BESS scheduling models that aim to capture all cost aspects were developed in Nguyen et al. (2012) to maximize the overall profit of an existing wind-storage system. Economic models were used in Ornelas-Tellez et al. (2014) to predict the market price to optimize the operation of existing energy resources in a microgrid, but no future investments were considered. Operational stochastic control and optimization in Zachar and Daoutidis (2016) were designed as an MPC to ensure sufficient energy as an economic dispatch problem.

Motivated by the need to find the optimal BESS investment as a function of time considering capital and O&M costs, as well as operational revenues, this paper proposes a stochastic optimization approach that leverages mixed integer and real (convex) optimization to formulate financially optimal BESS sizing solutions. The stochastic optimization is used to address the variability in prediction and forecasting of energy and BESS pricing to determine when is the optimal time to invest in a BESS. The convex optimization is used to compute globally optimal solutions for BESS sizing parameters, given the operational model and the price variability in the day-ahead market.

The paper is outlined as follows. First, the problem formulation and the system

topology for financial optimization are summarized in Section 5.2. The mathematical framework is summarized in Section 5.3, explaining the optimization techniques, objective functions and the constraints. Different operating scenarios are discussed and compared in Section 5.4 to cover cases of extreme high/low power variability in solar, wind and demand patterns. In Section 4.4, different BESS installation cases and optimal BESS sizing for a case study of a real microgrid are presented.

5.2 System Topology and Pricing

5.2.1 Microgrid and Market Structures

Fig. 5.1 illustrates the structure of power market and microgrids used in this paper. The microgrid is modelled as a subset of the market $\mu G \subset \mathcal{N}$, and demand, renewable generation, and BESS power in both market (m) and microgrid (μ) are denoted by P_d, P_{RE}, and P_b, as illustrated in Fig. 5.1.

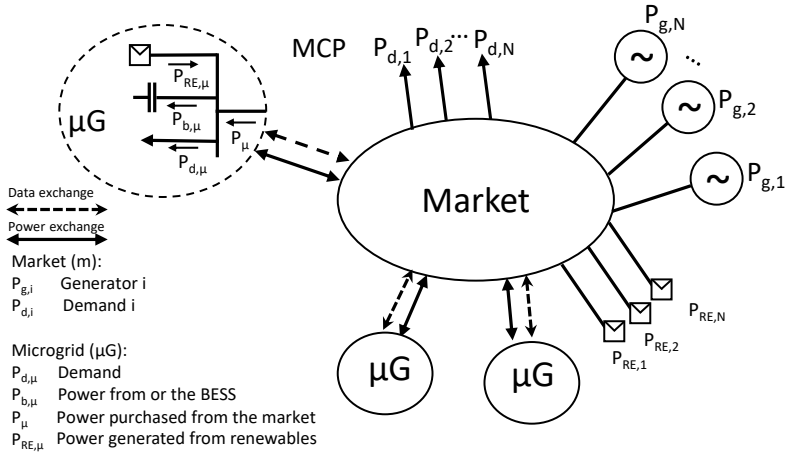

Figure 5.1. Power market system architecture.

The net demand P_{net}, which is the actual market demand (including all microgrids' demand) minus the total renewable power available in the market, is computed via

$$P_{net} = \Sigma_{i \in \mathcal{N}} \left(P_{d_i} - P_{RE_i} \right) = \Sigma_{i \in \mathcal{N}} P_{g_i} \tag{5.1}$$

where P_{g_i} indicates power provided by generator i and

$$P_{\mu} = \Sigma_{j \in \mu G} \left(P_{d_j,\mu} + P_{b_j,\mu} - P_{RE_j,\mu} \right) \tag{5.2}$$

5.2.2 Market Clearing Price Modeling

Assuming that the microgrids will pay the hourly market clearing price (MCP) in the future instead of predefined constant or time-of-use (TOU) rates, a price model is required to anticipate the MCP at different times for optimal operation of microgrids.

Typically, Independent System Operators (ISO) aggregate the bids received from generators and cross it with the net demand hourly profile of the market to define hourly MCP. It is assumed that the MCP is solely a function of the net demand in that λ_P is linearly correlated with the market net demand P_{net} via

$$\lambda_P = \alpha \, P_{net} + \beta. \tag{5.3}$$

This pricing modeling has been validated in the literature Huang et al. (2015); Verzijlbergh et al. (2014). It is assumed for simplicity that the parameters of the MCP model (α, β) remain constant throughout the 15 year modeling horizon. However, the optimization could consider more detailed and dynamic models where the pricing model parameters vary as generators are added or removed.

To model the effects of different generators' bidding strategies and maintenance schedules on different days of the week (weekdays and weekend) and different seasons (summer and non-summer) on MCP, four distinct MCP models are fit from historical CAISO demand and pricing data.

5.2.3 Microgrid and Power Market Growth

For realistic financial predictions and optimal sizing of the BESS, the financial model considers the annual growth of both the market and the microgrid. The growth of the market and the microgrid takes into account all components, i.e. demand, solar and wind.

For simplicity, we assume a fixed annual solar growth (ASG) defined by

$$ASG = \frac{S_{t+1y} - S_t}{S_t} \times 100\%$$

where S_t represents the vector of hourly solar profiles of the current year. Hence, with a fixed ASG, the net solar power S_{t+1} contribution is predicted to grow exponentially as

$$S_{t+1} = \left(\frac{ASG}{100} + 1\right) S_t$$

with $ASG > 0$. Similarly, we assume a fixed annual wind growth (AWG) as

$$AWG = \frac{W_{t+1y} - W_t}{W_t} \times 100\%.$$

The CAISO historical demand data shows different rates of increase at different hours of the day, specifically power demand at the peak hour has grown faster than at off-peak hours. to account for this effect, we define an annual demand growth profile (ADGP) that varies by hour of the day as

$$ADGP = (D_{t+1} - D_t) \oslash D_t \times 100\%,$$

where D_t is the vector of hourly power demand at year t and $\oslash$ denotes element-wise division.

5.3 Stochastic BESS Optimization

5.3.1 Objective Function

A stochastic programming model is developed to capture all possible scenarios of solar and wind generations, demand variations, and supply bidding strategies in the BESS sizing and operation problem.

The objective function is defined to minimize the expected energy cost, i.e. the sum of energy purchase costs and the BESS investment cost over a time period T while considering annual growth in solar, wind and demand. Mathematically, for an optimization horizon T and scenario set of Ω, the objective function is defined as

$$\min_{P_{b_{\max}}, P_b} \Sigma_{t \in T} \left\{ J_{b,t} + \Sigma_{i \in \Omega} Pr_i J_{i,t} \right\} \cdot v_t \; - v_{b,t} \cdot v_t, \tag{5.4}$$

where $P_{b_{\max}}$ and P_b are the power rating and the vector of dispatched power of the battery respectively. Pr_i refers to the probability of a scenario i and

i $J_{b,t}$ refers to the investment cost of BESS installed in year t.

ii $J_{i,t}$ is the total cost of energy purchased from the market in year t for the scenario i, and is given by

$$J_{i,t} = \Lambda_{i,t}^{T} \mathrm{P_{i,t}} \Delta \mathrm{t}.$$

$\mathrm{P_{i,t}}$ and $\Lambda_{i,t}$ are respectively the hourly vectors of power demand from the energy markets and MCP in year t and scenario i, and Δt is the time difference between two consecutive time steps.

iii $v_{b,t}$ accounts for the remaining value of the unexpired BESS purchased at time t at the end of the simulation period.

iv As is common in economic models $v_t = (1-\gamma)^t$ discounts the monetary value in future years using an annual interest rate of γ.

5.3.2 Constraints

Resource Adequacy:

At any time step, the microgrid control center (MGCC) must ensure that there is adequate power to supply demand. Therefore, any mismatch between the power demand and the summation of solar power output, and BESS discharging power must be purchased from the market to keep the power balance at any time step t and scenario i. This constraint is summarized as

$$P_{RE_{i,t}} + P_{b_{i,t}} + P_{i,t} = L_{i,t} \tag{5.5}$$

where $P_{i,t}$ is the power purchased from the market.

Battery Constraints:

First, the battery charging/ discharging power must be between the limits, *i.e.*

$$-P_{b_{max}} \leq P_{b_{i,t}} \leq P_{b_{max}}$$

To avoid damages due to a deep (dis)charge cycle of the battery, the stored energy in the battery is constrained by its maximum and minimum SOC limits (ρ_{min}, ρ_{max}) as

$$\rho_{min} E_{b_{max}} \leq E_{b_{i,t}} \leq \rho_{max} E_{b_{max}}$$

where ρ_{min} and ρ_{max} are typically around 10% and 95%. The energy stored in the battery

is denoted by $E_{b_{i,t}}$ and calculated via

$$E_{b_{i,t}} = \Sigma_{h=1}^{t} P_{b_{i,h}} \Delta t + E_{b_{i,0}}$$

with $\mathrm{E}_{b_{i,0}}$ as the initial BESS energy.

It is also desired to keep the final SOC of the BESS equal to its initial value at the end of each day. This constraint is needed to avoid transferring energy between days and included via

$$E_{b_{i,t_1}} = E_{b_{i,0}}$$

for any $t_1 \in \{24k \text{ hours},\ k \in \mathbb{N}\}$. Finally, the ratio between the nominal power rating and energy rating of the BESS implemented by

$$2 \times E_{b_{max_i}} = P_{b_{max_i}}$$

as the last battery constraint. Obviously, more advanced battery constraints that take into account parasitic loss and efficiency parameters could be used to provide even more realistic battery constraints.

Power Congestion Constraint

A power congestion constraint limits the power purchased from the market due to the physical limit of the microgrid at the point of common coupling (PCC) or upstream power lines. Power congestion constraints may, for example, limit the BESS' ability to charge at $P_{b_{max_i}}$ during (or within) the cheapest price. By including a power congestion constraint

$$-P_L \leq P \leq P_L \tag{5.6}$$

the BESS will be charged over a longer time frame to accommodate the congestion limit P_L.

5.3.3 Scenarios

The most accurate results would be obtained by simulating a typical meteorological and climatologically representative timeseries over a year (or longer), but this is computationally intensive. Instead, we consider year's (2015) worth of data, downsampled to a set of typical days and these days are repeated each year.

Subsequently, a manual clustering is applied to classify demand profiles in representative patterns. The clustering assembles the data into four main groups that resemble a summer/non-summer and weekday/weekend separation. Fig. 5.2 illustrates all demand profiles clustered in those four groups, each identified by a distinct color. The clustering can then be used to formulate an average for each group as depcited in the top plot of Fig. 5.3.

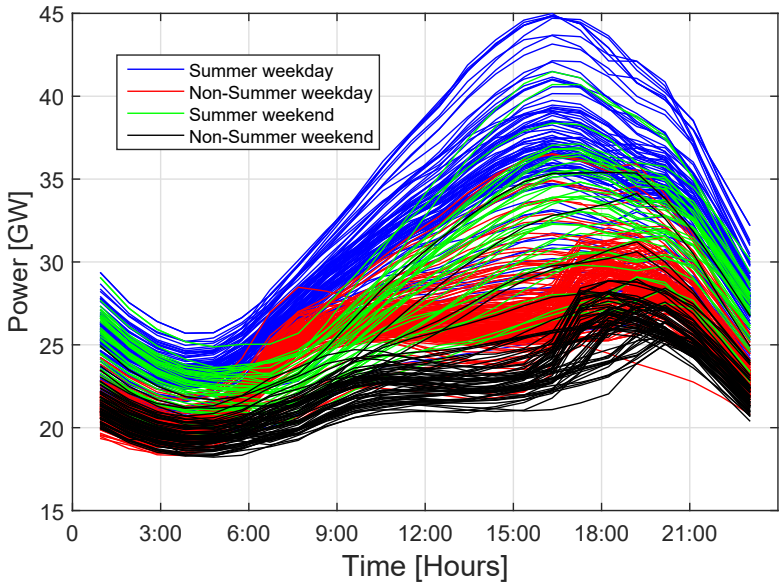

Figure 5.2. Daily demand profiles for the CAISO market for one year (2015). Colors denote different clusters classified by (week)days and (non)summer season.

Although usually intermittent in nature, solar and wind power profile over the complete state of California tends to be smooth and easily separable into a small number of distinctive patterns. Only a binary classification of *high* and *low* is applied in this paper to cover the state-wide range of patterns in solar and wind power generation. Clusters were obtained by the popular k-means clustering method MacQueen (1967), which aims to partition time series data into two clusters. Clear days are presented as the *high* solar case, whereas overcast days are denoted by *low* solar case. The bottom plot of Fig. 5.3 illustrates the 4 different scenarios for high/low solar and wind.

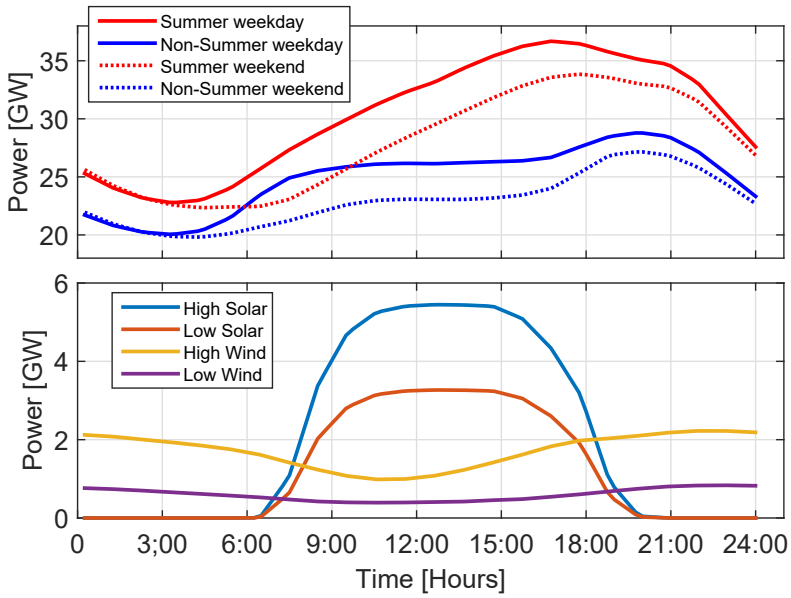

Figure 5.3. Top: average of demand profiles clustered in 4 categories. Bottom: the 4 categories of high/low solar/wind and used as λ_P in (5.3) for pricing modeling.

For unambiguous notation we use H and L as abbreviated notations for the *high* and *low* and summer weekday and summer weekend and non-summer weekday and summer weekend as $\{SWD,SED,NSWD,NSED\}$ for power/demand conditions, while S, W, and D are used for *solar*, *wind* and *demand*. The binary classification with the demand scenarios allows $4 \cdot 2 \cdot 2 =$ 16 scenarios. A summary of the 16 scenarios based on the

binary classification of *high* and *low* solar, wind and demand

$$\begin{aligned}\Omega = &\{HS, LS\} \times \{HW, LW\} \\ &\times \{SWD, SED, NSWD, NSED\}\end{aligned} \tag{5.7}$$

is given in Table 5.1. Clearly, more granular clustering, e.g. by adding seasonal effects on variables such as (solar, wind), will increase the accuracy of the optimization, but also the computational cost.

Table 5.1. Scenarios i for CAISO demand and renewable generation. The probability of each scenario Pr_i is given in the last row.

Demand	Summer								Non-Summer							
	weekday				weekend				weekday				weekend			
Solar	H		L		H		L		H		L		H		L	
Wind	H	L	H	L	H	L	H	L	H	L	H	L	H	L	H	L
Scen.	1	2	3	4	5	6	7	8	9	10	11	12	13	14	15	16
Pr	3.2	7.4	4.7	11.0	1.2	2.8	1.8	4.1	5.4	12.7	8.1	19.0	2.2	5.2	3.4	7.8

Each scenario is assigned a probability consistent with climatological data in a certain location. The probability of each scenario is defined by multiplying the corresponding individual probabilities and is used as a weighting of that scenario in the optimization of (5.4), e.g.

$$Pr(\{HS, LW, SWD\}) = Pr(HS) \cdot Pr(LW) \cdot Pr(SWD). \tag{5.8}$$

Individual probabilities of solar, wind and demand are mutually independent and the probability of all possible scenarios sums to 100%.

5.4 Case Studies and Simulations

5.4.1 Market Clearing Price Models

The MCP models developed for each demand cluster are shown in Fig. 5.4.

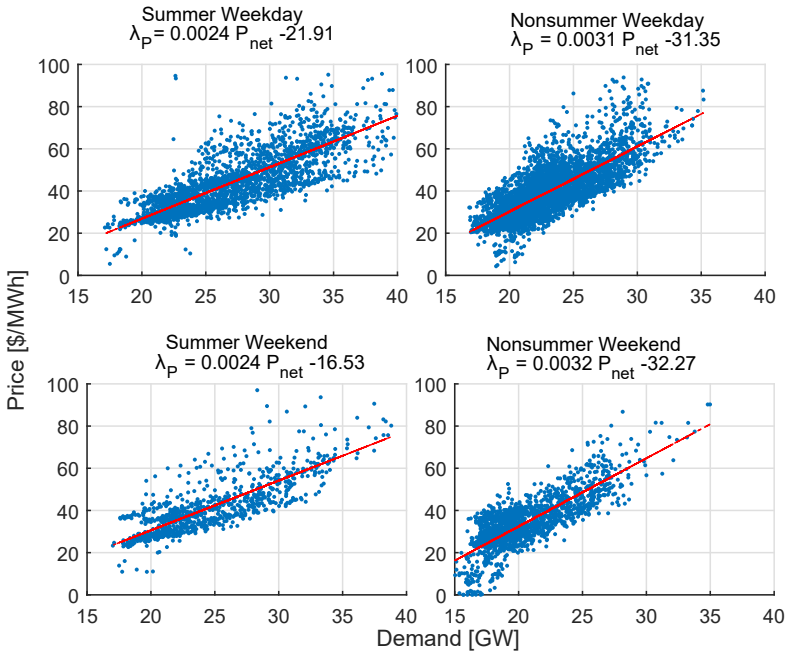

Figure 5.4. CAISO price model fits as a function of net demand for each demand type (title).

The CAISO MCP λ_P derived from Eq. (5.3) is the main input to the market model to determine the size and the daily operation of the BESS. The parameter λ_P varies based on the different scenarios as shown in Fig. 5.5. The highest market price is associated with low solar, low wind and summer weekday demand (scenario 4). Conversely, the scenario with non-summer weekend demand, high solar, and high wind results in the smallest λ_P. Negative pricing may appear also as a result of the assumed inability to curtail renewables; after renewable generators lose their protected "must-take" status, they will be curtailed in such a situation to avoid negative pricing. In this case, it is cheaper to temporarily pay market participants to take power rather than turning off

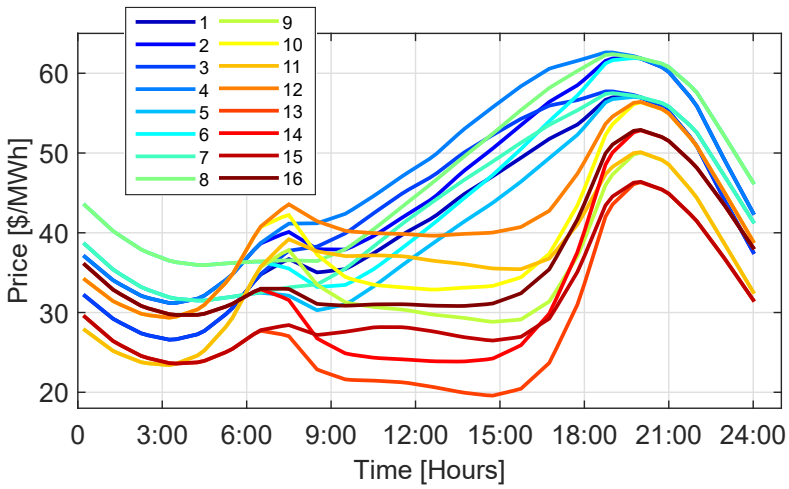

Figure 5.5. Market clearing price (MCP) λ_P for different scenarios (Table 5.1) for the first year.

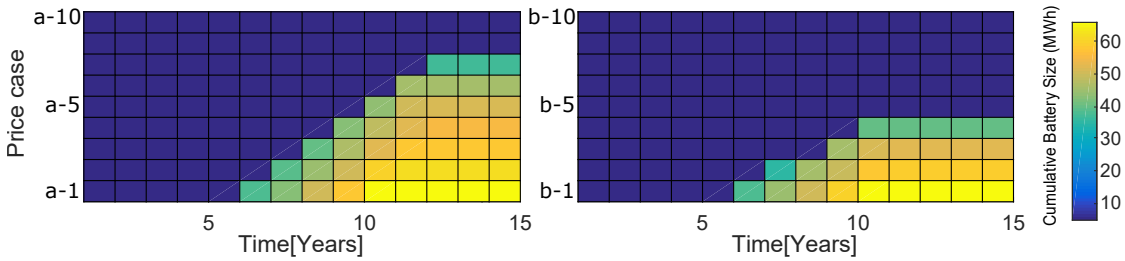

Figure 5.6. BESS installation schedule by year for BESS price scenarios (a) on the left and (b) on the right.

base-load power plants.

5.4.2 Case Study

The case study uses CAISO demand data and the location marginal pricing (LMP) node (UCM_6_N001) located at (32°53'00.9"N 117°13'21.2"W) which is the trading node containing UC San Diego. The simulated case has a peak market demand around 45 GW and a low demand (base-load) around 18 MW. The 2015 utility scale solar and wind peaks are around 5.7 and 2 GW respectively. Clear solar days are assumed to occur 30% of the time, overcast days 70%, and high wind 40% of the time and low wind 60%. Different demand scenarios follow the calendar with 96 and 36 days for

summer (May 1 to Oct 31) weekday and weekend, respectively and 165 and 68 days for non-summer weekday and weekend, respectively. By that, the Pr shown in (5.8) is given by $Pr(Scen1) = Pr(\{HS, HW, SWD\}) = 0.30 \cdot 0.40 \cdot 96/365 = 3.2\%$. The time step for all data and optimization schedules is 15 minutes.

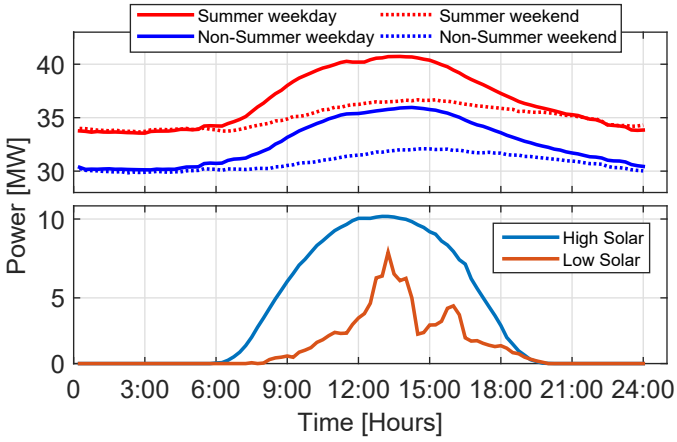

Figure 5.7. Microgrid demand (top) and solar (bottom) profiles.

The characteristics of the microgrid conform to the UC San Diego microgrid. Similar to CAISO, demand is split into summer and non-summer weekday and weekend based on actual demand data collected from campus with demand peaks of (42, 36, 35, and 32) MW for summer weekday, summer weekend, non-summer weekday, and non-summer weekend and base-load of 34 MW for both summer scenarios and 30 MW for non-summer as shown in Fig. 5.7 (top plot). Those profiles are matched with the existing market scenarios in Table 5.1. Microgrid generation is 20 MW from gas turbines and solar power of peak-to-peak ratio is 10 MW and both *high* and *low* solar clusters are shown in Fig. 5.7 (bottom plot). Noted here that the *low* solar profile for the microgird is more intermittent compared to the market case because of the geospatial effect. The maximum allowable power demand from the grid (P_L) is 45 MW. Since microgrid energy sales to the market are not permitted, overgeneration would have to be curtailed.

The growth rates of solar and demand are both 3% for the microgrid. The growth

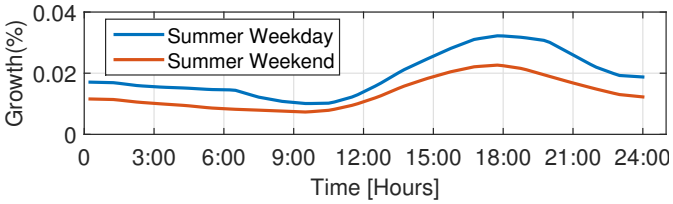

Figure 5.8. The market annual demand growth profiles for summer.

of solar and wind are both assumed to be 7% for the microgrid. To compute annual demand growth profile, CAISO demand data in 2013–2015 is used. The market annual demand growth profiles for non-summer scenarios are assumed scalar and equal to 2% while those for summer scenarios are shown in Fig. 5.8.

The BESS pricing cases ($J_{b,t}$ in Eq. (5.4)), which all include government subsidies and incentives, are divided into two categories named a and b.Each category includes 10 cases (called a-1,$\cdots$,a-10,b-1,$\cdots$,b-10) which start from a price value between 117 \$/kWh and 175.5 \$/kWh. The price functions of all cases in category a converge to 100 \$/kWh within 15 years Nykvist and Nilsson (2015) while those of the cases in category b decay with a constant rate of 1% every year. The life cycle of BESS is assumed 10 years for all cases.

5.5 Numerical Results

Fig. 5.6 shows optimization results for the BESS installation by year. On the y axis prices increase from lower to higher. On the x axis prices decrease from left to right as the years progress. For both cases no installation was applied before the year 5 (Y5) but as the BESS prices drop faster in case a compared to case b the installation went up to case a-8 compared to case b-4. The yearly installation plan of the BESS results to be large at one year followed by smaller installation few years before and after. After case a-8 and case b-4 no installations have resulted.

Fig. 5.9 shows a sample day of price case a-8 as P_u, P_b and λ_P, where microgrid

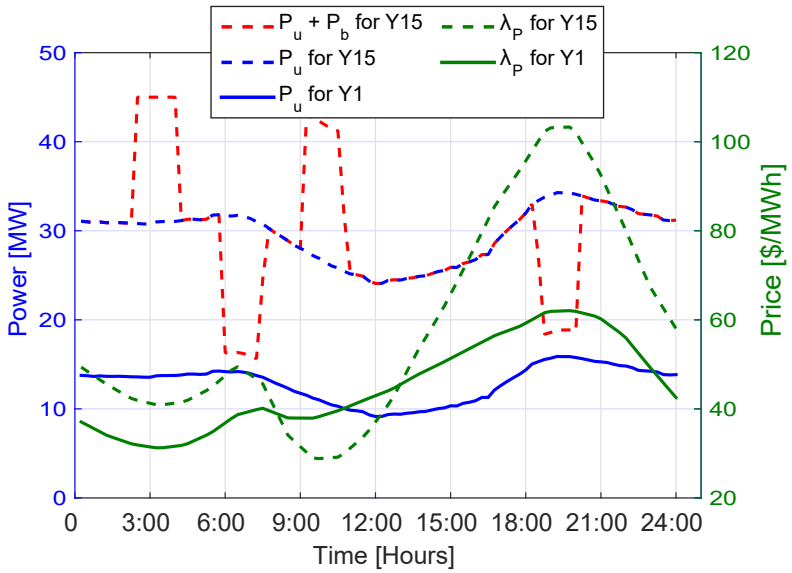

Figure 5.9. First and last year microgrid demand and storage profile (left axis) and price (right axis). Data are for the first scenario {SWD,HS,HW}. During Y1 no BESS installation was present and no data is plotted.

power purchase with storage is presented in the left axis and λ_P is presented in the right axis for Y1 and Y15. Adding BESS in the microgrid changes the behavior of the microgrid demand with a new peak between 1 and 3 AM during a market price depression. Specifying $P_L = 45$ MW limits the charging of the BESS from hour 1AM to 3AM to not exceed a total microgrid demand of 45 MW. Comparing λ_P in Y1 and Y15 shows the effect of larger solar for a midday price minimum and stronger peak demand growth in the evening. Therefore the price curve shows two peaks and a pronounced evening peak in Y15. The price curve triggers two BESS cycles per day to leverage the margins between minima and peaks.

5.6 Conclusions

As the need for Battery Energy Storage System (BESS) is increasing to cope with intermittent energy production from renewable energy sources, optimal BESS sizing from an economical perspective is a challenging problem. To optimally size the BESS in

the design stage of a microgrid, the trade-off between BESS cost, energy bill savings, and lifetime must be taken into account. Using a stochastic optimization approach we optimally size and schedule a BESS in a microgrid based on market energy pricing. Variability of wind and solar energy resources, the variability of energy demand, and a dynamic market price model that considers feedback from microgrid energy decisions are considered. Decreasing BESS costs over time are also modeled. The modeling framework contains significant flexibility and realism for microgrid planning.

Assuming the market clearance price model and net demand forecasts in our case study for CAISO and a particular trading node, the results show that a microgrid can start saving money with wholesale market energy trading once BESS prices drop below $150/kWh. The operational scheduling of BESS is not targeted to shave the microgrid peak but rather to profit from wholesale energy cost margins. Additional constraints could be added to achieve a hybrid between local and market objectives.

The text and data in Chapter 5, in full, is a reprint of the material as it appears in "Market-Driven Energy Storage Planning for Microgrids with Renewable Energy Systems Using Stochastic Programming,". Habib, Abdulelah; Disfani, Vahid R.; Kleissl, Jan; de Callafon, Raymond, *IFAC-PapersOnLine*, vol. 50, iss. 1, pp. 183-188, 2017. The dissertation author is the primary investigator and author of this article

Chapter 6

Concluding Remarks

In this dissertation, the two main operation mode (grid connected and off-grid) were discussed in the theme of improving system efficiency whether in seeking sizing or scheduling problems. In the case of islanding, the dissertation's Chapter 2 and 3 studied the optimal design for standalone system with a specific load type to be on or off (no partial operation is allowed). This setup is suitable for applications such as water treatment facility powered by a solar farm in a rural area, where facility consists of a discrete number of units. Each unit is required to operate on design point (no partial operation is applicable), the algorithm will determine the optimal number of units and the size of the units in a given location by studying the annual solar data. The storage then was introduced to the problem for optimal sizing as well as load scheduling. The techniques can also be applied to large loads operating in island modes - such as motors or pumps, steel manufacturing, and data centers. Mixed integer linear programming is used for sizing and scheduling the loads, whereas historical solar data is used to optimally schedule the available resources in a selected location. The approach is illustrated for both static and dynamic loads. As further work for this part of the dissertation will carry the more realistic application for dynamical loads. Also, another application is load with nonlinear efficiency for instance if a load is designed to operate without $\pm 20\%$ of the design point but with high efficiency at the design point. This kind of constraints are

nonlinear/convex and required to different relaxation techniques to be studied.

In Chapter 4, we investigated methods for mitigating macrogrid power outages by utilizing available Distributed Energy Resources (DER) to supply load locally, but across several customers. The algorithm schedules load and demand to meet certain objective functions such as minimizing power losses or maximizing solar energy utilization and is implemented in the framework of mixed integer linear programming. Reliability metrics increased significantly through power sharing and the approach is illustrated on power data from actual households when subjected to a power outage. One year worth of data for ten houses was processed from the Australian grid. The algorithm of power sharing can achieve improvement up to 35% in power system reliability with the availability of storage and up to 20% with solar only. As future work on this area, there is a lot of work to proof the concept and implement the hardware and the communication. Although we proposed that the algorithm can be implemented in the existing power system component such as smart metering, and smart inverters, but there is a lot of work to be done on the controls side.

Finally in Chapter 5 an investment and installation scheduling tool to help microgrid owners decide on when is the best time to install and size Battery Energy Storage Systems (BESS) from an economic perspective. As BESS can mitigate effects of intermittent energy production from renewable energy sources they play a critical role in peak shaving and demand charge management. The trade-off between BESS investment costs, lifetime, and revenue from utility bill savings along with microgrid ancillary services are taken into account to determine the optimal size of a BESS. The optimal size of a BESS is solved via a stochastic optimization problem considering wholesale market pricing. A stochastic model is used to schedule arbitrage services for energy storage based on the forecasted energy market pricing while accounting for BESS cost trends, the variability of renewable energy resources, and demand prediction. The approach is illustrated with

an application to various realistic case studies based on pricing and demand data from the California Independent System Operator (CAISO). The case study results give insight in optimal BESS sizing from a cost perspective, based on both long-term installation schedules and daily BESS operation. This tool can also help government and decision makers to determine the incentive program to promote storage installation. In future plans for this part of the dissertation, the pricing model used is very simplistic to one price node. This can be improved by matching models for more nodes in a similar black-box way or in a more advanced neural network approach. The rest of the modeling component can be tuned and fixed as needed.

Bibliography

Amir, L., Tam, T. K., Pita, M., Meijler, M. M., Alfonta, L., Katz, E., 2008. Biofuel cell controlled by enzyme logic systems. Journal of the American Chemical Society 131 (2), 826–832.

Ashok, S., 2007. Optimised model for community-based hybrid energy system. Renewable Energy 32 (7), 1155 – 1164.

Atia, R., Yamada, N., 2015. More accurate sizing of renewable energy sources under high levels of electric vehicle integration. Renewable Energy 81, 918–925.

Bahiense, L., Oliveira, G. C., Pereira, M., Granville, S., 2001. A mixed integer disjunctive model for transmission network expansion. Power Systems, IEEE Transactions on 16 (3), 560–565.

Bakelli, Y., Arab, A. H., Azoui, B., 2011. Optimal sizing of photovoltaic pumping system with water tank storage using lpsp concept. Solar Energy 85 (2), 288–294.

Balasubramaniam, K., Saraf, P., Hadidi, R., Makram, E. B., 2016. Energy management system for enhanced resiliency of microgrids during islanded operation. Electric Power Systems Research 137, 133 – 141.

Belloni, A., Piroddi, L., Prandini, M., 2016. A stochastic optimal control solution to the energy management of a microgrid with storage and renewables. In: 2016 American Control Conference (ACC). IEEE, pp. 2340–2345.

Blake, E. S., Kimberlain, T. B., Berg, R. J., Cangialosi, J., Beven II, J. L., 2013. Tropical cyclone report: Hurricane sandy. National Hurricane Center 12, 1–10.

Bonami, P., Kilinç, M., Linderoth, J., 2012. Algorithms and software for convex mixed integer nonlinear programs. In: Mixed integer nonlinear programming. Springer, pp. 1–39.

Bouabdallah, A., Bourguet, S., Olivier, J., Machmoum, M., 2013a. Photovoltaic energy

for the fixed and tracking system based on the modeling of solar radiation. In: Industrial Electronics Society, IECON 2013-39th Annual Conference of the IEEE. IEEE, pp. 1821–1826.

Bouabdallah, A., Bourguet, S., Olivier, J.-C., Machmoum, M., 2013b. Optimal sizing of a stand-alone photovoltaic system. In: Renewable Energy Research and Applications (ICRERA), 2013 International Conference on. IEEE, pp. 543–548.

Bouabdallah, A., Olivier, J., Bourguet, S., Machmoum, M., Schaeffer, E., 2015. Safe sizing methodology applied to a standalone photovoltaic system. Renewable Energy 80, 266–274.

Chen, Y., Gai, P., Xue, J., Zhang, J.-R., Zhu, J.-J., 2015. An on–off switchable power output of enzymatic biofuel cell controlled by thermal-sensitive polymer. Biosensors and Bioelectronics 74, 142–149.

Doll, C. N., Pachauri, S., 2010. Estimating rural populations without access to electricity in developing countries through night-time light satellite imagery. Energy Policy 38 (10), 5661 – 5670, the socio-economic transition towards a hydrogen economy - findings from European research, with regular papers.
URL http://www.sciencedirect.com/science/article/pii/S030142151000385X

Donadee, J., Sept 2013. Optimal operation of energy storage for arbitrage and ancillary service capacity: The infinite horizon approach. In: North American Power Symposium (NAPS), 2013. pp. 1–6.

Egido, M., Lorenzo, E., 1992. The sizing of stand alone pv-system: A review and a proposed new method. Solar Energy Materials and Solar Cells 26 (1), 51–69.

Energy, G., 2010. Western wind and solar integration study. Citeseer.

FERC, N., 2012. Arizonasouthern california outages on september 8, 2011: Causes and recommendations.

Ferhatbegovic, T., Zucker, G., Palensky, P., 2011. Model based predictive control for a solar-thermal system. Proceedings of 10th IEEE AFRICON, 1–6.

Fux, S. F., Benz, M. J., Guzzella, L., 2013. Economic and environmental aspects of the component sizing for a stand-alone building energy system: A case study. Renewable Energy 55, 438–447.

Griva, I., Nash, S. G., Sofer, A., 2009. Linear and nonlinear optimization. Siam.

Gupta, S., 2011. Dr. y. kumar1, dr. gayatri agnihotri1. J. Electrical Systems 7 (2), 206–224.

Habib, A. H., Disfani, V. R., Kleissl, J., de Callafon, R. A., Mar 2017. Optimal switchable load sizing and scheduling for standalone renewable energy systems. Solar Energy 144, 707–720.
URL http://dx.doi.org/10.1016/j.solener.2017.01.065

Habib, A. H., Kleissl, J., de Callafon, R. A., July 2016a. Model predictive load scheduling using solar power forecasting. In: 2016 American Control Conference (ACC). pp. 3200–3205.

Habib, A. H., Pecenak, Z. K., Disfani, V. R., Kleissl, J., de Callafon, R. A., April 2016b. Reliability of dynamic load scheduling with solar forecast scenarios. In: 2016 Annual IEEE Systems Conference (SysCon). pp. 1–7.

Habib, A. H., Ratnam, E. L., Disfani, V. R., Kleissl, J., de Callafon, R. A., Dec 2016c. Optimization-based residential load scheduling to improve reliability in the distribution grid. In: 2016 IEEE 55th Conference on Decision and Control (CDC). pp. 2419–2424.

Habib, A. H., Zamani, V., Kleissl, J., 2015. Solar desalination system model for sizing of photovoltaic reverse osmosis (PVRO). In: ASME 2015 Power Conference. Vol. 9.

Hanley, C. J., Peek, G. H., Boyes, J. D., 2008. Solar energy grid integration systems-energy storage. Sandia Report, SAND2008-4247.

Holbert, K. E., Chen, Z., 2015. Contemplating a residential battery system for the Southwestern US. In: North American Power Symposium (NAPS), 2015. pp. 1–6.

Horowitz, S. H., Phadke, A. G., Renz, B. A., 2010. The future of power transmission. Power and Energy Magazine, IEEE 8 (2), 34–40.

Houchois, P., Dewhurst, J., Gandolfi, A., 2014. Global utilities, autos & chemicals.

Huang, S., Wu, Q., Oren, S. S., Li, R., Liu, Z., 2015. Distribution locational marginal pricing through quadratic programming for congestion management in distribution networks. Power Systems, IEEE Transactions on 30 (4), 2170–2178.

Hung, J. T., Robertazzi, T. G., 2008. Scheduling nonlinear computational loads. Aerospace and Electronic Systems, IEEE Transactions on 44 (3), 1169–1182.

IEA, International Energy Agency, 2013. 2013 Key world energy statistics. Tech. rep.,

OECD/IEA.

Ioli, D., Falsone, A., Prandini, M., 2015. An iterative scheme to hierarchically structured optimal energy management of a microgrid. In: Decision and Control (CDC), 2015 IEEE 54th Annual Conference on. IEEE, pp. 5227–5232.

Jaworsky, C., Turitsyn, K., June 2013. Effect of storage characteristics on wind intermittency mitigation effectiveness. In: 2013 American Control Conference. pp. 3649–3654.

Kellogg, W. D., Nehrir, M. H., Venkataramanan, G., Gerez, V., Mar 1998. Generation unit sizing and cost analysis for stand-alone wind, photovoltaic, and hybrid wind/pv systems. IEEE Transactions on Energy Conversion 13 (1), 70–75.

Kim, B.-G., Ren, S., van der Schaar, M., Lee, J.-W., 2013. Bidirectional energy trading and residential load scheduling with electric vehicles in the smart grid. Selected Areas in Communications, IEEE Journal on 31 (7), 1219–1234.

Kobayakawa, T., Kandpal, T. C., 2015. Analysis of electricity consumption under a photovoltaic micro-grid system in india. Solar Energy 116, 177–183.

Kousksou, T., Bruel, P., Jamil, A., Rhafiki, T. E., Zeraouli, Y., 2014. Energy storage: Applications and challenges. Solar Energy Materials and Solar Cells 120, 59 – 80. URL http://www.sciencedirect.com/science/article/pii/S0927024813004145

Lasseter, R. H., 2002. Microgrids. In: Power Engineering Society Winter Meeting, 2002. IEEE. Vol. 1. pp. 305–308 vol.1.

Lasseter, R. H., 2011. Smart distribution: Coupled microgrids. Proceedings of the IEEE 99 (6), 1074–1082.

Lee, M., Soto, D., Modi, V., 2014. Cost versus reliability sizing strategy for isolated photovoltaic micro-grids in the developing world. Renewable Energy 69, 16–24.

Liscouski, B., Elliot, W., 2004. Final report on the august 14, 2003 blackout in the united states and canada: Causes and recommendations. A report to US Department of Energy 40 (4).

Ma, Z., Chen, D., 2015. Optimal power dispatch and control of a wind turbine and battery hybrid system. In: American Control Conference (ACC), 2015. IEEE, pp. 3052–3057.

MacQueen, J., 1967. Some methods for classification and analysis of multivariate observations. In: Proceedings of the fifth Berkeley symposium on mathematical statistics

and probability. Vol. 1. Oakland, CA, USA., pp. 281–297.

Mandelli, S., Brivio, C., Colombo, E., Merlo, M., 2016. A sizing methodology based on levelized cost of supplied and lost energy for off-grid rural electrification systems. Renewable Energy 89, 475–488.

Mansfield, M., Linzey, W., 2013. Hurricane sandy multistate outage & restoration report. Tech. rep., Technical Report 9308, National Association of State Eenergy Officials.

Mellit, A., Kalogirou, S. A., 2008. Artificial intelligence techniques for photovoltaic applications: A review. Progress in energy and combustion science 34 (5), 574–632.

Mellit, A., Kalogirou, S. A., Drif, M., 2010a. Application of neural networks and genetic algorithms for sizing of photovoltaic systems. Renewable Energy 35 (12), 2881–2893.

Mellit, A., Kalogirou, S. A., Drif, M., 2010b. Application of neural networks and genetic algorithms for sizing of photovoltaic systems. Renewable Energy 35 (12), 2881–2893.

Miller, D. N., de Callafon, R. A., 2012. Identification of linear, discrete-time filters via realization. LINEAR ALGEBRA–THEOREMS AND APPLICATIONS, 117.

Mohammadi, M., Hosseinian, S., Gharehpetian, G., 2012. Optimization of hybrid solar energy sources/wind turbine systems integrated to utility grids as microgrid (MG) under pool/bilateral/hybrid electricity market using pso. Solar energy 86 (1), 112–125.

Morais, H., Kadar, P., Faria, P., Vale, Z. A., Khodr, H., 2010. Optimal scheduling of a renewable micro-grid in an isolated load area using mixed-integer linear programming. Renewable Energy 35 (1), 151–156.

Negnevitsky, M., Wong, K., 2015. Demand-side management evaluation tool. Power Systems, IEEE Transactions on 30 (1), 212–222.

Nguyen, D. A., Ubiratan, P., Velay, M., Hanna, R., Kleissl, J., Schoene, J., Zheglov, V., Kurtz, B., Torre, B., Disfani, V. R., 2015. Impact research of high photovoltaics penetration using high resolution resource assessment with sky imager and power system simulation.

Nguyen, M. Y., Nguyen, D. H., Yoon, Y. T., 2012. A new battery energy storage charging/discharging scheme for wind power producers in real-time markets. Energies 5 (12), 5439–5452.

Nouni, M., Mullick, S., Kandpal, T., 2008. Providing electricity access to remote areas

in india: An approach towards identifying potential areas for decentralized electricity supply. Renewable and Sustainable Energy Reviews 12 (5), 1187 – 1220.
URL http://www.sciencedirect.com/science/article/pii/S136403210700010X

Nykvist, B., Nilsson, M., 2015. Rapidly falling costs of battery packs for electric vehicles. Nature Climate Change 5 (4), 329–332.

Olcan, C., 2015. Multi-objective analytical model for optimal sizing of stand-alone photovoltaic water pumping systems. Energy Conversion and Management 100, 358–369.

Ornelas-Tellez, F., Zuiga-Neria, G. C., Rico, J. J., Sanchez, E. N., Calderon, F., 2014. Optimized operation of a micro-grid for energy resources. IFAC Proceedings Volumes 47 (3), 4578 – 4583, 19th IFAC World Congress.
URL http://www.sciencedirect.com/science/article/pii/S1474667016423207

Pickard, W. F., Abbott, D., 2012a. Addressing the intermittency challenge: Massive energy storage in a sustainable future. Proceedings of the IEEE 100 (2), 317.

Pickard, W. F., Abbott, D., 2012b. Addressing the intermittency challenge: Massive energy storage in a sustainable future. Proceedings of the IEEE 100 (2), 317.

Pitz-Paal, R., Geuder, N., Hoyer-Klick, C., Schillings, C., 2011. How to get bankable meteo data. DLR solar Resource Assessment. Cologne (Alemanha): DLR [Deutschen Zentrums für Luft-und Raumfahrt].

Ratnam, E. L., Weller, S. R., Kellett, C. M., Murray, A. T., 2015. Residential load and rooftop pv generation: an australian distribution network dataset. International Journal of Sustainable Energy, 1–20.

Reno, M. J., Hansen, C. W., Stein, J. S., 2012. Global horizontal irradiance clear sky models: Implementation and analysis. SANDIA report SAND2012-2389.

Rickerson, W., Uppal, J., Glassmire, J., Lilienthal, P., Sanders, E., Colson, C., Solano-Peralta, M., Vallvé, X., Couture, T., 2012. Renewable energies for remote areas and islands (remote). International Energy Agency-Renewable Energy Technology Deployment (IEA-RETD). Paris, France.

Saber, A. Y., Venayagamoorthy, G. K., 2012. Resource scheduling under uncertainty in a smart grid with renewables and plug-in vehicles. Systems Journal, IEEE 6 (1), 103–109.

Sachs, S., 2014. Indigenous developments (winter 2015). Indigenous Policy Journal 25 (3).

Savkin, A. V., Khalid, M., Agelidis, V. G., 2014. Optimal size of battery energy storage and monotonic charging/discharging strategies for wind farms. In: Control Applications (CCA), 2014 IEEE Conference on. IEEE, pp. 1372–1376.

Sevilla, F. S., Knazkins, V., Park, C., Korba, P., 2015. Advanced control of energy storage systems for pv installation maximizing self-consumption**the work reported in this paper was financed by the swiss competence center for energy research, sccer-furies. IFAC-PapersOnLine 48 (30), 524 – 528, 9th IFAC Symposium on Control of Power and Energy Systems CPES 2015.
URL http://www.sciencedirect.com/science/article/pii/S240589631503075X

Shafie-khah, M., Heydarian-Forushani, E., Golshan, M., Siano, P., Moghaddam, M., Sheikh-El-Eslami, M., Catalão, J., 2016. Optimal trading of plug-in electric vehicle aggregation agents in a market environment for sustainability. Applied Energy 162, 601–612.

Smaoui, M., Abdelkafi, A., Krichen, L., 2015. Optimal sizing of stand-alone photovoltaic/wind/hydrogen hybrid system supplying a desalination unit. Solar Energy 120, 263–276.

Sreeraj, E., Chatterjee, K., Bandyopadhyay, S., 2010. Design of isolated renewable hybrid power systems. Solar Energy 84 (7), 1124–1136.

Sun, C. C., Puig, V., Cembrano, G., 2014. Two-layer scheduling scheme for pump stations. In: Control Applications (CCA), 2014 IEEE Conference on. IEEE, pp. 1741–1746.

Teleke, S., Baran, M. E., Bhattacharya, S., Huang, A. Q., Oct 2010. Rule-based control of battery energy storage for dispatching intermittent renewable sources. IEEE Transactions on Sustainable Energy 1 (3), 117–124.

Thevenard, D., Pelland, S., 2013. Estimating the uncertainty in long-term photovoltaic yield predictions. Solar Energy 91, 432–445.

UN, 2014. Universal Access to Modern Energy for the Poor [Online]. Available: http://www.undp.org/content/undp/en/home/ourwork/environmentandenergy/focus-areas/sustainable-energy/universal-access/.

Vermeulen, H., Nieuwoudt, T., 2015. Optimisation of residential solar pv system rating for minimum payback time using half-hourly profiling. In: Domestic Use of Energy

(DUE), 2015 International Conference on the. IEEE, pp. 215–221.

Verzijlbergh, R. A., De Vries, L. J., Lukszo, Z., 2014. Renewable energy sources and responsive demand. do we need congestion management in the distribution grid? Power Systems, IEEE Transactions on 29 (5), 2119–2128.

Viana, A., Pedroso, J. P., 2013. A new MILP-based approach for unit commitment in power production planning. International Journal of Electrical Power & Energy Systems 44 (1), 997–1005.

Vieira, J. A. B., Mota, A. M., 2010. Implementation of a stand-alone photovoltaic lighting system with mppt battery charging and led current control. In: Control Applications (CCA), 2010 IEEE International Conference on. IEEE, pp. 185–190.

Wan, Y., January 2012. Long-term wind power variability [Online]. NREL: Technical Report TP-5500-53637.

Wissem, Z., Gueorgui, K., Hédi, K., 2012. Modeling and technical–economic optimization of an autonomous photovoltaic system. Energy 37 (1), 263–272.

Yang, Y., Li, H., Aichhorn, A., Zheng, J., Greenleaf, M., 2014. Sizing strategy of distributed battery storage system with high penetration of photovoltaic for voltage regulation and peak load shaving. Smart Grid, IEEE Transactions on 5 (2), 982–991.

Zachar, M., Daoutidis, P., 2016. Economic dispatch for microgrids with constrained external power exchange. IFAC-PapersOnLine 49 (7), 833–838.

Zhang, D., Zarghami, M., Liang, T., Vaziri, M., Oct 2015. A state-space model for integration of battery energy storage systems in bulk power grids. In: 2015 North American Power Symposium (NAPS). pp. 1–5.

Zhang, H., Vittal, V., Heydt, G. T., Quintero, J., 2012. A mixed-integer linear programming approach for multi-stage security-constrained transmission expansion planning. Power Systems, IEEE Transactions on 27 (2), 1125–1133.

Zheng, Y., Hill, D., Meng, K., Luo, F., Dong, Z., 2015. Optimal short-term power dispatch scheduling for a wind farm with battery energy storage system. IFAC-PapersOnLine 48 (30), 518 – 523, 9th IFAC Symposium on Control of Power and Energy Systems CPES 2015.
URL http://www.sciencedirect.com/science/article/pii/S2405896315030748